A MULTI-PROXY LOOK AT DEGLACIAL SOUTHWEST PACIFIC OCEAN SEA SURFACE TEMPERATURE AND THERMOCLINE SOURCE WATER CHANGES

By

BENEDETTO SCHIRALDI JR.

A thesis submitted to the
Graduate School-New Brunswick Rutgers, The State University of New Jersey
in partial fulfillment of the requirements for the degree of
Master of Science
Graduate Program in Oceanography
written under the direction of
Dr. Elisabeth L. Sikes
and approved by

_____
Dr. Elisabeth Sikes, PhD

_____
Dr. James D. Wright, PhD

_____
Dr. Yair Rosenthal, PhD

_____
John Wilkin, Ph.D

New Brunswick, New Jersey
May, 2013

ABSTRACT OF THE THESIS

A Multi-Proxy Look At Deglacial Southwest Pacific Ocean

Sea Surface Temperature and Thermocline Source Water Changes

By BENEDETTO SCHIRALDI JR.

Thesis Direction:
Dr. Elisabeth L. Sikes

Glacial-interglacial changes in global and regional temperature have been linked to changes in insolation, winds, and ocean circulation. This study reconstructs sea surface temperature (SST) and source water provenance across the last deglaciation (~30-5 kyr BP) in five sediment cores in the Bay of Plenty, New Zealand and places these in a regional context by comparing these results to previously published work.

SST reconstructions from Mg/Ca ratios in the planktonic foraminifera *Globogerina bulloides* and alkenones ($U^{37}_{'}$) track different seasons' SST spring and summer, respectively. During the last glacial maximum (LGM, 26-22 kyr BP), summer SSTs average 16.4°C while spring SSTs were 13.6; about 4°C cooler than modern. The seasons track well with each other and maintain a constant offset of 3.3-2.8°C as temperatures increase into the Holocene, peaking at 21.7°C for summer and 18.4°C for spring. Comparison to model reconstructions of local insolation yielded correlation to winter insolation from the LGM (~26 kyr BP) to the Antarctic Cold Reversal ACR (~14.1 kyr BP) after which SSTs correlate well to their respective seasonal insolation. Comparison of this study's temperatures to published SSTs indicate that deglacial warming of subtropical waters differ from subantarctic waters that warmed later and by 2°C more than subtropical waters.

$\delta^{18}O$ and $\delta^{13}C$ from planktonic foraminifera *G. bulloides* and *Globorotalia*

inflata were used to reconstruct δ18O of seawater ($\delta^{18}O_{sw}$) and track source water provenance. In the LGM, depleted $\delta^{18}O_{SW}$ averaging 0.2‰, and enriched $\delta^{13}C$ ranging between -0.4-0.1‰ indicate shallow water masses had a strong local Southern Ocean component. A step change occurs at 20.1 kyr BP where $\delta^{13}C$ depletes to -1.3‰ that suggests a deglacial shift in shallow subsurface water mass source location to a distal subtropical component likely sourcing through the equatorial Pacific that persists into the Holocene. A regional comparison indicates numerous switches between distal-subtropical and proximal- subantarctic influences during the early deglaciation. This ends at the ACR, which figures as a tipping point for stabilization and onset of modern circulation.

ACKNOWLEDGEMENTS

The completion of this thesis was one of the most difficult tasks I have ever had to complete and would not have been possible unless for the emotional support of my many friends and family. For this reason I am taking a moment to thank both of my parents, my siblings Nick, Elizabeth, and Brian for their love and support throughout this entire process. I will also like to take a moment to thank my loving and devoted girlfriend Patricia for always being there to help me deal with the stress of Graduate School no matter what the hour. I could not have completed this research without the support of my many friends including: cool Tom, Mike, Sean, Tony, Bill, Danny, Collin, sweet Tom, Sheng, Alex, Chris, Dylan, Omar, Jason, Jesse, and of course my fellow IMCSers and friends: Anna, Kevin, Aboozar, Jack, Kat, Mikaela, and Brittany.

I thank my advisor Dr. Elisabeth Sikes for the countless hours she put in to not only ensuring my research was good science but also well written and well thought out science. I am grateful for the support of my committee members Dr. Yair Rosenthal, and Dr. James D. Wright and the members of their labs including Rick Mortlock, Nicole Abdul, Julie, Audrey, and Tali, especially for their help and guidance in the data acquisition. Finally, I would like to thank Dr. Aurora Elmore for sharing the data from her post-doc work at Rutgers University.

Lastly, this research would not have been completed without the financial support of the National Science Foundation, Rutgers Graduate School, and the knowledge shared by the International School of Foraminifera and the Gryzbowski Foundation.

TABLE OF CONTENTS

LIST OF TABLES

LIST OF FIGURES

Figure 1.3| a)The distribution of $\delta^{13}C$ of ΣCO_2 in the modern western Atlantic [Kroopnick, 1985] . b) A of δ13C of foraminferal calcite of benthic forams used to reconstruct a glacial transect for the western Atlantic Ocean basins(Curry and Oppo, 2005). A simple three-component model is used to explain the water mass distribution and gradients in both time slices. During the glaciation, patterns in the South Atlantic imply that the northern source water at 1500 m penetrated as far as 30°S latitude. The penetration of the deep Southern Ocean water mass can be observed as far as 60°N. The shallow, southern source water mass (AAIW) did not penetrate to 25°N, but there are too few data at intermediate water depths between about 25°S and 25°N in the western Atlantic to constrain its northward extent. (Taken from Curry and Oppo, 2005)

Figure 1.4| The relation between $\delta^{18}O$ (top two graphs) and salinity (bottom two graphs) and latitude of the surface waters of the Atlantic and Pacific Oceans. Variations with respect to latitude are similar for these two indicating that the rain water that dilutes at high latitudes is highly dependent in $\delta^{18}O$. Redrawn from Broecker (2002).

Figure 1.5| Bathymetric map of New Zealand. Our five coring locations are located to the north of the North Island of New Zealand in the Bay of Plenty: RR0503-JPC64 (37° 25.34′ S, 177° 00.41′ E; 651 m; pink triangle), RR0503-JPC79 (36°57.52’ S, 176°35.57; 1165 m; red triangle), RR0503-JPC/TC83 (36°44.25’S, 176°38.39’E; 1627m; white triangle), RR0503-JPC/TC87 (37°15.81’S, 176°39.86’E; 663m; blue triangle), RR0503-JPC125 (36°11.9’S. 176°53.35’E; 2,541m, cyan triangle). Modern surface conditions have subtropical flow (red) sourced from lower latitudes into the Bay of Plenty. The subtropical front (STF; purple) marks the convergence zone where subtropical waters meet subantarctic water (blue) sourced from higher latitudes in the Southern Ocean.

Figure 3.19 .Schematic maps of the suggested changes in circulation a) glacial b) deglacial surface circulation. Note that during the LGM subantarctic waters were a component of surface waters in the Bay of Plenty but after the onset of the deglaciation the Bay of Plenty is dominated by distally sourced Subtropical Mode Water (STMW; red) while the south Chatham Rise is dominated by proximally source Southern Ocean Subantarctic Mode Water (SAMW; blue). SAMW is getting passed the Subtropical Front (STF; purple) resulting in a deglacial battle for competing influence of SAMW and STMW at Hawkes Bay 99

Chapter 1

1.1 Introduction

A key to understanding driving forces in the climate system is determining how these forces manifested themselves regionally in past climate modes. A natural climate forcing is a naturally occurring physical or chemical phenomenon which takes a system out of balance and forces that system to respond and find a new homeostasis. Natural changes in climate can be recorded by environmental archives, which preserve some characteristic of the environmental conditions from the past. Some examples of proxy climate records include ice cores, in which past atmospheric conditions are preserved in the ice and gas bubbles, and in the calcite shells of foraminifera, found in oceanic sediment. These single shell eukaryotes preserve oceanic conditions such as sea surface temperature through their stable isotopes and trace metals composition during calcification. By providing us with a glimpse of past atmospheric and oceanic conditions climate proxy records have been fundamental in providing scientists information about past climate variability.

1.2 Natural Climate Variability

1.2.1 Orbital Theory

In the past million years the Earth has gone through major glacial-interglacial cycles which are believed to have resulted from changes in incoming insolation due to variations in orbital parameters which affect Earth's insolation balance (Milankovitch, 1930). *Milankovitch* (1930) established that the incoming solar radiation is determined by the combination of three cyclical changes in Earth's orbit: the precession of the equinox, obliquity, and eccentricity. Precession of the equinox refers to wobble of the earth's axis; this oscillation has a 20 thousand

year (kyr) cycle whereas the tilt of the spin axis relative to the position in the eccentric orbit primarily governs the seasonal cycle of mid to high latitudes. Obliquity is a 40 kyr oscillation in Earth's axial tilt. This oscillation primarily impacts insolation at high latitudes and may result in insolation anomalies up to ~10 W/m^2 (e.g., Huybers and Wunsch, 2005). Finally, eccentricity refers to the shape of the overall orbit, whether it is circular or elliptical. Changes in eccentricity vary on a 100 kyr cycle and will alter Earth's distance at the aphelion, the time in the orbit when the Earth is furthest from the sun, and perihelion, the time in the orbit when the earth is closest to the sun, thus altering integrated annual incoming solar insolation.

Many studies invoke 65^{o}N to be the critical latitude for controlling the growth and decline of northern ice sheets (e.g., Milankovitch, 1930; Hays et al. 1976; Broecker 1982). *Broecker* (1982) hypothesized that the Milankovitch cycles impact insolation at 65°N governing the volume of northern hemisphere ice sheets. In turn, arguing the growth and collapse of ice sheets can accelerate or halt Atlantic Meridional Overturning Circulation (AMOC) which causes insolation at 65°N to govern global climate. Studies from the northern and the southern hemisphere (e.g., Barrows et al., 2007; Pahnke et al., 2006; etc.), compare reconstructions of the insolation at 65^{o}N, the latitude that forces northern hemisphere ice sheets, to proxy records of temperature to illustrate the high correlation of paleo-temperature estimates and the insolation at high northern latitude ice sheets. Studies in the southern hemisphere routinely attribute variability in local proxy records to northern hemisphere insolation intensity (e.g., Pahnke et al., 2006; Imbrie et al. 1992). *Shakun et al.* (2012) argue that CO_2 is the key driver of global deglacial warming but that changes in AMOC cause an apparent phase lag in the initial timing of the deglacial termination between the northern hemisphere and southern hemisphere. In contrast to studies that argue for non-local causes for

the apparent similarities in large scale hemispheric changes, *Laepple and Lohmann* (2009) highlight linear/nonlinear responses of the local seasonal cycle extrapolated to astronomical time scales as a possible explanation for region-specific climate change. In other words, *Laepple and Lohmann* (2009) illustrate that when interpreting a paleo temperature proxy, how local insolation affects the region of the proxy must be considered, it is not sufficient to interpret these trends as a global signal. Also supporting the hypothesis that local insolation drives local warming, *Huybers and Denton* (2008) show that changes in the intensity of northern hemisphere summer are in phase with changes in the overall length of southern hemisphere summers, which may account for the high correlations of southern hemisphere proxy records with northern hemisphere insolation. Therefore, before jumping on the band wagon that 65°N insolation controls all, it is essential that the proxy record be interpreted and assessed in terms of a local insolation signal driving the regional climate.

1.3 Modern Oceanography of the mid-latitude South Pacific Ocean

1.3.1 Modern Day Circulation in the New Zealand Region

In the New Zealand region, ocean circulation that would otherwise be zonal is partitioned by the presence of the New Zealand land mass. At roughly 34ºS the southward flowing East Australian Current (EAC) deflects east towards New Zealand along the north Tasman Sea (Hamon, 1965; **Figure 1.1**). As the East Australian Current flows across the Tasman Sea it gives rise to the southeast flowing East Auckland Current which allows STMW to flow along the northern edge of the North Island into the Bay of Plenty (Heath, 1972). When this flow reaches the East Cape of the North Island, it turns and flows south along the eastern side of the North Island giving rise to the East Cape Current (ECC). The ECC flows out of the

Figure 1.1

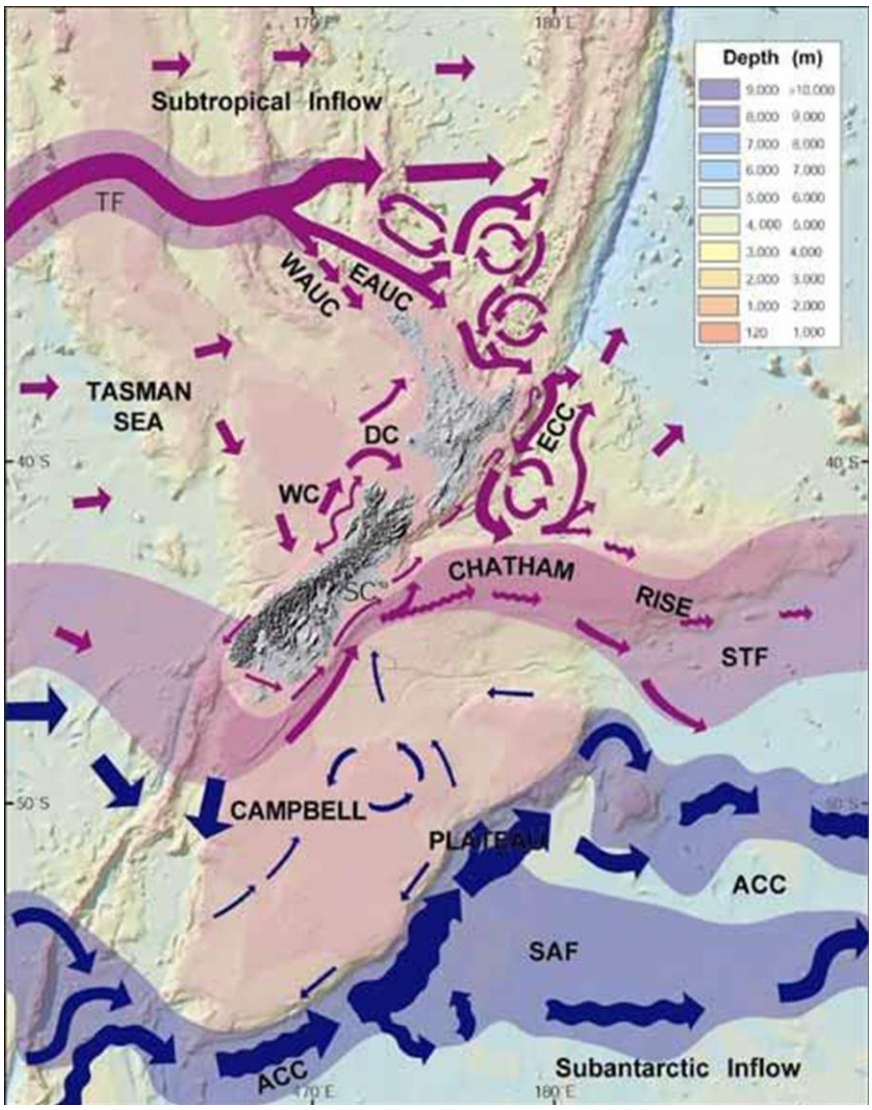

Figure 1.1| New Zealand Circulation. Summarizing the characteristics of the surface current systems, oceanic fronts and main water masses including Subtropical Water [STW]; Subtropical Front [STF]; Subantarctic Water [SAW]; Subantarctic Front [SAF]; Antarctic Circumpolar Current [ACC], the northern limit of which is defined by the SAF; Circumpolar Surface Water [CSW]. Currents are annotated as follows: East Australian Current [EAC]; East Auckland Current [EAUC]; North Cape Eddy [NCE]; East Cape Eddy [ECE]; East Cape Current [ECC]; Wairarapa Eddy [WE]; Southland Current [SC]; Southland Front [SF]; Westland Current [WC], and D'Urville Current [DC]; Tasman Front [TF].

(Taken from Carter, et al. 1998)

Bay of Plenty, south through Hawks Bay, until it reaches the Chatham Rise where it deflects to the east meeting up with the northward flowing Southland Current at the STF (Heath, 1968) this convergence is known as the subtropical front (STF).

The dominant subsurface water mass in the Bay of Plenty and northern New Zealand is Subtropical Mode Water (STMW) delivered by the East Auckland current. In the Bay of Plenty below STMW sits the subantarctic mode water (SAMW), which, based upon salinity measurements at 37°S, is roughly 300m thick and occupies depths of roughly 200-500m (**Figure 1.2b;** World Ocean Experiment; WOCE). Salinity profile data from WOCE indicates the average depth of Antarctic Intermediate water (AAIW) is between 500m and 1500m.

1.3.2 Surface Water Mass Structure

An important hydrographic feature in the surface water mass structure of the southwest Pacific Ocean, and this study region, is the STF. The subtropical front marks the northernmost edge of the Southern Ocean and the front divides the cooler fresher waters of the Southern Ocean from the warm salty subtropical surface water to the north (Orsi et al., 1995; Belkin and Gordon, 1996). The shallow sub-surface ocean in the New Zealand sector of the South Pacific Ocean is composed of three major subsurface water masses: the STMW, SAMW, and underlying these AAIW. In the New Zealand Region the SAMW is at the surface south of the STF (**Figure 1.2b**). North of the STF, subtropical surface waters are underlain by STMW which have a wide range of temperature of 13.5-22°C and salinity ranging from 34.3-36.2 psu to the north (~7°S; Wong and Johnson, 2003). SAMW has a lower temperature ranging from 5-14°C and a salinity range of 34.2-34.6 psu (McCartney, 1977; Tsuchiya and Talley, 1996). In the sector east of New Zealand, the STF is bathymetrically fixed by the Chatham Rise at ~42°S (Heath, 1981, 1985; Chiswell 1994; Belkin and Gordon, 1996). Despite being bathymetrically

Figure 1.2

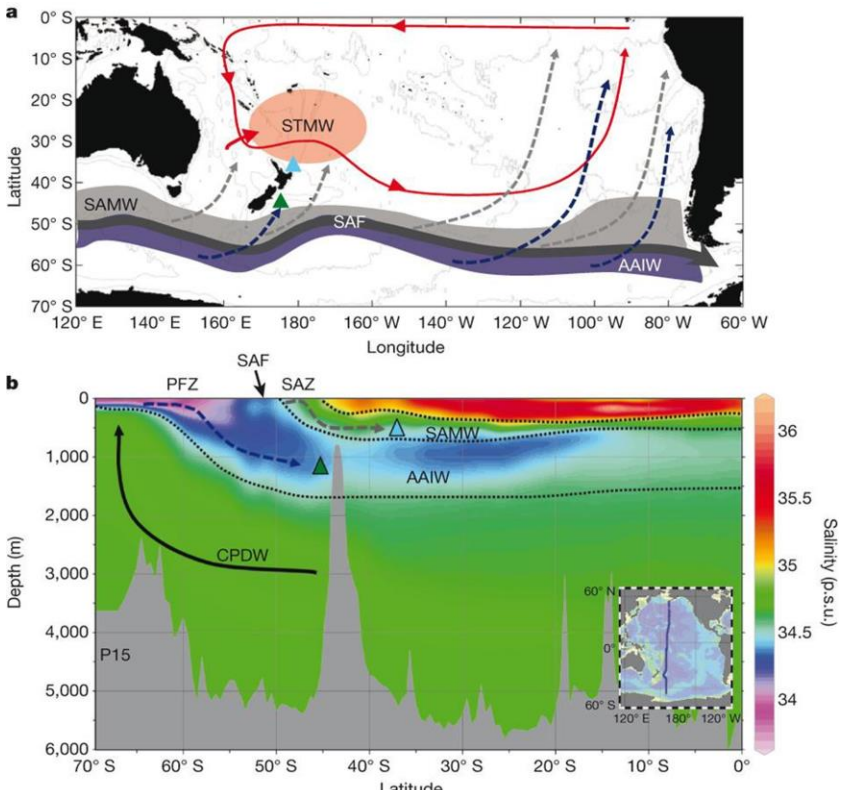

Figure 1.2| a, Schematic presentation of major currents. The bold solid line marks the approximate location of the sub-Antarctic front (SAF), which separates cold and fresher polar surface waters, to the south, from the warmer and saltier surface waters in the sub-Antarctic zone (SAZ), to the north. SAMW forms in the SAZ (grey shaded area) and becomes entrained in the South Pacific subtropical gyre circulation (solid red line). At the equator, its chemical signal can be identified in STMW (~100–300-m water depth) in the western basin. Denser AAIW (~800–1,400-m water depth) forms south of the SAF, in the polar frontal zone (PFZ, blue shaded area), and flows northwards below SAMW. The triangles mark the core sites used in this study including: the RR0503 Bay of Plenty Ensemble (37° S, 177° E; turquoise triangle) and MD97-2120 (43° 32.06′ S, 174° 55.85′ E; 1,210 m; green triangle). **b**, Wind-driven upwelling in the Southern Ocean causes shallow, mid-depth and deep-water masses to shoal. Cores RR0503-JPC64 and MD97-2120 are proximal to the formation zones of SAMW and AAIW and are positioned within the flow paths of both water masses as they are advected to the north and ventilate the South Pacific thermocline. In the Pacific, circumpolar deep water (CPDW) resides below SAMW and AAIW, providing a source for upwelled waters in the Southern Ocean. In the modern ocean, CPDW carries a strong contribution from North Atlantic Deep Water (NADW) flowing out of the Atlantic Ocean at abyssal depths. Inset, ship's track/sampling transect for the salinity vertical profile shown in the main panel. p.s.u., practical salinity units.
(taken from *Rose et al.* 2010)

fixed on the Chatham Rise, the surface expression of the front has been shown to migrate in the domain between the northern edge of the Chatham Rise and the southern edge of the Chatham Rise (Belkin and Gordon, 1994). This meandering in the surface expression of the STF across the Chatham Rise may affect how nearby sea surface temperature (SST) proxies respond to climate changes in the deglaciation.

Further south, the subantarctic front (SAF) marks the northern edge of the Antarctic Circumpolar Current (ACC). The ACC is the northern edge of the formation region of AAIW, where denser sub-polar water masses advect north below SAMW (Deacon, 1937). AAIW is colder in temperature ranging from 3.5 -10^{o}C but higher in salinity, 34.3-34.5 psu than SAMW (McCartney, 1977; Tsuchiya and Talley, 1996). South of the SAF, strong westerly winds drive the ACC causing deep isopycnal mixing (Deacon, 1937; Kennet, 1982; Orsi et al., 1995; Toggweiler and Key, 2001) allowing for the ventilation of circumpolar deep water (CDW). CDW possesses a large component of North Atlantic Deep Water (NADW; Callahan, 1972; Toggweiler and Key, 2001). On modern time scales, the impact of this high latitude circulation on both deep water masses and subsurface water masses of the New Zealand study region is well characterized. However, on glacial time-scales changes in deep water source and Southern Ocean upwelling regime have been shown to affect subsurface waters throughout the South Pacific and into the tropical latitudes of the Pacific Ocean (Spero and Lea, 2002). These changes affected the characteristics and source locations of the subsurface water masses in the study region.

1.3.3 Isotopes Signal of Regional Water

The $\delta^{13}C$ of planktonic foraminifera is a useful tracer for primary productivity and circulation (Emerson and Hedges, 2008). Subsurface water masses become depleted, or lower,

in $\delta^{13}C$ because they accumulate DIC released from remineralized organic carbon, which is significantly $\delta^{13}C$ depleted (Emerson and Hedges, 2008). Surface waters can also become enriched in $\delta^{13}C$ when biological activity preferentially takes up ^{12}C from the DIC leaving surrounding waters enriched in ^{13}C (Emerson and Hedges, 2008). In the South Pacific Ocean the deeper water masses are relatively depleted in $\delta^{13}C$ owing to the respired CO_2 signal accumulated along the long flow path from the North Atlantic (**Figure 1.3**; Curry & Oppo, 2005). The flow path and source locations of STMW, SAMW, and AAIW dictate the isotopic signature of these water masses in the Bay of Plenty water column. Presently in the Bay of Plenty, STMW and SAMW have a more proximal and ventilated source making them enriched in $\delta^{13}C$ relative to older more depleted CDW. In the region north of New Zealand SAMW and STMW possess $\delta^{13}C$ ranging from 1.4-2‰ (WOCE, P15 station 110). AAIW is advected northward under SAMW and STMW accumulating isotopically depleted carbon as it flows north, by the time it reaches the water column around New Zealand it has a $\delta^{13}C$ signature of 0.6-1.0‰ (WOCE, P15 station 110). Any changes in $\delta^{13}C$ signature throughout the Bay of Plenty water column on glacial-interglacial time scales will reflect shifts in the proximity of the source location or changes in the flow path from the source location of these water masses.

The primary driver of changes in the relative abundance of oxygen isotopes in seawater is the balance between evaporation and precipitation. In areas where evaporation is greater than precipitation, the preferential evaporation of isotopically lighter ($H_2{}^{16}O$) water, leaves the more saline waters isotopically enriched in ^{18}O. Generally at lower latitudes there is net evaporation leaving waters more saline and isotopically enriched, while at higher latitudes cooler temperature result in net precipitation leaving waters fresher and isotopically depleted. Therefore, there is a correlation between the $\delta^{18}O$ of surface water to sea surface salinity

Figure 1.3

a) Western Atlantic GEOSECS $\delta^{13}C$ (PDB)

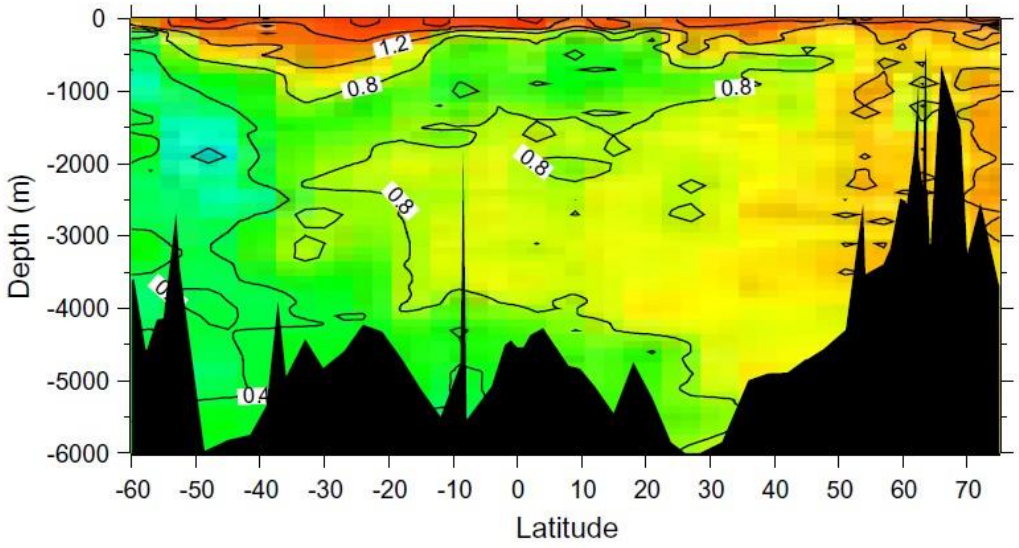

b) Western Atlantic Glacial $\delta^{13}C$ (PDB)

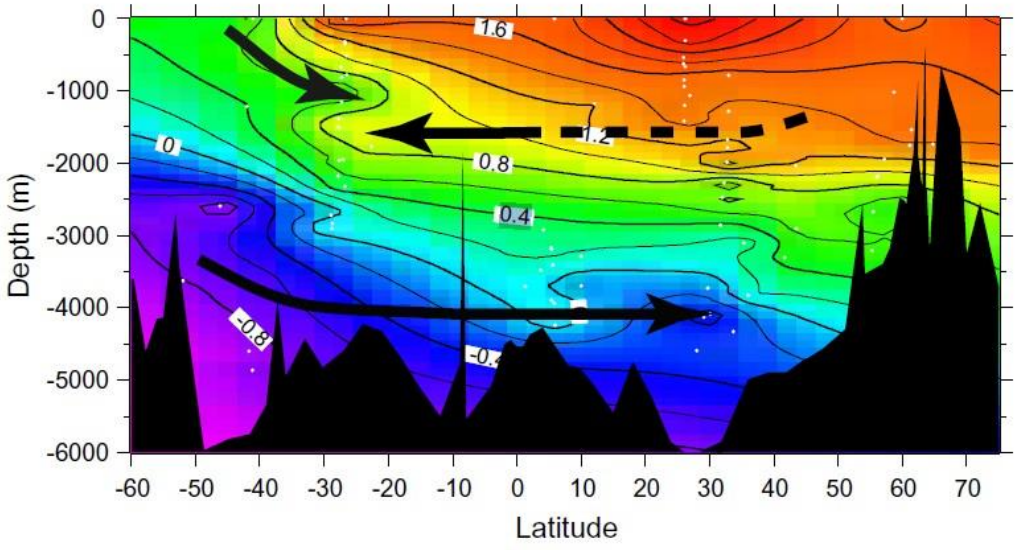

Figure 1.3| a) The distribution of $\delta^{13}C$ of ΣCO_2 in the modern western Atlantic [Kroopnick, 1985]. b) A of δ13C of foraminferal calcite of benthic forams used to reconstruct a glacial transect for the western Atlantic Ocean basins (Curry and Oppo, 2005). A simple three-component model is used to explain the water mass distribution and gradients in both time slices. During the glaciation, patterns in the South Atlantic imply that the northern source water at 1500 m penetrated as far as 30°S latitude. The penetration of the deep Southern Ocean water mass can be observed as far as 60°N. The shallow, southern source water mass (AAIW) did not penetrate to 25°N, but there are too few data at intermediate water depths between about 25°S and 25°N in the western Atlantic to constrain its northward extent. (Taken from Curry and Oppo, 2005)

evident latitudinally (**Figure 1.4**). The salinity effect can also operate on very local scales with areas of high net evaporation more enriched and areas of high net precipitation isotopically depleted. The effect of net evaporation, or net precipitation, on millennial time scales causes oxygen isotopes of global seawater to track well with global ice volume. As more isotopically depleted fresh water is removed from the ocean and stored at polar latitudes in ice caps, sea level is lowered and salinity increases. As ice volume increases, the isotopic composition of sea water ($\delta^{18}O_{sw}$) becomes heavier by roughly 0.01‰ per meter of sea level decrease (Fairbanks, 1989). Because the time scale of glaciations is millennial, which is on the same order of the residence time of water in the ocean basin, the ice volume, or sea level effect, is a global signal (Shackleton, 1987). Thus, when interpreting $\delta^{18}O$ changes on glacial-interglacial time scales the effect of ice volume, salinity, and temperature must be considered independently. For example, during glaciations ice volume will result in isotopically enriched waters globally because isotopically depleted water is permanently stored in the form of ice. The increased storage of fresh water, in the form of ice, will serve to make the whole ocean more saline. Finally, lower global temperatures will reduce the energy for evaporation and precipitation resulting in localized changes in salinity. All three of these effects are essential in the interpretation of the local $\delta^{18}O$ of seawater on glacial interglacial timescales.

1.4 Glacial Oceanography of the mid-latitude South Pacific Ocean

During the LGM Atlantic Meridional Overturning Circulation was weaker than it is in the modern era (e.g. McManus et al. 2004; Shakun et al., 2012). Weakened overturning circulation and reduced upwelling in the Southern Ocean (Anderson et al., 2009) contributed to the lower exchange between deep waters and the atmosphere. The reduced exchange caused

Figure 1.4

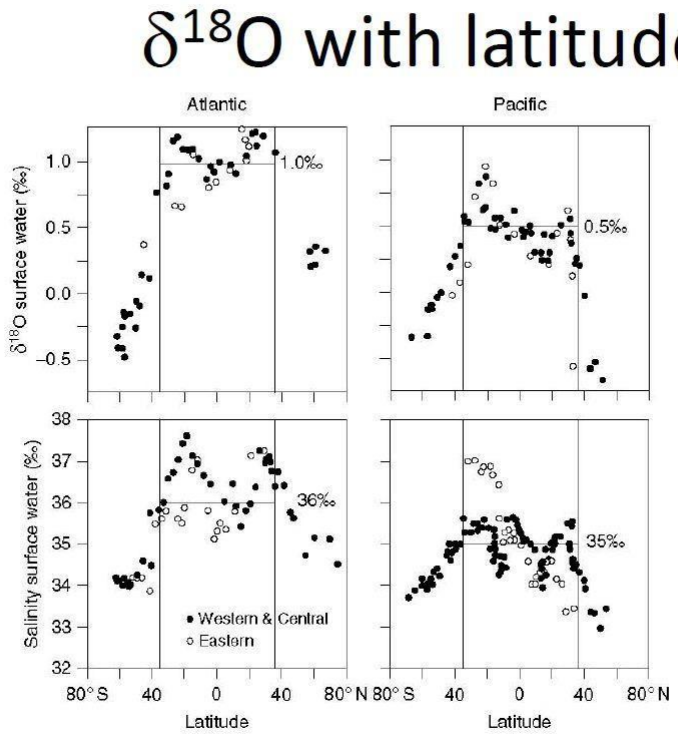

Figure 1.4| The relation between $\delta^{18}O$ (top two graphs) and salinity (bottom two graphs) and latitude of the surface waters of the Atlantic and Pacific Oceans. Variations with respect to latitude are similar for these two indicating that the rain water that dilutes at high latitudes is highly dependent in $\delta^{18}O$. Redrawn from Broecker (2002).

(Figure 5.12 from Emerson and Hedges, 2008)

the deep ocean to accumulate depleted $\delta^{13}C$ due to older water masses inhabiting the abyssal ocean (e.g. Sikes et al., 2000; Curry and Oppo, 2005; Skinner, 2010). The weakening of the southern hemisphere westerlies caused reduced upwelling of the deep Southern Ocean water masses and is hypothesized to have resulted in a northward shift in their mean position (Toggweiler, 1999). Sea surface temperature (SST) reconstructions indicate that during the LGM the STF was shifted 2-3^{o} north of its current position south of Australia, pressing up against Tasmania (Sikes et al. 2009). Studies from the Indian Ocean have also shown a northward migration of the STF (Wells and Connell, 1997; Weaver et al. 1998; Nees et al., 199; Barrows et al., 2000; Schafer et al., 2005; Hayward et al., 2008). The northward shift of the STF points to an increase in the surface area of the southern ocean, the formation region of SAMW and AAIW. On the eastern side of New Zealand it has been shown that cooler subantarctic surfaces waters penetrated as far north as Hawks Bay (Carter et al., 2008; Pahnke and Sachs, 2006) despite the bathymetrically fixed position of the STF. To the west of New Zealand, surface temperatures decrease, indicating that the STF may have shifted further to the north by ~3° (Hayward et al., 2012). The southward advection of subtropical waters into the Bay of Plenty also may have been less owing to the weakened influence of the EAC (Bostock et al., 2004) that diminished subtropical surface water flow across the Tasman Sea into the East Auckland Current and Bay of Plenty. These studies suggest that glacial circulation in the New Zealand region was different from modern.

1.5 Early Deglacial Oceanography of the mid-latitude South Pacific (19-14.5 kyr BP)

Deglacial warming in the southern hemisphere began ~19.5 kyr BP leading northern hemisphere warming by roughly two thousand years (Blunier et al., 1998). Causes for the

earlier onset of the deglaciation in the Southern Hemisphere are still being debated, however, *Shakun et al.* (2012) suggest that the mechanism responsible for the deglacial onset starts with a rise in boreal summer insolation causing high latitude northern hemisphere warming at 19 kyr BP (Alley et al., 2000). At this time, the rise in temperature reduced AMOC circulation by increasing the fresh water forcing at high northern latitudes (Clark et al., 2009). *Shakun et al.* (2012) suggest that the transfer of heat from the southern to northern hemisphere via AMOC, commonly referred to as the bi-polar see saw, was reduced causing the southern hemisphere to warm. *Huybers and Denton* (2008) challenge the hypothesis that northern hemisphere changes are responsible for southern hemisphere warming suggesting there is no well-defined mechanism for the changes in northern hemisphere summer to drive changes in the southern hemisphere. Instead they use paleo insolation models to exam how seasonal changes in the high latitude southern hemisphere may have resulted in the warming. *Huybers and Denton* (2008) show that while the intensity of glacial austral summers weren't at their peak, the length of summer was, linking local seasonal changes to southern hemisphere warming. This agrees with *Laepple and Lohmann* (2010) suggestion that local seasonal changes are likely the driving influence of southern hemisphere warming. Moreover, *Huybers and Denton* (2008) illustrate high latitude austral summer length changes in phase with high latitude boreal summer intensity, thus explaining the misleading high correlation between southern hemisphere temperature records and northern hemisphere insolation. Therefore, local insolation is a key variable in the explanation of deglacial warming.

As the deglaciation progressed (17.5-14.1 kyr BP) global temperatures warmed concurrently with a rise in atmospheric CO_2 (Shakun et al. 2012). Global climate models

suggest that a rise in global temperatures would cause an intensification and subsequent poleward shift of the southern hemisphere westerlies (Russell et al., 2006). Evidence of increased Southern Ocean upwelling during the early deglaciation (17.5-14.1 kyr BP; Anderson et al., 2009) supports a deglacial wind shift (Toggweiler et al., 2006) and is coincident with a $\delta^{13}C$ minimum across much of the Southern Ocean at ~15 kyr BP (e.g., Carter et al., 2008; Pahnke and Zahn, 2005; Spero and Lea, 2002; Ninnemann and Charles, 1997). Carbon isotopic minima are hypothesized to be a result Southern Ocean ventilation of depleted of $\delta^{13}C$ waters transmitted into the source region of AAIW and SAMW (Spero and Lea, 2002; Ninnemann and Charles, 1997). However, the $\delta^{13}C$ minima widely seen in Southern Ocean sites, are delayed by as much as 5kyr relative to the minimum seen at the southwest Pacific subtropical sites (Anderson et al., 2009; Carter et al., 2008; Bostock et al. 2004; Pahnke and Zahn, 2005; Spero and Lea, 2002). The non-contemporaneous nature of the carbon isotope minima may be an indication that the early carbon isotope minimum (Carter et al., 2008) is decoupled from the 15 kyr BP isotopic minimum (Spero et al., 2002).

As the deglaciation progressed, southern hemisphere temperatures and atmospheric CO_2 continued to rise plateauing for 1.7 kyr (Monnin et al., 2001), beginning 14.1 kyr BP, known as the Antarctic Cold Reversal (ACR; Jouzel et al., 1987a; Jouzel et al., 2001; Blunier and Brook, 2001). The ACR was accompanied by a weakening of Southern Ocean upwelling (Anderson et al., 2009) likely owing to the northward migration of the southern westerly winds (Toggweiler et al., 2006; Russell et al., 2006). During the ACR, surface ocean $\delta^{13}C$ values in the subantarctic Southwest Pacific Ocean begin a phase of enrichment that persisted into the Holocene (Carter et al., 2008; Pahnke and Zahn, 2005; Spero and Lea, 2002). Further north, in

the Australia region of the subtropical Pacific, a $\delta^{13}C$ minimum after the onset of the ACR coincided with the reinvigoration of the East Australian Current, indicating a change in the source water formation region of Australian surface waters (Bostock et al., 2004). At the end of the ACR (12.1 kyr BP), Southern Ocean upwelling resumed (Anderson et al., 2009) marking a further southward migration of the southern hemisphere westerlies (Toggweiler et al., 2006). The resumption of the Southern Ocean upwelling after the ACR is concurrent with a second phase of deglacial warming and CO_2 rise (Blunier and Brook, 2001; Monnin et al., 2001; Anderson et al., 2009). Unlike the early deglacial Southern Ocean upwelling pulse, the post ACR pulse is not concurrent with a depletion in southwest Pacific Ocean surface $\delta^{13}C$ (Carter et al., 2008; Pahnke and Zahn, 2003; Bostock et al., 2004; Spero and Lea, 2002, this study). The dissimilarity of this phase to the early deglacial upwelling pulse suggests that by the end of the ACR the Southwest Pacific Ocean circulation had already gone through its most drastic changes and was already approaching modern circulatory conditions.

1.6 Importance of this study

One goal of this study is to assess how local seasonal insolation relates to the SSTs in the Bay of Plenty, New Zealand (**Figure 1.5**) since the LGM. This will be done through the examination of foraminiferal Mg/Ca and alkenones as proxy for SST. In the reconstruction of sea surface temperature the validity of the *Laepple and Lohmann* (2009) seasonal insolation hypothesis will be assessed alongside the interpretation of seasonal SST records. The treatment of Bay of Plenty SST reconstructions will then be put in a regional context through the comparison with Mg/Ca and alkenone records from nearby sites. This regional analysis will focus on what the proxy evidence suggests about seasonal deglacial temperature changes in the New Zealand region.

Figure 1.5

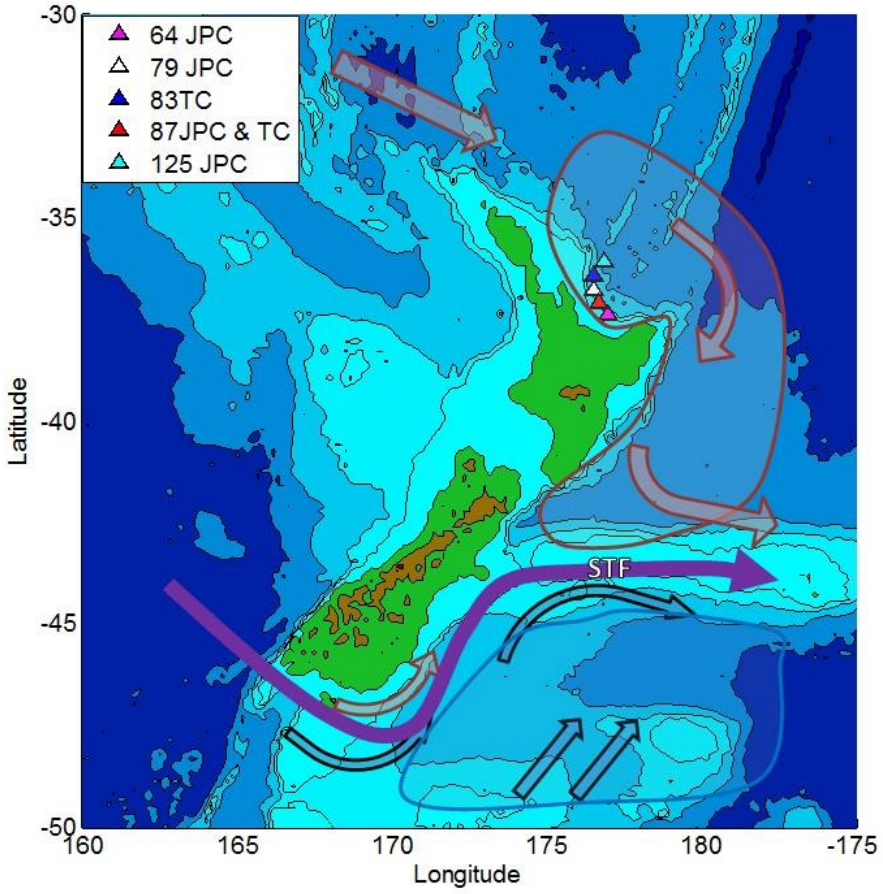

Figure 1.5| Bathymetric map of New Zealand. Our five coring locations are located to the north of the North Island of New Zealand in the Bay of Plenty: RR0503-JPC64 (37° 25.34′ S, 177° 00.41′ E; 651 m; pink triangle), RR0503-JPC79 (36°57.52’ S, 176°35.57; 1165 m; red triangle), RR0503-JPC/TC83 (36°44.25’S, 176°38.39’E; 1627m; white triangle), RR0503-JPC/TC87 (37°15.81’S, 176°39.86’E; 663m; blue triangle), RR0503-JPC125 (36°11.9’S. 176°53.35’E; 2,541m, cyan triangle). Modern surface conditions have subtropical flow (red) sourced from lower latitudes into the Bay of Plenty. The subtropical front (STF; purple) marks the convergence zone where subtropical waters meet subantarctic water (blue) sourced from higher latitudes in the Southern Ocean.

This study also presents and analysis of stable isotopic evidence from the Bay of Plenty to acquire a greater understanding how the oceanography of the New Zealand region changed throughout the transition from the LGM into the Holocene. The $\delta^{18}O_{SW}$ of surface ocean water is reconstructed from planktonic foraminifera $\delta^{18}O$ that is corrected for both deglacial ice volume changes (Peltier and Fairbanks, 2006) and local SST changes. $\delta^{18}O_{SW}$ interpretations can be used as indicators of salinity and source latitude. These are augmented $\delta^{13}C$ reconstructions based on foraminifera to get a qualitative reconstruction of shallow subsurface water displacement from the source location. The combined interpretation of $\delta^{13}C$ and $\delta^{18}O_{sw}$, leads to a more thorough determination of the causes of the post-LGM $\delta^{13}C$ minima. The goal of the isotope analysis is to better understand whether isotopic depletions in the southwest Pacific Ocean were a result of source water and circulatory changes, deep ocean ventilation, or a combination of both processes.

An additional aim of this study focuses on how these changes impacted seasonal SSTs throughout the New Zealand region. In combination, the two sections of this thesis focus on the evolution of temperatures and major source water changes in the New Zealand region from the LGM to the Holocene. Independently these two sections provide valuable insight on how southern ocean circulation and deglacial warming manifested through the mid-latitude southern hemisphere. The use of multiple proxies allows for a more comprehensive understanding of how deglacial SST changes in the New Zealand region are interwoven with major changes in southern hemisphere ocean circulation.

Chapter 2

2. Comparison of Alkenones and Mg/Ca as Seasonal Rectifiers

2.1 Introduction

It is becoming widely recognized that the use of multiple proxies can lead to a greater understanding of the climate in a region than the use of a single technique. Multi-proxy comparisons have expanded from correlating general agreement among proxies to infer a broad regional climate to interpreting finer scale differences among proxies to achieve an improved, detailed understanding of paleoceanographic conditions (Mix et al., 2000; Bard, 2001; Mix et al., 2001; Sikes et al., 2009). In this study, two widely used proxies for sea surface temperature (SST), the Mg/Ca ratio in foraminifera (e.g., Mashiotta et al., 1999; Rosenthal et al. 2000) and the $U^{K'}_{37}$ index of alkenones (e.g., Prahl et al. 1988; Sikes and Volkman, 1993), were applied to the same core taken from the New Zealand region (**Figure 2.1**). These proxy records have been used independently in numerous studies to quantify glacial interglacial SST changes in the New Zealand region (Pahnke et al., 2003; Pahnke and Zahn, 2005; Pahnke and Sachs, 2006; Sikes et al., 2002, Sikes et al., 2009, Samson et al., 2005). However, when foraminifera and alkenone temperature reconstructions from the same or nearby cores are compared, there are often differences between the records (Sikes and Keigwin, 1994; Chapman et al., 1996; Mix et al., 2000; Sikes et al., 2002; Pahnke and Sachs 2006; Sikes et al., 2009). The disagreement may be a result of non-thermal influences on the proxies such as seasonal growth preference (Sikes et al. 2009) or nutrient stress (Prahl et al., 2003; Sikes et al., 2005) biasing the proxy and compromising the ability to fully reconstruct past climate.

Figure 2.1

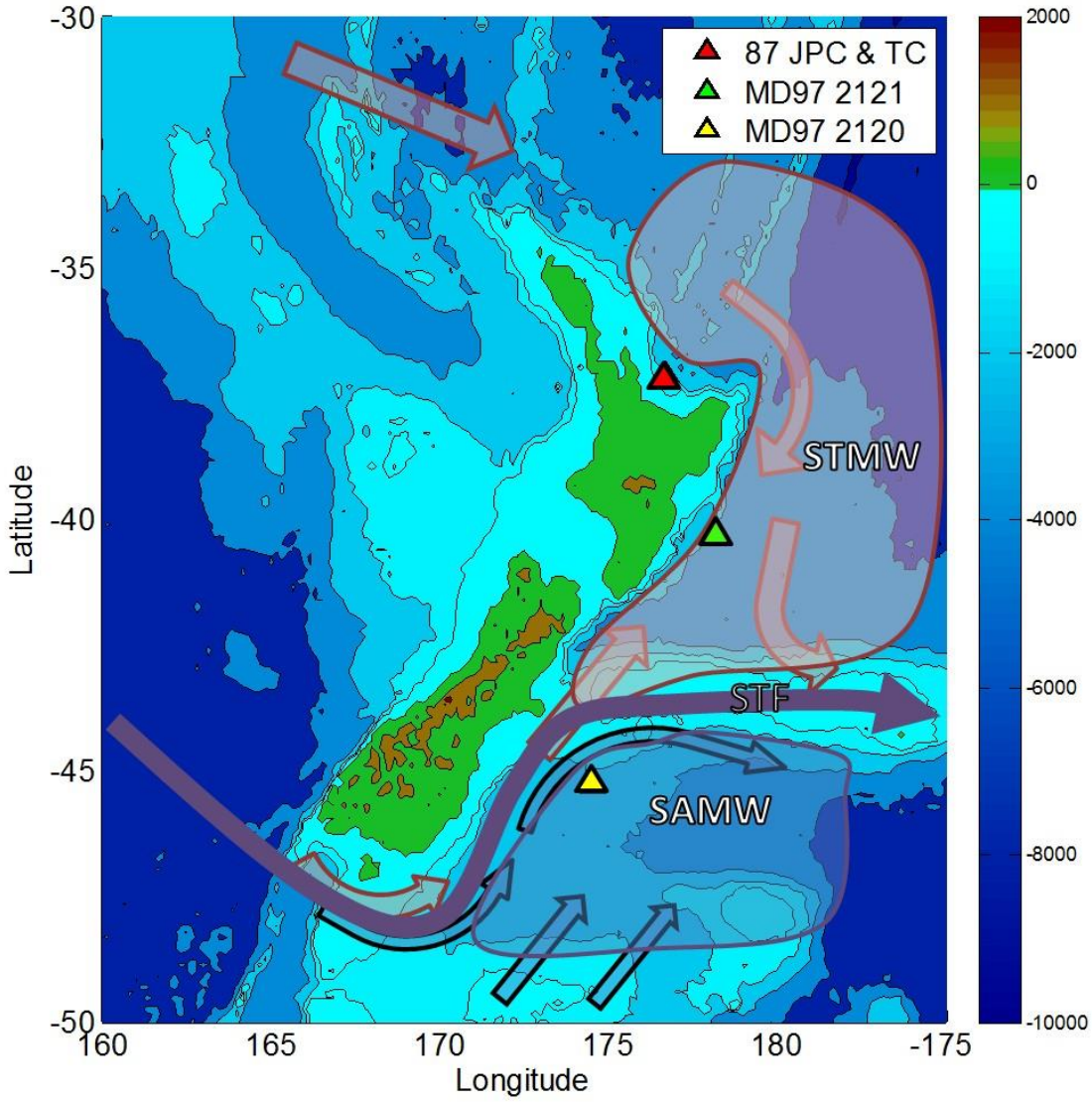

Figure 2.1| A bathymetric map of the New Zealand region. The red triangle marks the location of cores 87 JPC and TC from which alkenone and Mg/Ca data was taken in this study. The Hawks Bay core published by Carter et al., 2008 (marked in green) and south Chatham Rise core published by Pahnke and Zahn, 2005 (marked in yellow) are also shown. Today the subtropical front (STF; purple arrow) separates subtropical mode water (STMW; red) and subantarctic mode water (SAMW; blue) and sits within this transect of cores.

Around New Zealand, sediment trap studies have illustrated key offsets in the timing of the peak alkenone and foraminifera flux into the sediment. Maximum foraminifera export occurs in the early austral spring while the maximum export production of alkenones does not occur until late austral spring to early summer (King and Howard, 2004; King and Howard, 2005, Sikes et al 2005). In the sediments, these modern seasonal growth offsets produce temperature disparities between these proxies as they can only record the conditions from the time in which they grew (e.g., Sikes et al. 2009). Thus, the hypothesis that seasonal growth causes inherent differences and rectification of the seasonal cycle among proxy records (Huybers and Wunsch, 2003), implies that down core alkenone SST reconstructions are biased towards the conditions of early summer while foraminifera reconstructions are biased towards spring, assuming that the seasonality or bias does not change on glacial interglacial time scales. Therefore, the intra-core temperature offsets in the Austro-New Zealand sector can arise when foraminifera proxies that record (Huybers and Wunsch, 2003) spring whereas alkenones are recorders for summer temperatures; the seasonality of the proxy is the driving factor of the disparity.

Seasonal temperature changes have been examined on glacial-interglacial timescales through the use of paleo-insolation modeling. Recent modeling work compared modern temperature data and an incoming solar radiation model output to better understand how local temperature responds to that radiation (*Laepple and Lohmann*, 2009). The response of daily temperature to daily insolation throughout the year can be either linear or nonlinear. In the New Zealand region, the response of temperature to insolation is linear throughout the year with approximately a sixty day offset in insolation and temperature extremes (personal communication T. Laepple, 2012). The modern relationship between local insolation and

temperature during the year can be extrapolated to past insolation changes, using models of insolation based on Milankovitch forcings to provide a basis for evaluating the seasonal temperature evolution on glacial-interglacial time scales (*Laepple and Lohmann*, 2009). Other modeling studies suggest a proxy that responds nonlinearly to the annual cycle, due to growth during a specific season, may reflect properties of that specific season on glacial-interglacial time scales (*Huybers and Wunsch* 2003). Earth's precession cycle is instrumental in determining seasonal disequilibrium in insolation forcing, while having no impact on total annual insolation. *Huybers and Wunsch* (2003) use a model of paleo insolation to illustrate that seasonal rectification can be seen by the expression of a high energy band at 20 kyr in the frequency spectra of a seasonal rectifier, provided the record is long enough to have multiple precession cycles. This rectification hypothesis lends itself to interpreting the alkenone and foraminifera records in this study as proxies for late austral spring/early austral summer and early spring respectively. If the modern seasonal response of temperature to insolation holds for glacial-interglacial time scales, then proxy records such as foraminifera and alkenones are rectifiers for their respective growth season through time and will follow the paleo-insolation model for their respective season. Models of paleo-insolation make it possible to assess the how well New Zealand SST proxies actually compare to the progression of seasonal insolation since the LGM.

The alkenone record at site 87JPC/87TC is a northern compliment to high resolution cores to the east of New Zealand which demonstrate glacial-interglacial variability in SST. The available cores with summer SST span from the southeast Chatham Rise, south of the subtropical front (STF), to the subtropical water masses of the Bay of Plenty (**Figure 2.1**). Northward shifts of the STF during the glaciation occurred in other parts of the Southern Ocean

including the Indian Ocean (Prell et. al., 1980), the Tasmanian sector (Sikes et al., 2009), the western Pacific sector (Luer et al., 2008), and the Atlantic sector (Hays et al., 1976). However, east of New Zealand it has been shown that the position of the STF in the last glacial maximum (LGM) was similar to that of today (Nelson et al. 1993; Carter et al. 2000; Sikes et al., 2002). Today the mean surface expression of the STF appears to flip-flop seasonally from the northern Chatham Rise to the southern Chatham Rise (Belkin and Gordon, 1994). In the past, the anchoring of the subtropical front along the Rise, kept waters north of the Chatham Rise including the Bay of Plenty subject to subtropical conditions through the glaciation and deglaciation. The south Chatham Rise proxies record subantarctic conditions throughout the entire period with possible frontal influences being meso-scale changes in the surface expression of the Front affecting the core.

During the deglaciation wind and current changes in the region may have impacted regional SST patterns. Modeling studies indicate that the circumpolar southern hemisphere westerlies may have shifted their position during the deglacial transition affecting the subantarctic (Toggweiler, 1999; Russell et al., 2006; Toggweiler et al., 2006) Southern Ocean upwelling, which is currently wind-driven. A deglacial shift of the westerlies is supported by evidence of major increases centered on the early deglaciation (17-14.1 kyr BP) and early Holocene (12.4-8.0 kyr BP), with a pause during the Antarctic Cold Reversal (ACR, 12.4-14.1 kyr BP; Anderson et al., 2009). During the glaciation, foraminifera proxy evidence points to a weakened East Australia Current in subtropical waters near Australia (Bostock et al., 2004). Today, the EAC supplies warm subtropical waters to the East Auckland Current which feeds directly into the Bay of Plenty (**Figure 2.2**). While the EAC is not a direct contributor to the surface waters of the Bay of Plenty a decrease in the regional influence of the EAC may have

Figure 2.2

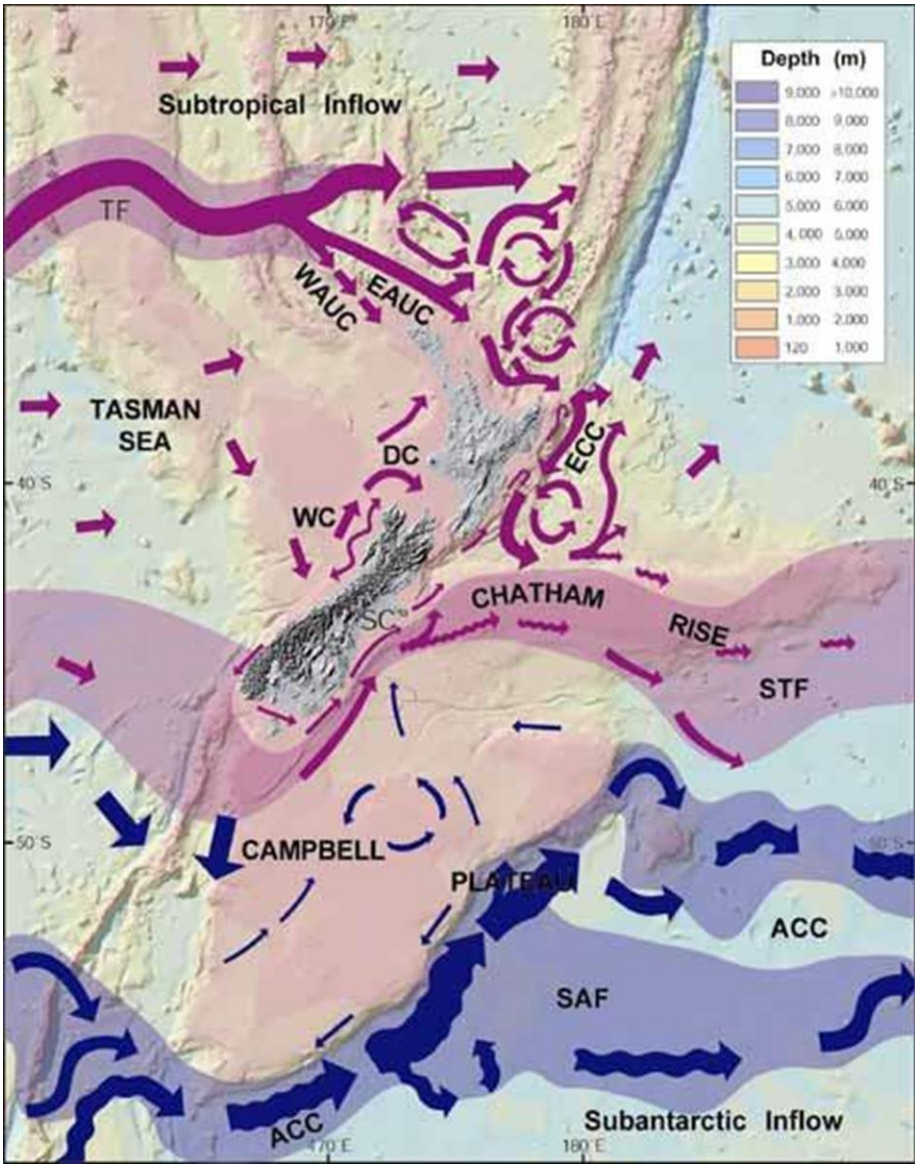

Figure 2.2| New Zealand Circulation. Arrows Summarize the characteristics of the surface current systems. Oceanic fronts and main water masses include Subtropical Water [STW]; Subtropical Front [STF]; Subantarctic Water [SAW]; Subantarctic Front [SAF]; Antarctic Circumpolar Current [ACC], the northern limit of which is defined by the SAF; Circumpolar Surface Water [CSW]. Currents are annotated as follows: East Australian Current [EAC]; East Auckland Current [EAUC]; North Cape Eddy [NCE]; East Cape Eddy [ECE]; East Cape Current [ECC]; Wairarapa Eddy [WE]; Southland Current [SC]; Southland Front [SF]; Westland Current [WC], and D'Urville Current [DC]; Tasman Front [TF].

(Taken from Carter, et al. 1998)

had an impact in the surface waters in the subtropics. A latitudinal transect of SST records makes it possible to investigate how Southern Ocean versus subtropical Pacific Ocean variations influenced conditions in the New Zealand sector of the southwest Pacific Ocean.

In this study we compare two proxies, an alkenone-based SST paleoclimate record and a Mg/Ca based SST paleoclimate record taken from a single sediment core in the Bay of Plenty north of New Zealand. The sea surface temperature records are compared to a paleo-insolation model with daily resolution (Huybers, 2006) to assess whether or not these paleo proxies track seasonal paleo-insolation. The new alkenone record in this study completes a latitudinal transect of alkenone records in the region permitting comparison of this alkenone SST record to the records from core MD97-2121 (40°22.80 S, 177°59.40 E; Pahnke and Sachs, 2006) in Hawkes Bay north of the STF and MD97-2120 (45°32.06 S, 174°55.85 E; *Pahnke* and Zahn, 2005) located south of the Chatham Rise south of the STF (**Figure 2.1**). These cores transect the area from the subtropical surface waters of the southwest Pacific north of New Zealand to the subantarctic surface waters of the Southern Ocean allowing a comparison of the response of both subtropical and subantarctic surface waters in the region across the deglaciation. Mg/Ca analyses of *G. bulloides* were conducted in one other core, MD97-2120 (Pahnke et al., 2003) allowing a seasonal comparison of SSTs for both the Southern Ocean and the Bay of Plenty. This study compares the deglacial SST response north and south of the STF across these seasons to examine seasonal changes in the deglaciation.

2.2 Methods

2.2.1 Mg/Ca Reconstruction

Sample Preparation

Five cc samples were taken from cores 87 JPC and 87TC from a 1cm thick quarter section of the core at an interval of every 4cm. Sediment samples were dried and then washed and wet sieved at 63µm to remove fine clays. The size fraction >63µm was then sieved into four bins, <150µm, 150-250µm, 250-350µm, and >350µm. Specimens of *G. bulloides* were picked from the size fraction between 350µm and 250 µm, collecting enough sample to reach a critical mass of 400-500µg; about 25-35 foraminifera per sample. Foraminifera were then brushed onto 2"x2" glass plates, crushed enough to open chambers, and subsequently stored in acid cleaned 0.5 mL polypropylene microcentrifuge vials following the methods of *Rosenthal et al.* (1997).

After all samples were picked and chambers were broken open, each sample was cleaned by the following process: First, fine clays were removed by filling vials with distilled de-ionized water (ddH_2O), placing vials in an ultrasonic bath, and then siphoning off liquid three times. This process was then repeated twice replacing ddH_2O with methanol. Once small clays were removed, 100µL of a reducing agent: 750 mL of anhydrous hydrazine, 10mL of ammonium hydroxide, and 10mL of a citric acid/ammonium solution, was added to each sample, ultrasonicated, then placed in a hot bath for 30 minutes, and siphoned out in order to remove metal oxides from calcite tests. Next, 250µL of an oxidizing agent consisting of 30mL of 0.1 N NaOH and 100µL H_2O_2 was added to each sample, ultrasonicated, placed in a hot water bath for 5 minutes, then siphoned off and rinsed with ddH_20 in order to remove organic matter. Samples were then transferred into acid cleaned 0.5 mL polypropylene microcentrifuge vials and briefly acid leached with 250 µL of .001 N HNO_3 to remove carbonates. After acid

leaching, samples were rinsed with ddH_2O, and the remaining liquid was siphoned off and samples were then refrigerated until running on the Inter-coupled Plasma Mass Spectrometer (ICP-MS). All Mg/Ca foraminifera analyses were performed at Rutgers University at the Institute of Marine and Coastal Sciences.

Before analysis on the ICP-MS samples were dissolved in 100µL of 0.065 N HNO_3, centrifuged to separate out any precipitates, and the liquid was subsequently transferred a final time into new acid cleaned 0.5 mL polypropylene microcentrifuge vials. Prior to the sample run, 3 consistency standards and a matrix of 6 differing concentrations of a combination of [Ca], spiked gravimetric standards (SGS), and 0.5 N HNO3, were run to test for sensitivity. Following the matrix, a blank, and a SGS were run followed by 5 samples. After every five samples a SGS and blank were run to provide a reference for machine sensitivity drift, normally caused by oxide precipitation along intake cones. After each run, a final sequence of 3 consistency standards, were re-run in order to check the consistency of the machine sensitivity.

Once all samples were analyzed, each was checked for outliers in Mg/Ca ratio and anomalously high metal concentrations. Any outliers with unrealistic metal concentrations, possibly due to machine error or contamination, are noted in Table 2.1 and are not included in the final data analysis.

Mg/Ca Conversion to SST

Early studies involving comparison of the Mg/Ca ratio in calcite shells to ocean temperature illustrate the existence of strong correlations between Mg incorporation into calcite shells and water temperature (Rosenthal and Boyle 1993) and that the incorporation of Mg/Ca into calcite shells is dependent both on temperature and biological factors (Rosenthal et al.,

1997). Thus, different calibrations must be used to convert the Mg/Ca of different species of foraminifera to temperature. The calibration equation of calibration equation of *Mashiotta et al.,* (1999; equation 2.1) is specifically calibrated for *G. bulloides* living in the southwest Pacific Ocean. This calibration also allows for the direct comparison of subtropical Bay of Plenty *G.* bulloides to the Mg/Ca SST results of *Pahnke et al.,* (2003).

This calibration yields a 1 σ uncertainty of +/- 0.8 ºC with a 95% confidence interval which

$$Mg/Ca = 0.474e^{0.107T} \quad (2.1)$$

varies along the regression from +/-0.3 at 16ºC to +/-0.6 ºC at both 10 ºC and 25ºC (*Mashiotta et al.,* 1999).

2.2.2 Alkenone Reconstruction

Sample Preparation

Core 87 JPC and the corresponding trigger core, 87 TC were sampled at 2 cm intervals in the same manner as for foraminiferal samples. Sediments were oven dried at 30°C then homogenized using a mortar and pestle and loaded into 22 ml stainless steel extraction cells of a Dionex 2000 Accelerated Solvent Extractor (ASE). Nonadecanone was added to each as an internal reference standard. Samples were extracted using a 1:4 mixture of methanol: dichloromethane with the ASE programmed to 150ºC and 2000 psi. Extracts were concentrated via evaporation under vacuum in a Rapidvap. Samples were subsequently analyzed by capillary Gas Chromatography with a flame ionization detector (FID), using a Shimadzu GC-17A fitted with a 30 m JW Scientific DB-5 (0.32mm i.d.). Samples were injected on-column using hydrogen as a carrier gas and the temperature program was 50–150°C at 30°C min^{-1} and 150–325°C at 3°C min^{-1} which ensured good separation of all

major constituents. Compounds were integrated using Shimadzu-provided software. C_{37} alkenone analysis for $U^{K'}_{37}$SST estimation were performed at Rutgers University.

$U^{k'}_{37}$ Paleothermometry

The long chained alkenones synthesized by *Emiliania huxleyi* have been shown to have a linear relation to water temperature across a wide range of temperatures (*Prahl et al.* 1988; *Muller et al.* 1988; *Sikes and Volkman* 1993). Although *Sikes and Volkman* (1993) calibrated this ratio Antarctic and subantarctic water masses, further studies in the New Zealand region (*Sikes et al.* 2002 and *Sikes et al.* 2005) have demonstrate that the calibration that best recreates modern SST in subtropical waters of the Bay of Plenty is the relationship of *Prahl et al.* (1988)

and thus this calibration is used to convert Bay of Plenty U^{37} to SST.

$$U^{K'}_{37} = 0.034T + 0.039$$

2.3 Results

2.3.1 Site 87 Core Stratigraphy

87JPC

The age model for the Bay of Plenty core RR0503-JPC-87 (36°44.25' S 176°38.39' E; 663m depth) was developed by Aurora Elmore for use in another study *Elmore et al*., (in prep) and was made available for this coordinating study. Stratigraphy was based on a combination of tie points from tephra chronology (Shane et al. 2006; Lowe et al. 2008) and benthic $\delta^{18}O$ correlations in the RR0503 cores (**Figure 2.3**). The benthic $\delta^{18}O$ data at the core top of this piston core was estimated to be 6.25 $\pm$ .03 thousand calendar years before present (kyr BP). A second benthic $\delta^{18}O$ stratigraphic point at 46cm depth in core provides an age of 7.27 kyr BP providing an initial sedimentation rate estimation of 7.3 cm/kyr. The presence of the boundary

Figure 2.3

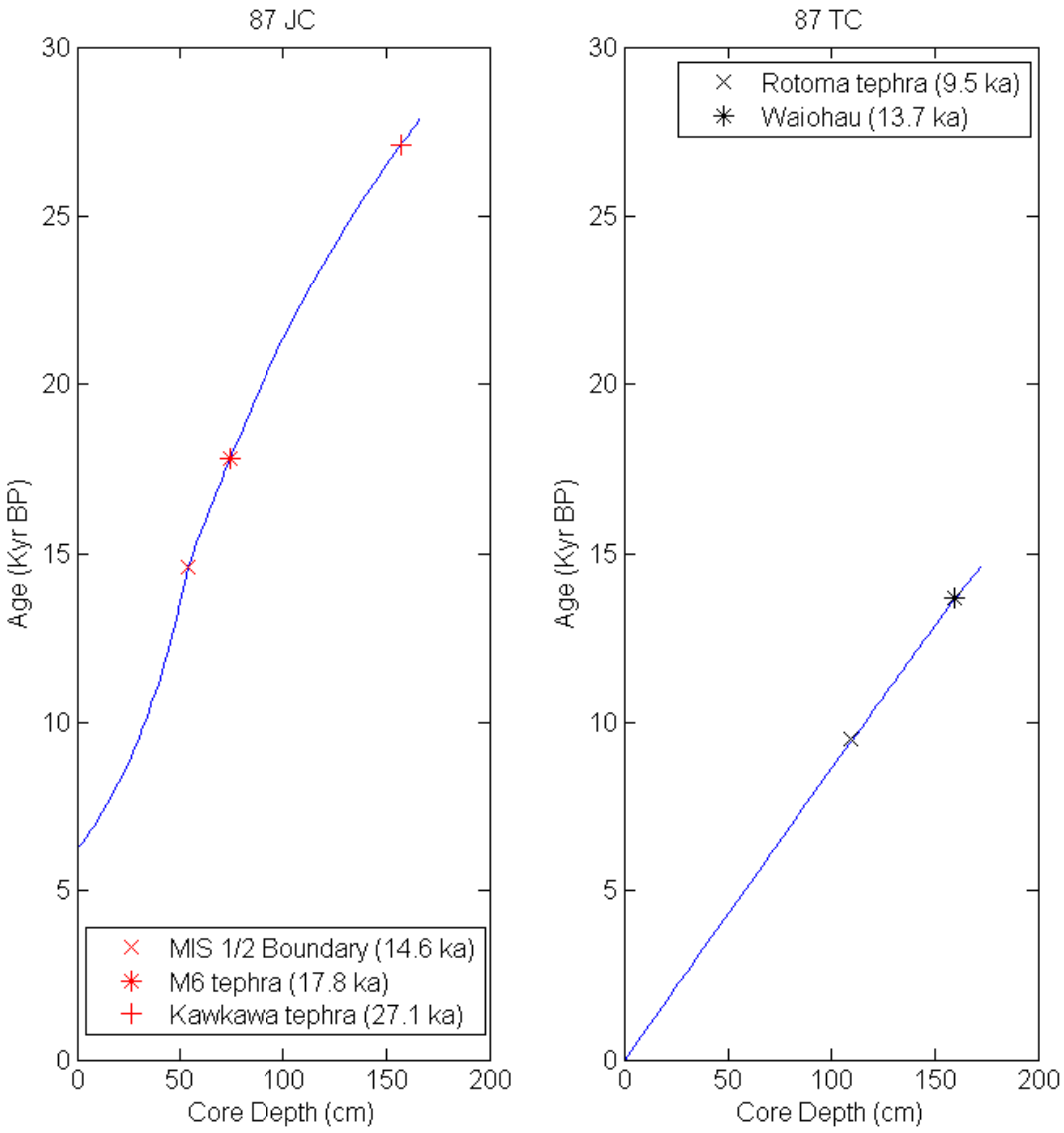

Figure 2.3| Chronology of RR0503 cores 87 TC (right) and 87 JPC (left) based of the stratigraphic interpretation of *Elmore et al.* (in prep) with age plotted on the y-axis and depth (cm) in core plotted on the x-axis. Stratigraphic tie points include the Rotoma tephra (9.5 kyr BP; black x), the Waiohau tephra (13.7 kyr BP; black star), the MIS ½ boundary (14.6 kyr BP; red x), the M6 tephra (17 17.8 kyr BP; red star), and the Kawkawa tephra (27.1 kyr BP, red plus).

between marine isotopes stages one and two (MIS 1/2; 14.6 kyr BP) at 54cm has a slight drop in sedimentation (4.0 cm/kyr) through the end of MIS 1 (Elmore in prep). The presence of the Mayor Island 6 (17.8±.03 kyr BP) Tephra and the Kawkawa Tephra (27.1±.03 kyr BP) illustrates a continuous sedimentation rate back into early deglacial times and the LGM.

87 TC

The age model for Bay of Plenty core RR0503-TC-87 (36°44.25' S 176°38.39' E; 663m depth) was similarly developed with the use of a tephra chronology. The top of the trigger core was assumed to be modern. The presence of the Rotoma Tephra (9.5±.03 kyr BP) at 110 cm and the Waiohau Tephra (13.5±.03 kyr BP) at 160 cm provide evidence of a steady sedimentation rate, of ~12cm/kyr, from the Holocene through the end of MIS 1. The presence of Mayor Island 6 tephra (17.8±.03 kyr BP) at 221 cm implies a slightly greater sedimentation rate, ~14.1cm/kyr, during early deglacial times.

Splice

The alkenone record reported in this study contains data from both core RR0503-JPC-87 and core RR0503-TC-87. In order to report down core data as a continuous timeline, the chronologies of both cores were spliced together. The presence of a layer of andesite in core JPC-87 at 34 cm and core TC-87 at 207 cm along with the aforementioned presence of the Mayor Island 6 Tephra in both cores made it possible to join the chronologies of both cores and report alkenone based SST data as a continuous chronology. For the remainder of this study all data will be reported using the above age model.

2.3.2 SST Reconstructions

Mg/Ca based SST

During the early glaciation between 26-21.3 kyr BP, the Mg/Ca based SST for the *G. bulloides* core 87 JPC averaged 13.6°C (**Figure 2.4**). LGM minimum temperatures had variability on the order of 2.5°C. At 21.3 kyr BP deglacial warming began with a rate of increase of 1°C/kyr with temperatures reaching 17.8 ºC at 16 kyr BP. Throughout this warming trend temperature data is quite variable with 20.8 kyr BP and 19.2 kyr BP spiking to 17.0°C. During the ACR, 14.1-12.4 kyr BP, there was a marked cooling and temperatures fall 1.0°C to an average of 16.2 ºC. This cooling has a temperature variability ranging from 15.2-17.1°C. The warming trend reinitiated into the Holocene, with temperatures reaching a maximum value of 18ºC at 8.6 kyr BP then leveling off in the mid-Holocene at 17.2ºC. Holocene temperatures varied between 15.1-18.0°C.

Alkenone Based SST

During the last glaciation the few available alkenone SST data were highly variable between 27-20 kyr BP (**Figure 2.5**). At the start of the record ~27 kyr BP temperatures were 16°C. SST then peaked at 19°C between 26.5 and 26 kyr BP after which there was a minimum of 15.5°C between 24.5 and 23.5 kyr BP. Temperatures reach 18°C by 21.5 kyr BP and then fell to 16.4°C at ~20.2 kyr BP. After this interval of highly variable SSTs there was a steady warming trend of ~1°C/kyr until 16 kyr BP when temperatures reach 19°C. This warming was interrupted by a temperature plateau with a mean value of 19.4ºC between 16.0 and 12.4 kyr BP; that largely coincided with the ACR. After this temperatures peaked at 21.6°C at 10 kyr BP and subsequently stabilized at an average value of 20.4ºC until 6 kyr BP. After this early-

Figure 2.4

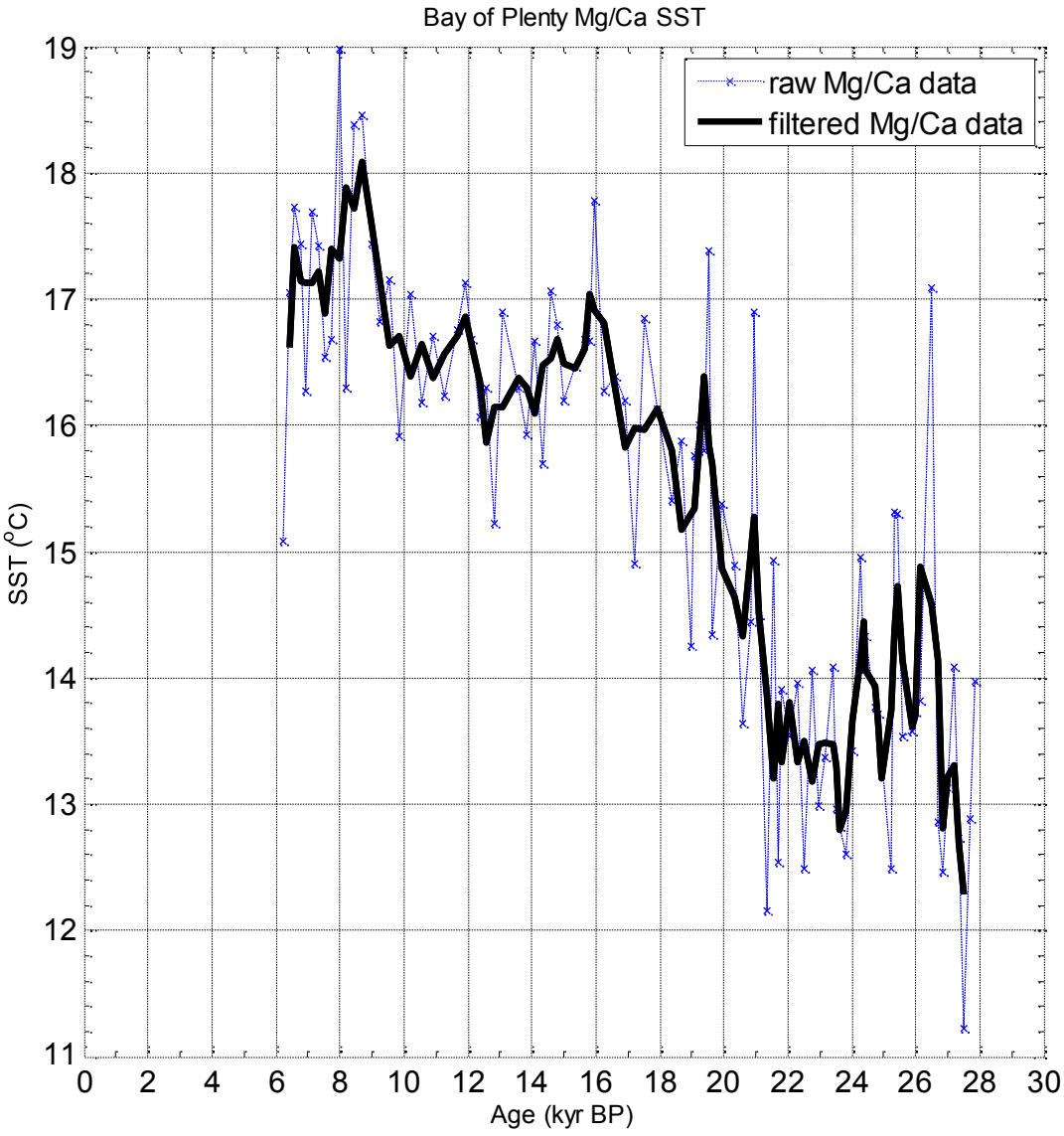

Figure 2.4| Mg/Ca based temperature estimates reported against age. Raw data from core 87 JPC (dotted blue line), and a 3-point running mean (solid black line). Note that the deglacial onset in this water mass appears to occur at 21.2 kyr BP and that within the filtered data there is a cooling trend between 14.1 and 12.4 kyr BP coincident with the Antarctic Cold Reversal. The glacial onset is followed by a steady rise in SST and two step changes differentiated by ~1ºC.

Figure 2.5

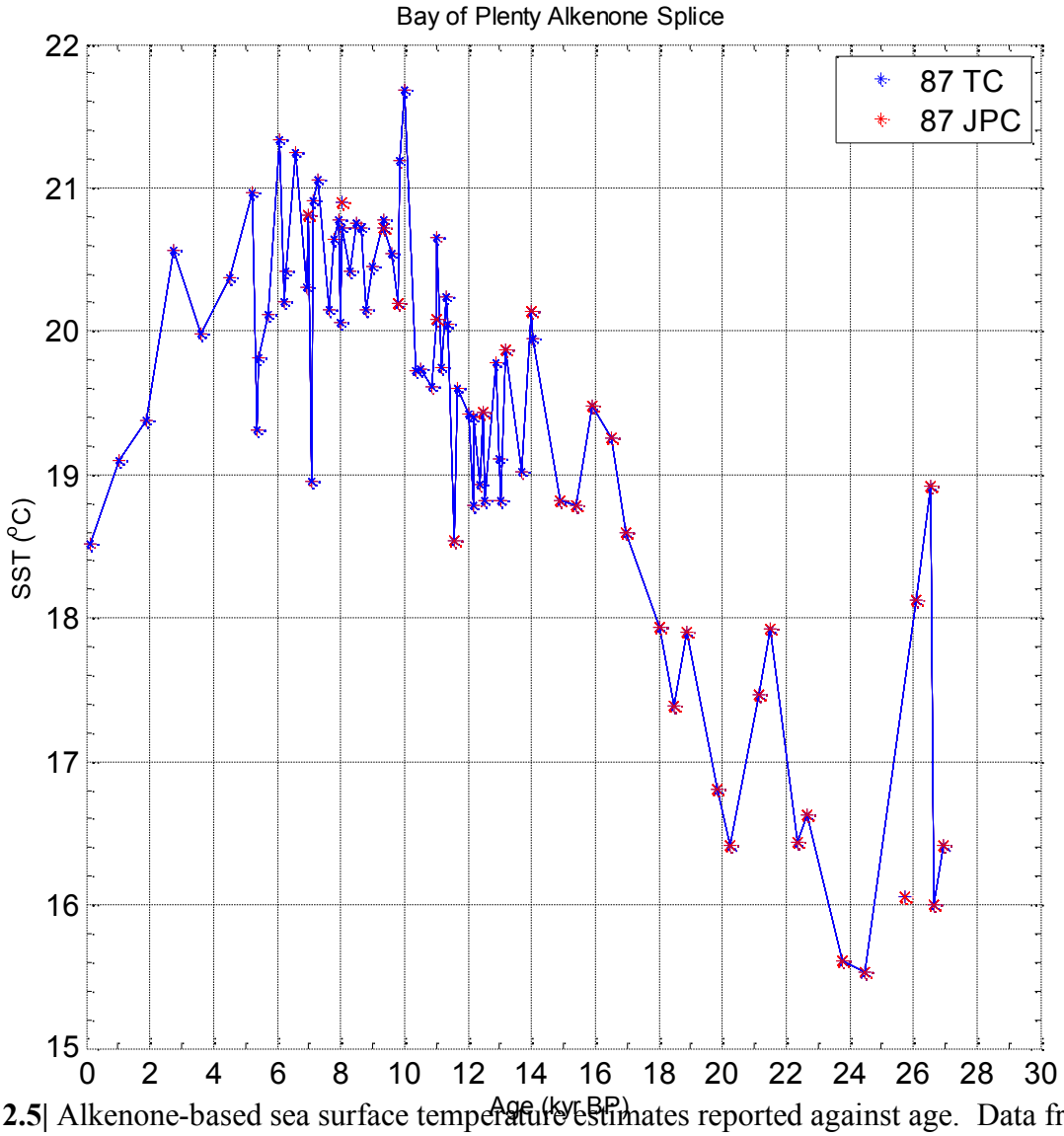

Figure 2.5| Alkenone-based sea surface temperature estimates reported against age. Data from the trigger core (87 TC; blue stars) and the piston core (87 JPC; red stars) are plotted as a continuous chronology. The reconstruction, a glacial minimum temperature occurs at 24 kyr BP and the onset of the deglaciation at 20.1 kyr BP. The transition of warming into the Holocene is fairly smooth with the exception of brief interruption of cooling between 14 and 10 kyr BP, coincident with the approximate timing of the Antarctic Cold Reversal. In the Holocene temperatures appear to reach a maximum of 22°C.

Holocene maximum, temperatures decreased at a steady rate of .4ºC/kyr until reaching 18.5°C in the modern era.

Proxy SST Comparison

To facilitate the comparison of the Mg/Ca reconstructions to the alkenones, high frequency variability in both records was removed from using a three point running mean filter through the Mg/Ca data (**Figure 2.4**). The glacial values were then binned by averaging the glacial interval 26.0 - 22.0 kyr BP, the ACR 14.1-12.4 kyr BP, the early Holocene interval 12.1-8.0 kyr BP, and Holocene values 8.0 – 6.0 kyr BP. These bins are reported as the mean value for the respective climatic period of each record (**Figure 2.6**).

Across the transition from LGM to Holocene both the alkenone and the Mg/Ca SST reconstructions show similar deglacial increases in SST, 4.1°C and 3.6°C, respectively (**Figure 2.6**). Alkenones had a mean glacial value of 16.4°C while foraminifera were 13.6°C. The glacial difference between the two proxy records was 2.8°C. During the deglaciation the alkenone and foraminifera temperatures rose at a similar rate, such that the difference between the two records was similar to the glacial offset. At the ACR, both the alkenones and foraminifera plateau with average values of 19.4 and 16.2°C respectively, making the offset between the proxies 3.2°C. Post-ACR, both proxy records increased by 0.6°C with the average offset being constant. In the early Holocene there was less than a 0.5°C average warming and a similar offset of 3.3°C between the proxy records. Throughout the entire deglaciation the offset between the two proxies remained similar given the ~1.0°C uncertainty in the estimates of both proxy records.

The Bay of Plenty record was placed in a regional context by comparing the SST reconstructions from this study with previously published high resolution SST records. Nearby

Figure 2.6

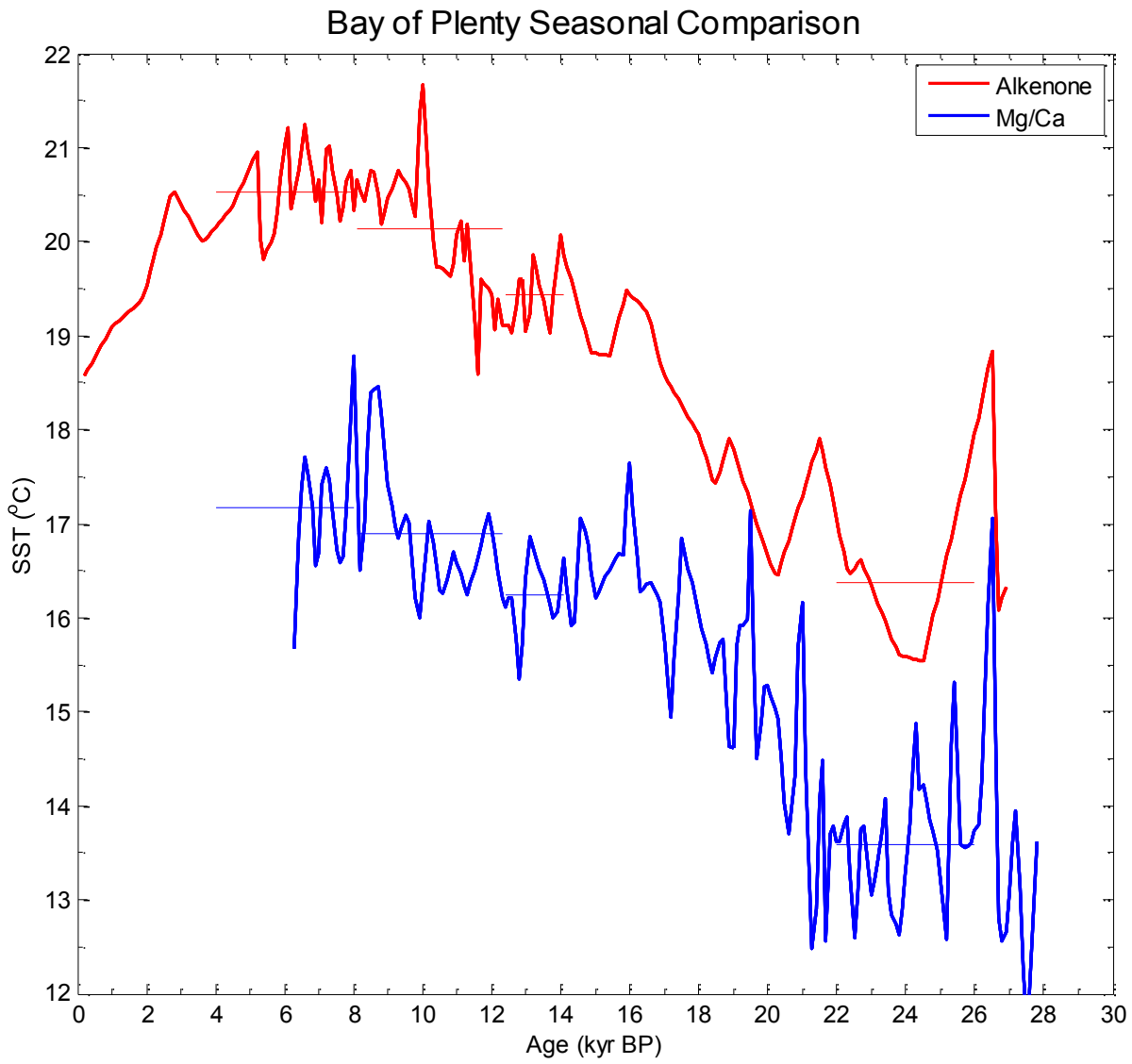

Figure 2.6| Comparison of Bay of Plenty alkenone (red) and Mg/Ca (blue) temperature reconstructions plotted to age. The solid horizontal lines indicate the average for the intervals including the Holocene, the Early Holocene, the Antarctic Cold Reversal, and the Last Glacial Maximum as described in text.

core MD97-2121 has an alkenone record (Pahnke and Sachs, 2006) Chatham Rise core MD97-2120 has both Mg/Ca and alkenone SST (Pahnke et al., 2003; Pahnke and Sachs, 2006). The comparison between alkenones (summer SST) for the two subtropical cores, Bay of Plenty and Hawkes Bay, track well with one another. In contrast, subantarctic SSTs from the south Chatham Rise core rise more rapidly than both subtropical sites the early deglaciation into the early Holocene.

Subtropical SST in core MD97-2121 rose steadily as did SST in core 87 JPC-TC through the deglacial transition with some minor variability in temperature offsets due to noise in the records (**Figure 2.7**). During the LGM MD97-2121 SST averaged 13.1°C with the deglacial onset in Hawkes Bay occurring at 18.9 kyr BP roughly 1.2 kyr later than in the Bay of Plenty. During the ACR temperatures in both subtropical cores hit a plateau. The temperatures in Hawkes Bay plateaued at 15.7°C, and subsequently rose until they stabilized at 17.0-18.0°C during the early and middle Holocene. Throughout the entire deglacial transition the latitudinal temperature difference between Hawkes Bay and the Bay of Plenty remained stable at 3.1-3.7°C.

The temperature offsets between the Bay of Plenty and subantarctic waters on the South Chatham Rise during the deglaciation were much more dynamic (**Figure 2.7**). At the LGM, mean SST on the Chatham Rise were 10.3°C and the difference between the Bay of Plenty and the south Chatham Rise was 5.8°C. As the deglaciation progressed, the temperature difference between the sites decreased by 2.3°C. By the ACR subantarctic water temperatures had rapidly risen to 14.0°C decreasing the temperature difference with the Bay of Plenty to 5.3°C. By the early Holocene, 12.1 kyr BP, subantarctic SSTs were 15.5°C reducing the temperature difference to ~4.6°C. At ~8.5 kyr BP subantarctic SST began to decline again at 2.0°C in 1.0

Figure 2.7

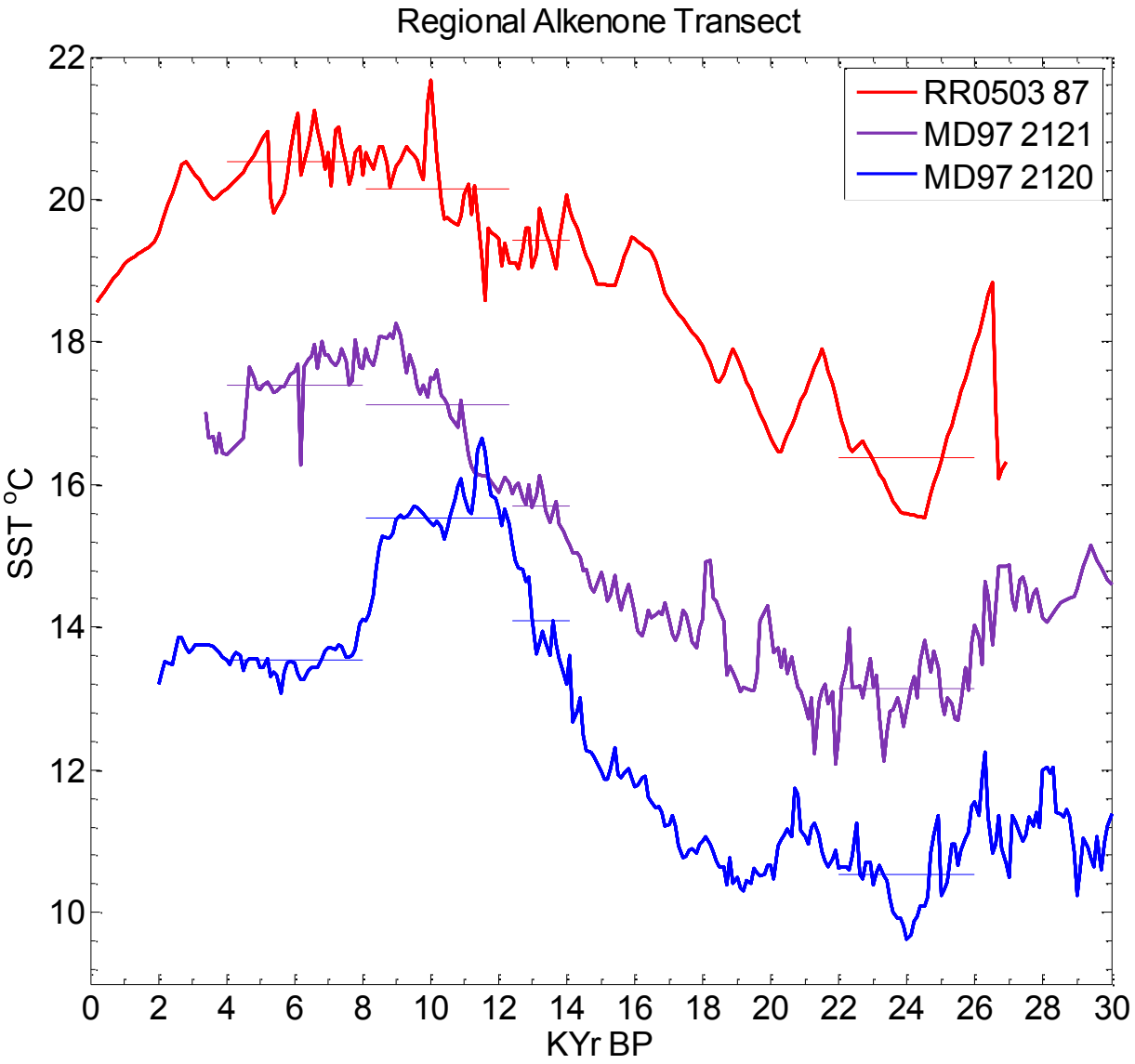

Figure 2.7| Alkenone SST reconstruction transect for the New Zealand Region. Alkenone SST from Bay of Plenty core 87 JPC and TC (red), Hawkes Bay core MD97-2121 (purple), and south Chatham Rise core MD97-2120 (blue). The average temperature values are denoted by the horizontal bars for four intervals: the LGM (26-22 kyr BP), the ACR (14.1-12.4 kyr BP), the early Holocene (12.3-8.0 kyr BP), and the mid-Holocene (8.0-6.0 kyr BP). Note that During the LGM and the mid-Holocene the differences between the cores are fairly similar but during the ACR and the early Holocene the differences between MD97-2120 and MD97-2121 are dramatically reduced. It is also apparent that the reduced differences during this interval are driven by greater temperature increase in core MD97-2120 relative to the change seen in the other two cores.

kyr, to 13.5°C throughout the mid-Holocene. The dramatic decrease at 8.5 kyr BP was not observed in either the subtropical record causing the difference between the South Chatham Rise and the Bay of Plenty to increase to 7.0°C. The deglacial temperature shift at the subantarctic site does not track well with changes in the subtropical sites.

The only previously existing Mg/Ca SST reconstruction in the region was the *G. bulloides* record from South Chatham Rise site MD97-2120 (Pahnke et al., 2003). New high resolution data in this study allows the comparison of spring SSTs north and south of the subtropical convergence that can be contrasted with the summer (alkenone) record discussed above (**Figure 2.8**). During the LGM Mg/Ca south Chatham Rise SSTs averaged 8.9°C about 4.7°C cooler than the Bay of Plenty. The onset of the deglacial warming at the subantarctic site occurred at 19.8 kyr BP, over a thousand years later than in subtropical waters, which initiated at ~21.3 kyr BP. This caused an increase in the offset between these two sites as the Bay of Plenty warmed and the south Chatham Rise remained cool. After this, subantarctic SST increased more rapidly reaching 12.6°C by the ACR and decreasing the SST difference between the two sites to 3.7°C. In the early Holocene, subantarctic SSTs peaked at 15.2°C, further reducing the temperature difference between the two areas to ~2.0°C. In the later Holocene subantarctic SSTs fell to 13.0°C while subtropical temperatures increased slightly to 17.2°C increasing the difference in the SST at these two sites results to 4.2°C during the Holocene. The comparison of Mg/Ca SSTs between the two sites had the greatest difference in the LGM and lowest the early Holocene.

Figure 2.8

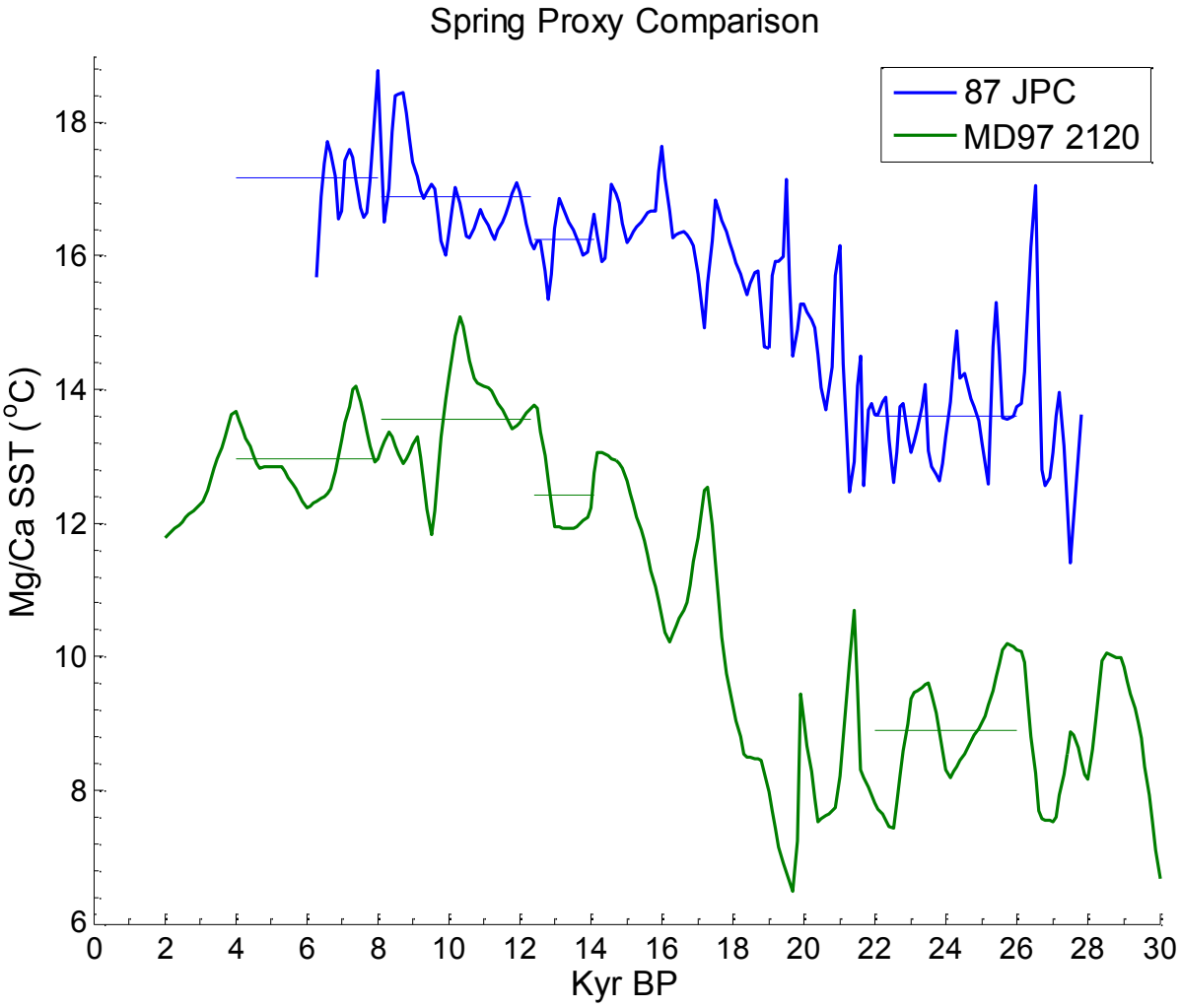

Figure 2.8| A comparison of *G. bulloides* Mg/Ca SST proxies from core 87 JPC in the subtropical Bay of Plenty (blue) and subantarctic core MD97-2120 from the south Chatham Rise (green). Note solid line represents the mean SST value across the interval of its domain.

2.4 Discussion

2.4.1 Oceanographic Implications of SST Estimates

The difference between the two Bay of Plenty SST estimates provides a proxy record of seasonality. The interval within the annual cycle an organism grows in the shallow ocean will impact the temperature that the proxy records. Thus, the seasonal growth preference of foraminifera and alkenones is an important factor which produces differences between alkenone based SSTs and foraminifera based SSTs (Sikes et al. 2009). In subtropical waters of the New Zealand region the vast majority of *G. bulloides* export flux has been shown by sediment trap data to peak in the month of October, giving modern *G. bulloides* an export flux based seasonality of early austral spring (King and Howard, 2001; King and Howard, 2003). Sediment trap results have also shown that the annual peak in alkenone export primarily occurs in late spring and early summer offset from that of *G. bulloides* with a secondary but lower peak occurring in late summer early autumn (Sikes et al., 2005). The mean Holocene difference between proxy records is 3.3°C which agrees well the range of modern values for those seasons. Today, the seasonal offset between early spring and early summer SSTs at the Bay of Plenty coring location is 3.6-4.1°C, based on a ten year monthly mean (*Park and Longdill*, 2006). The fact that the mean Holocene difference between the two proxy records approximates modern seasonal temperature difference supports the assumption that the difference between the two proxy records is primarily based on seasonal differences in SST.

Glacial seasonality in SSTs, as estimated by the differences in the two SST records in the Bay of Plenty was 2.6°C, slightly lower than the modern. The error of estimates, $\pm$0.8°C, is within the magnitude of ΔT. It is well established that the subtropical front remained fixed with a northern boundary at the Chatham Rise (Fenner et al., 1992; Nelson et al. 1993; Weaver et al.,

1998; Sikes et al., 2002) meaning temperature changes in the Bay of Plenty reflect variations in subtropical SST through the LGM and deglacial transition. During the LGM the strength of the East Australian Current (EAC), which contributes to the East Auckland Current that flows into the Bay of Plenty, was significantly reduced (Bostock et al. 2004; **Figure 2.2**). Planktonic and benthic foraminiferal stable isotopes from off shore Australia suggest this current did not increase to modern strength until after the ACR (Bostock et al., 2004). The reduced difference between spring and summer SSTs in the LGM may have been related to a weakened EAC, decreasing the sourcing of warmer tropical waters from the western equatorial Pacific for entraining in the EAUC and into the Bay of Plenty in austral summer. The seasonality, driven by greater warming of summer SSTs, increased to modern values when the strength of the EAC increased during the ACR (Bostock et al. 2004) and reflected in the Bay of Plenty data set (**Figure 2.6**). The nearly constant offset between alkenone and *G. bulloides* SSTs reflects small differences between growth seasons of these proxies on glacial-interglacial time scales (**Figure 2.6**).

2.4.2 Seasonal Insolation Hypotheses

Variability in the offsets between the seasonal proxy SSTs may reflect changes that occurred during their season of growth throughout the deglaciation. The difference between the Bay of Plenty proxies exists because foraminifera are recording spring SSTs while the alkenones record early summer SSTs. These proxies may be rectifiers of these specific seasons on glacial-interglacial time scales. In order to assess how well Bay of Plenty seasonal proxies track changes in seasonal insolation they were compared to paleo-insolation models. The modeling study *Laepple and Lohman* (2009) present the hypothesis that local insolation is

driving proxy records on astronomical time scales in a way similar to how local insolation drive the seasonal cycle on annual time scales.

Presently, in the New Zealand region there is a linear temperature response of local SSTs to modeled local insolation throughout the annual cycle with a lag of approximately 60 days (Laepple and Lohmann, 2009). The modeling study of *Huybers and Wunsh* (2003) suggests that proxy records which have nonlinear responses may be representative of a specific season; termed seasonal rectification. Alkenones appear to be a summer rectifier, which, if the time series was longer *Huybers and* Wunsch (2003) hypothesize that there would be a high energy band at 20 kyr indicating the effect of precession on seasonality. Even with the short time series available, it appears the low latitude summer temperatures have a strong precession component. The stable offset between the Bay of Plenty SST proxies persists from the LGM to the Holocene (**Figure 2.6**). One caveat to this interpretation is that on glacial-interglacial time scales Bay of Plenty SST records do not track with the respective modeled seasonal insolation values as predicted by *Laepple and Lohmann* (2009); there is a low correlation to the insolation that drives the seasonal temperatures. The low correlation occurs mostly from the LGM to the ACR, whereas after the ACR SST values appear to track well with local modeled spring insolation values (**Figure 2.9**).

At the Bay of Plenty the progression of weakest annual insolation value tracks well with the progression of spring and summer temperatures from the LGM to the ACR. This suggests a link between the seasonal temperatures to the progression of annual minimum insolation values. The insolation model of *Huybers et al.* (2006) outputs daily insolation values for the entire interval of this record, making it is possible to both isolate an individual seasonal insolation and the progression of values such as the annual minimum insolation across the

Figure 2.9

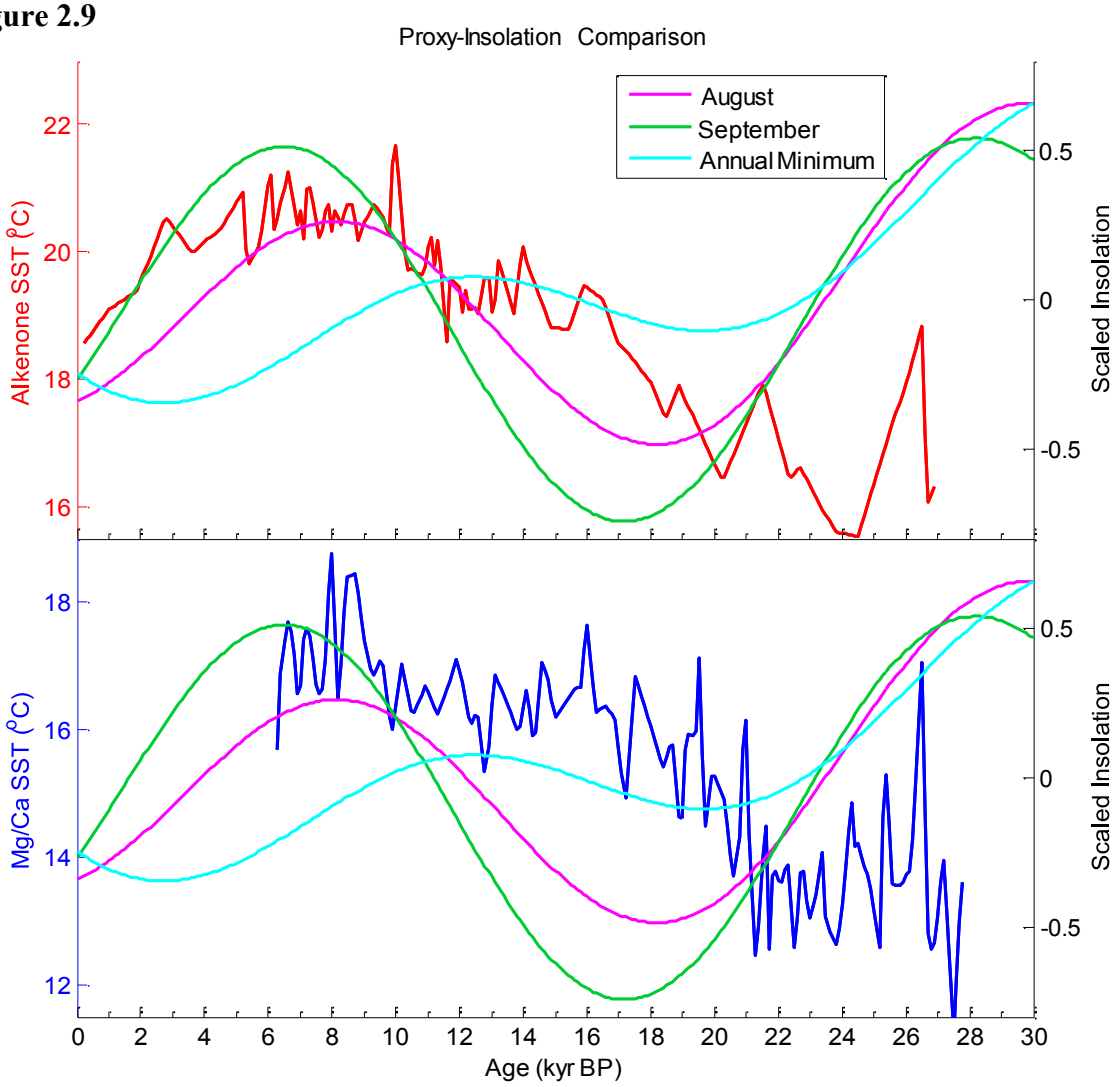

Figure 2.9| Bay of Plenty SST and modeled insolation. Core site 87 SST proxy records (alkenones thick red and Mg/Ca blue scale on left axis) plotted with the average August insolation (pink), September insolation (green), and the annual minimum insolation (blue) scaled on right axis. Seasonal insolation is scaled by removing the mean value from each point and then dividing each point by the amplitude of the curve. Note that the proxy records appear to follow the winter minimum insolation during the interval from the LGM to the ACR. After the ACR Mg/Ca peaks with August insolation while alkenones peak with September insolation verifying that the seasonal insolation hypothesis of *Laepple and Lohmann* (2009) at least holds true in the Holocene. The ACR appears to be a transition from the proxy records tracking with minimum insolation to the proxy records tracking with the insolation values that drive their respective seasonal SSTs as predicted by the 60 day lag of SST with insolation.

entire interval (**Figure 2.9**). From the LGM to the ACR the proxy records track well with austral winter insolation values whereas from the ACR to the Holocene the proxies track well with local spring insolation **(Figure 2.9).** *Laepple and Lohmann* (2009) compare SST data to modeled insolation to illustrate that in a mid-latitude region where there is a linear response of temperature to insolation in a given year such as this one, the minimum insolation value is highly correlated to the minimum annual temperature. The relationship between SSTs and the annual minimum insolation from the LGM to the ACR can be interpreted as the annual minimum insolation establishing a base temperature which forces glacial/early deglacial spring and summer temperatures to be low. If glacial spring and summer temperatures are dependent on the winter minimum, perhaps due to a reduced greenhouse effect (Petit et al., 1999), it can explain the close tracking of temperatures to the annual minimum insolation during this time. Another possibility is that the proxy organisms changed their season of growth, but it is unlikely that blooms shifted towards winter, when insolation was at its lowest value. Minimum insolation was more likely driving local climate system in New Zealand region by setting a minimum temperature which served as a base or limiting factor, against which the spring and summer temperatures were set.

After the ACR, both proxy SSTs began to track early spring insolation. The alkenone SSTs began to track well with and peak with the September insolation whereas the foraminifera begin to track and peak with August insolation values (**Figure 2.9**). Alkenones have a November or late spring growth peak. The tight correlation to September insolation values can be attributed to the demonstrated 60 day lag of SST to insolation, the tight correlation of alkenone SST and spring insolation from the ACR to the Holocene affirms the interpretation of *Laepple and Lohmann* (2009). Similarly, foraminifera have peak growth in October. With a

two month lag, October temperatures are tightly correlated to August insolation and there is a tight correlation of the Mg/Ca proxy to August insolation from the ACR into the Holocene. This suggests that SST at that time was driven by mid-latitude climate into the Holocene, with a seasonal temperature cycle that is tightly correlated to but lagged with insolation values. In summary, the Bay of Plenty proxy records appear to track well with local insolation values, however, the nature in which they follow insolation appears to vary on glacial interglacial time scales.

2.4.3 Latitudinal variation in SST: Alkenone Transect

To place the Bay of Plenty alkenone record in a regional context, data from this study was compared to published records in two other cores creating a latitudinal transect of high resolution SST records across the New Zealand region. The SST difference between the Bay of Plenty SSTs and Hawkes Bay SSTs remained stable, at ~4.0°C, since the LGM (**Figure 2.7**). This offset likely reflects a steady latitudinal offset in incoming solar radiation during the deglacial progression indicating summer SST throughout the deglaciation was similar at the Bay of Plenty and Hawkes Bay.

The difference between subtropical and subantarctic SSTs was more variable, with differences between the Bay of Plenty and south Chatham Rise ranging from 4.6-7.0°C the deglaciation (**Figure 2.7**). MD97-2120 sits in close proximity to the southern flank of the STF in subantarctic water masses. The response of subantarctic SSTs at the south Chatham Rise is fundamentally different from the Bay of Plenty and the Hawkes Bay. The SST rise in subantarctic waters was more rapid and overshot Holocene values by as much as 4°C during the early Holocene interval (12.1-8.5 kyr BP). This caused the subtropical-subantarctic SST difference to decrease, with the SST difference reaching zero in the ACR and remaining low in

the early Holocene. The overall warming in subtropical waters were more than at the south Chatham Rise (4.0 versus 3.0°C; **Figure 2.7**).

This regional comparison shows that initial rates of deglacial warming were slower in the Bay of Plenty than at the south Chatham Rise (**Figure 2.7**). Rapid early warming of subantarctic waters with a temperature overshoot in the early Holocene values has been seen in other proxy records from south of the STF (Sikes et al., 2009; Sikes et al., 2002). At the South Tasman Rise a southward deglacial frontal shift is responsible for the overshoot (Sikes et al., 2009). The use of multiple proxies established a seasonal asymmetry in the frontal movement, with greater displacement occurring in the summer (Sikes et al., 2009). *Sikes et al.* (2002) used a latitudinal transect of cores along the subtropical convergence further offshore eastern New Zealand and determined the STF off eastern New Zealand remains fixed along the Chatham Rise (Heath, 1972; Jillet, 1969; Shaw and Vennel, 2001; Sikes et al., 2002) with the position of the STF at the LGM the same as the modern position. Nevertheless, a minor, 1°C, SST overshoot is also present in subantarctic waters at this location, though not as dramatic as the 4°C overshoot in MD97-2120.

Site MD97-2120 sits in the armpit of the Chatham Rise, very close to the front as the Chatham Rise redirects the northward flow along the Southland current to the eastward flow along the Chatham Rise. Today, the position of the STF near eastern New Zealand has been shown to shift between two mean seasonal positions: along the northern and the southern edge of the Chatham Rise proximal to the core site (Belkin and Gordon, 1996). During the LGM, the difference between SST in the Bay of Plenty and Hawkes Bay and the south Chatham Rise may have been greatest because the surface expression of the STF was along the northern edge of the Chatham Rise in spring (**Figure 2.10a)**. As the deglaciation progresses the more rapid

SST increase at the south Chatham Rise, may have been caused by the mean surface expression of the front being displaced in spring more strongly to the southern side of the Rise. The overshoot in the early Holocene suggests the mean position of the STF sat more extensively to the south edge of the Chatham Rise allowing the seasonal presences of subtropical waters at the site (**Figure 2.10b**). This overshoot in temperatures may have been enhanced by the early Holocene intensification of the EAC current (Bostock et al., 2004). At 8.5 kyr BP the SSTs at the South Chatham Rise core rapidly drop 4°C while both cores north of the STF show a moderate decrease in temperatures. This may indicate the surface expression shifted back to the northern side of the Chatham Rise in spring and summer (Chiswell, 1996). The addition of the Bay of Plenty alkenone data suggests that subtropical waters masses may have been able to influence frontal positioning on the Chatham Rise.

The Bay of Plenty SST difference between LGM and mid-Holocene is 4°C while at the south Chatham Rise the difference is 3°C. The temperature difference occurs despite the mean position of the STF being exactly the same in the LGM as it was in the Holocene (Sikes et al., 2002). During the Holocene there is a greater influence of low latitude, equatorial, conditions in the Bay of Plenty causing an enhanced deglacial warming which is only evidenced south of the STF during the brief SST overshoot.

Relatively colder glacial temperatures in the Bay of Plenty may have been enhanced by a northward shift in the southern hemisphere westerly winds. Russell et al. (2006) use a coupled climate model to show that a northward shift and weakening of the circumpolar westerlies may have accompanied cooling in the glaciation. This suggests that during the LGM the westerly winds might have dominated at latitudes several degrees northward of their modern position (Toggweiler et al., 2006). This is supported by records of Southern Ocean

Figure 2.10

a) b)

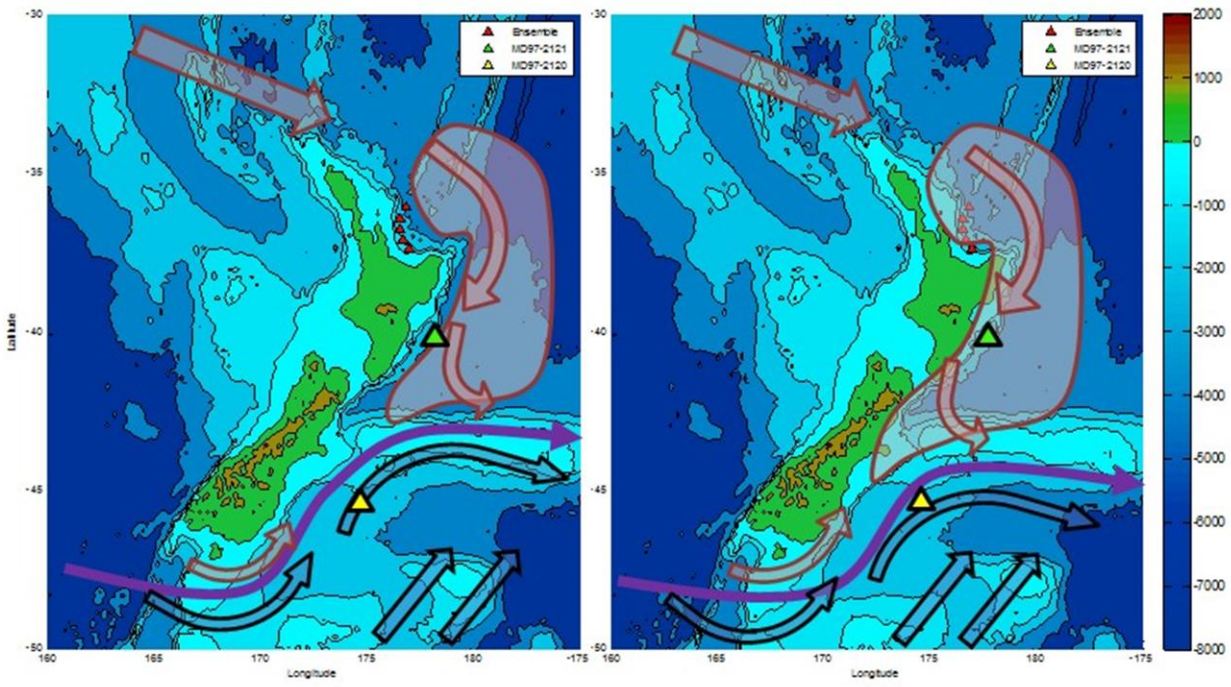

Figure 2.10| Representation of surface circulation in the New Zealand sector, based on interpretation of Belkin and Gordon (1996). The mean position of the Subtropical Front (STF; purple) is along the north Chatham Rise in colder months (a) and the south Chatham Rise in warmer months (b). Note that when the front sits further south along the rise the south Chatham Rise core (yellow triangle) is within the influence of subtropical mode waters (red), whereas when the front is along the northern Chatham Rise, subantarctic mode (blue) waters dominate the at the core location.

upwelling was much weaker than in the modern (Anderson et al., 2009). This northward shift would have caused greater cooling than if subtropical atmospheric conditions alone were affecting the Bay of Plenty during the LGM. The increasing low latitude influences as the deglaciation progressed can explain the greater amplitude warming in the Bay of Plenty. This may also be the main reason for the shift seen from austral winter insolation forcing to austral spring insolation after the ACR. Changes in the EAC which transport equatorial waters that become entrained in the EAUC are a possible conduit for equatorial influence. Isotopic evidence from offshore Australia document that the LGM EAC was significantly weaker than it is in the modern, it is not until after the ACR that the EAC intensifies carrying greater volumes of water from the equatorial Pacific into the Tasman Sea (Bostock et al. 2004) and possibly, the Bay of Plenty and Hawkes Bay to enhance deglacial warming.

2.4.4 Multi-proxy Discussion

Like the Bay of Plenty, the south Chatham Rise core has both alkenone (Pahnke and Sachs, 2006) and foraminifera Mg/Ca (Pahnke et al., 2003) SST reconstructions. In the Bay of Plenty the average glacial-interglacial seasonal SST difference is higher, at ~3°C, than the South Chatham Rise, ~2°C. In the Bay of Plenty that offset remains steady, 2.8-3.3°C, from the LGM to the Holocene, while on the south Chatham Rise the difference between seasons is more variable, 0.8-2.0°C, through the record (**Figure 2.11**).

The steady temperature offset between spring and summer at the Bay of Plenty and the variable temperature difference south of the Chatham Rise can be interpreted in two ways: 1) the temperature proxies change their seasonality during the deglacial progression as a result of nutrient and/or light stress or 2) at the south Chatham Rise the seasonal response to the deglaciation is impacted by seasonal changes in where the STF sits on the Chatham Rise. In

Figure 2.11

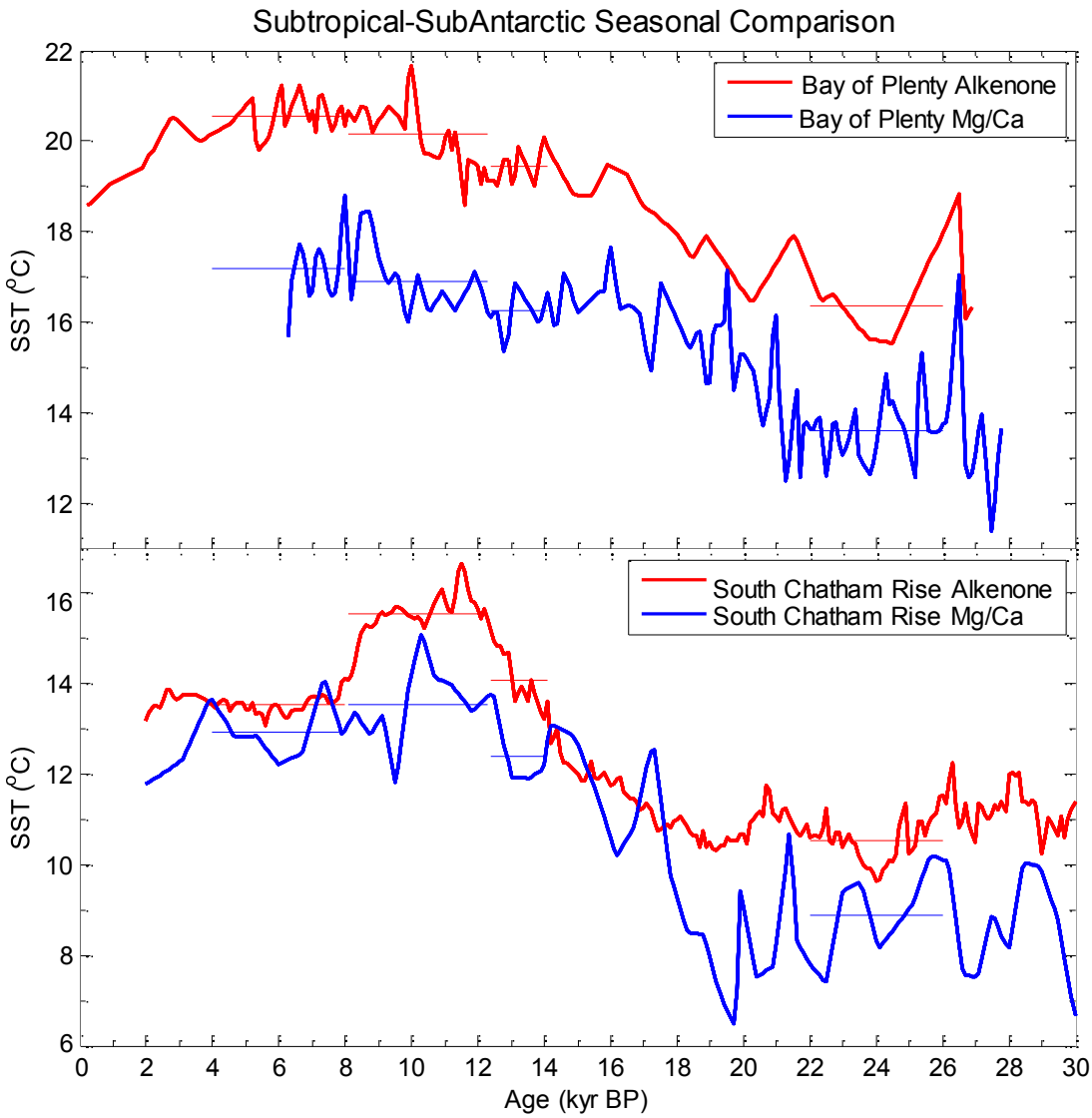

Figure 2.11| Seasonal temperatures in the Bay of Plenty and at the south Chatham Rise. Alkenones represent summer SST and Mg/Ca, spring based on the growth seasons of the organisms on which they are based. The comparison between subtropical and subantarctic SST indicates a very steady seasonal difference in the Bay of Plenty while the seasonal SST difference is more variable at the South Chatham Rise. This is especially apparent when looking at average values across intervals such as the LGM (26-22 kyr BP), the ACR (14.1-12.4 kyr BP), and comparing them with Early Holocene (12-8 kyr BP) and Holocene (8-4 kyr BP) averages.

the Bay of Plenty the steady offset between the spring and summer temperatures indicate that neither proxy changed its seasonality nor did the seasonal SST differences change as a response to the regional glacial-interglacial changes. Because the south Chatham Rise core sits so close to the front, the highly variable spring-summer offset may result from variability in nutrients delivered at the front or, the seasonal surface expression of the front, throughout the deglaciation.

During the early Holocene the south Chatham Rise summer SSTs warm much more than spring SSTs causing the greatest seasonal temperature difference for that site in the record, (2.0°C), whereas immediately following, the summer SSTs drop reducing the seasonal difference to the lowest in the record, (less than 1.0°C; **Figure 2.10b**). Similar differences between the responses of the similar SST proxies on the South Tasman Rise are attributed to seasonal variability in the position of the front (Sikes et al., 2009). On the Chatham Rise, an offshore latitudinal transect across the STF determined that the STF was in the same position in the LGM as it is in the Holocene (Sikes et al., 2002). At first glance this interpretation raises doubt that seasonal variability is related to frontal movement, however, the proxies in that study gave differing estimates of SST, that were attributed to mesoscale eddies causing differing estimates between alkenone and foraminifera SSTs (Sikes et al., 2002). Mesoscale movements of the front could be invoked to explain both the 4.0°C summer SST overshoot and enhanced seasonality during the early Holocene by increasing the component of subtropical surface waters to the south of the Rise in the summer.

It is clear that the pattern of deglacial warming in the subantarctic Pacific differs from the deglacial warming in the subtropical Pacific. These differences may not result only from frontal meandering but also from orbital forcings. It is well-known that Milankovitch forcing,

specifically precession and obliquity, impact high latitudes and low latitudes differently (e.g., Huybers, 2011; Huybers and Wunsch, 2005). The effect of obliquity at high latitudes can create insolation anomalies as high as $10W/m^2$. The differential temperature response at these two locations may also result from high latitudes being impacted more by obliquity while low latitudes are impacted more by precession.

2.5 Conclusions

In the Bay of Plenty and the southwest Pacific Ocean Mg/Ca records from *G. bulloides* are believed to be recorders of early spring while alkenone records reflect for late spring early summer temperatures. At the Bay of Plenty, Mg/Ca SSTs track well with austral spring insolation while alkenone SSTs track well with austral summer insolation throughout the Holocene. However, from the LGM to the ACR, SSTs track well with the progression of minimum insolation values. At the LGM temperatures are cooler, and based on the latitudinal comparison there may have been a greater influence of subantarctic waters to the Bay of Plenty causing a greater LGM-Holocene temperature difference than seen in subantarctic waters. Temperatures may have been forced by higher latitude insolation during this interval. This leads to the hypothesis that in a longer SST record from this region an obliquity signal would be seen during intervals when subantarctic waters masses made up a component of surface waters.

When the Bay of Plenty proxy records are put in a regional context via comparison to Hawkes Bay and South Chatham Rise proxy records, several nuances in the deglaciation are revealed. The deglacial warming was more intense in subtropical water masses whereas in subantarctic water masses the initial warming was more rapid causing an Early Holocene overshoot. This overshoot may have been related to mesoscale movements in the STF along

the Chatham Rise in summer months. In conclusion, the use of multiple proxies enhances the picture of the deglaciation by adding a seasonal component to the deglacial story in the southwest Pacific Ocean.

Chapter 3

3. Deglacial Source Water Shifts in the Southwest Pacific

3.1 Introduction

The deglacial transition is marked by major changes in large scale ocean and atmospheric circulatory patterns (e.g., Pahnke and Zahn, 2005; Anderson et al., 2009; Toggweiler 1999; Toggweiler et al., 2006; Bush and Philander, 2002). Deglacial initiation of the southern hemisphere warming leads that in the northern hemisphere (Sowers and Bender, 1995; Blunier et al., 1998; Stott et al., 2007, Shakun et al 2012). Despite general consensus that the southern hemispheric changes lead those in the northern hemisphere, the mechanism linking southern hemisphere deglacial events to those in the tropical and northern hemisphere is still a topic highly debated in the paleoclimate field (e.g., Ninneman and Charles, 1995; Smith et al., 1999; Spero and Lea, 2002; Huybers and Denton, 2008). One way to examine how high-latitude climate changes are related to low-latitude climate changes is by studying the mid-latitude climate records across which climate changes propagate (Bostock et al., 2004; Pahnke and Sachs 2006; Carter et al., 2008; Spero and Lea 2002).

During the LGM, global ocean deep circulation was different than that of today. Meridional overturning circulation is believed to have been slower due to reduced formation of North Atlantic Deep Waters (NADW; e.g., Broecker 1982, 2002). Diminished meridional over turning was accompanied by decreased upwelling in the Southern Ocean (e.g., Anderson et al., 2009) and reduced ventilation of the deep abyssal ocean (e.g., Sikes et al., 2000). A number of

mechanisms have been proposed including a weakening and northward shift in the southern Hemisphere westerlies (Sigman et al, 2010, Toggweiler 1999; Toggweiler et al., 2006).

The LGM ended with the warming of the Southern Hemisphere which was accompanied by a depletion in the $\delta^{13}C$ composition of shallow interior water masses and deeper subsurface water masses in both the subtropical Pacific and the subantarctic region of the Southern Ocean surrounding New Zealand (**Figure 3.1**; Anderson et al., 2009; Carter et al., 2008; Pahnke and Zahn, 2005; Bostock et al., 2004; Spero and Lea, 2002). In the South Pacific, subtropical shallow interior waters $\delta^{13}C$ depletions were abrupt (Carter et al., 2008). Deeper in the subsurface of the subtropical south Pacific Ocean (Carter et al., 2008) and in the shallow subsurface ocean in the subantarctic sector of the Southern Ocean the isotopic depletion is more gradual and resulting in an isotopic minimum event centered at ~15 kyr BP (Anderson et al., 2009; Carter et al., 2008; Pahnke and Zahn, 2005; Spero and Lea, 2002). The more gradual depletion in the mode waters coincides with initiation of the Southern Ocean upwelling system (Anderson et al., 2009) which is thought to cause the isotopic depletion in atmospheric CO_2 (Schmitt et al., 2012). It has been suggested that these isotopic depletions may have been a direct result of the upwelling of a low $\delta^{13}C$ signal being transmitted through the Pacific Ocean via SAMW and AAIW (Spero and Lea, 2002) but the earlier more abrupt change in subtropical waters is not consistent with this hypothesis suggesting these two depletions are decoupled.

Because $\delta^{13}C$ of DIC of subsurface water is primarily a proxy for primary productivity or respired CO_2, this data alone is not enough to constrain the geographical shift in origin of these isotopically depleted waters. Unlike $\delta^{13}C$, the $\delta^{18}O$ of ocean water ($\delta^{18}O_{SW}$) signal has embedded within it a latitudinal and a salinity component of source water caused by Rayleigh

Figure 3.1

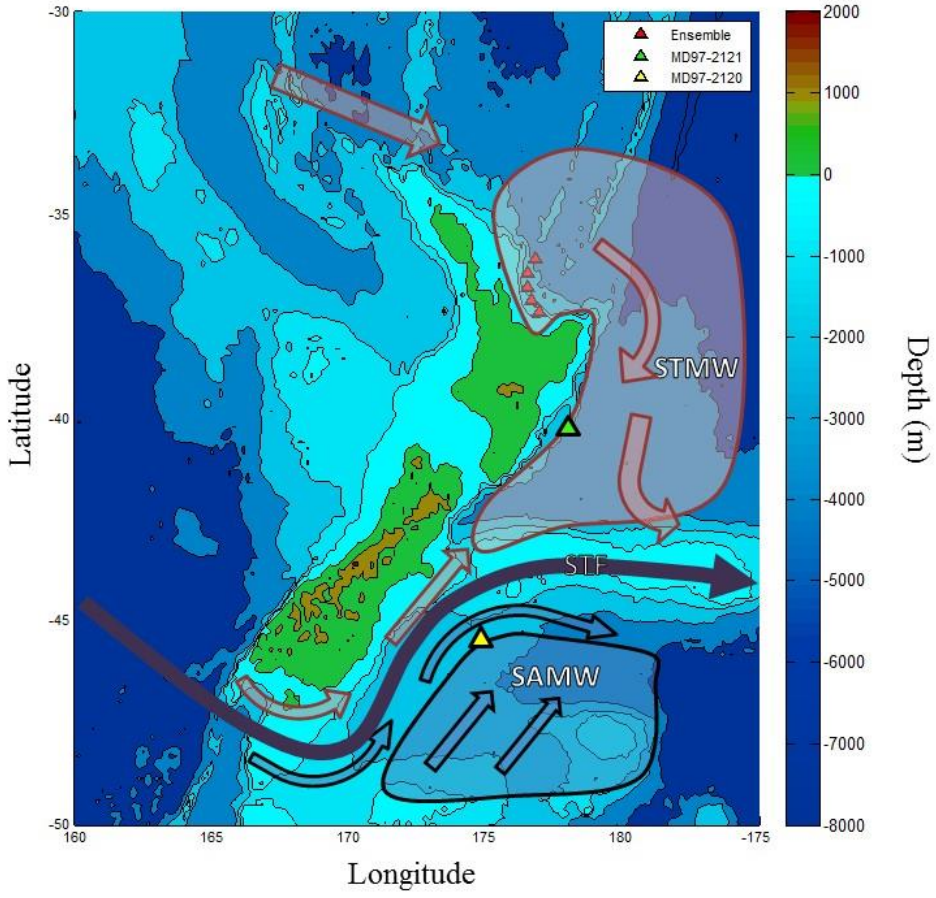

Figure 3.1| Schematic map of modern shallow surface circulation surrounding New Zealand. Subtropical mode water (STWM; red) advects in from the northwest carried in part by the East Auckland Current (straight red arrow). STMW is bounded to the south by the subtropical front (STF; purple). Further south subantarctic mode water (SAMW; blue shaded area) dominates with waters advecting in from the south. The coring sites referenced in this study include: the Bay of Plenty (red triangles; this study), Hawkes Bay (green triangles; Carter et al., 2008), and the south Chatham Rise (yellow triangle; Pahnke and Zahn, 2003).

distillation (Broecker, 2002). In order to better test the hypothesis that abrupt $\delta^{13}C$ change in the regional subsurface waters is not solely related to Southern Ocean upwelling it is necessary to combine paleo $\delta^{13}C$and $\delta^{18}O_{SW}$ reconstructions to interpret the provenance of the water mass.

In this study, high resolution stable isotope records from five cores in the Bay of Plenty were compiled to examine changes in the provenance of interior water masses from the LGM into the Holocene. The two isotopes, $\delta^{13}C$ and $\delta^{18}O$, of two planktonic foraminifera, *G. bulloides* and *G. inflata,* that grow at different depths, provide insight into deglacial water mass provenance changes and surface stratification in the subtropical New Zealand region. This Bay of Plenty record is compared to nearby records from Hawkes Bay and the south Chatham Rise to create a regional deglacial reconstruction. This study focuses on the mid-latitudes, such as the area surrounding New Zealand, as a key region in deciphering deglacial changes in Southern Hemisphere source water shifts.

3.1.1 Planktonic Foraminifera Stable Isotopes as Environmental Tracers

Planktonic foraminifera are single celled protozoans that live and calcify in surface ocean. Foraminifera tests are made of calcite ($CaCO_3$) and the isotopic composition of the carbon and oxygen within the shell is assumed to be in equilibrium the ocean during the time of growth, provided it is not a species with photosynthetic symbionts (Be, 1982). Two non-symbiont bearing species well adapted to live in the southwestern Pacific Ocean and used in this study are *Globigerina bulloides* and *Globigerina inflata* (Darling and Wade, 2008). *G. bulloides* is a spinose species of foraminifera which has been shown to live in the shallow depths of subpolar transitional zones (Be and Tolderlund, 1971; Be, 1977; Hemleben et al.,

1989; Darling and Wade, 2008; Chapman, 2010). *G. inflata* is a non-spinose foraminifera known to dominate subantarctic and subtropical transitional regions of the world's Oceans (Be, 1960; Be and Hemlin 1967). Furthermore, *Cleroux et al.* (2007) suggest that *G. inflata* prefers to live at the base of the thermocline and to record seasonal thermocline water mass conditions.

The degree to which the isotopic compositions of foraminifera track the isotopic composition of the local water mass has been established for the southwest Pacific Ocean. The sediment trap data of *King and Howard* (2004, 2005) document the relationship of modern *G. bulloides* and *G. inflata* to the $\delta^{18}O$ of the water mass of our specific study region. The maximum export flux out of the photic zone of *G. bulloides* and *G. inflata* is in early October, or early austral spring. The amplitude of the isotopic signal in *G. bulloides* over the annual cycle is similar to the $\delta^{18}O$ range of the surface ocean (King and Howard, 2005) confirming that these foraminifera live in the shallowest 50m of the water column in the (*Field* 2004). Comparison with the predicted $\delta^{18}O$ values of the surface waters in the New Zealand sector suggest *G. bulloides* has a constant $\delta^{18}O$ offset from the water of roughly 0.4+/-.03‰ (King and Howard, 2005). King and Howard (2005) also analyzed the annual isotopic amplitude of *G. inflata* illustrating that this species live between 50-100m depth deeper in the subsurface water column. Unlike *G. bulloides, G. inflata* $\delta^{18}O$ does not have an offset with the actual $\delta^{18}O$ value of the water it inhabits. The $\delta^{13}C$ of *G. bulloides* records the $\delta^{13}C$ of DIC with a constant disequilibrium offset of 1.5‰ while the *G. inflata* records the $\delta^{13}C$ of the DIC with a constant disequilibrium offset of 0.3‰ relative to the dissolved inorganic carbon (DIC) of the water (*King and Howard* 2004). These sediment trap studies in the New Zealand region establish that the isotopic composition of *G. bulloides* and *G. inflata* calcite tracks the isotopic composition of surface water masses with an isotopic offset (King and Howard, 2002, 2004, 2005).

Knowing foraminiferal isotopes track the isotopes of the modern ocean allows the interpretation of past changes in ocean circulation. The $\delta^{13}C$ of foraminiferal tests have been used as deep water mass tracers in the South Pacific because they carry a respired CO_2 signal which corresponds to the distance from water mass provenance (Broecker, 1994; Bostock et al., 2004; Bostock et al., 2010; Carter et al., 2008; Loubere and Bennett, 2008; Spero et al. 2003). The $\delta^{18}O$ records global ice volume, local temperature, and salinity. For the purpose of this study, the salinity component of the $\delta^{18}O$ is linked to the latitude of water mass formation (Broecker, 2002). The isotopic composition of *G. bulloides* and *G. inflata* will be used to interpret changes in the structure of the surface water column in the Southwest Pacific Ocean since the LGM.

3.2 Methods

3.2.1 Sample Preparation and Analysis

A depth transect of five cores (**Table 3.1**) from the subtropical Southwest Pacific Ocean in the Bay of Plenty off the coast of northern New Zealand were chosen for this study (**Figure 3.1**). Sampling for all of the cores in this study were 5cc. The sampling intervals for each core varied between 1, 4, and 8 cm depending on the individual sedimentation rates in the cores. For most cores, resolution was increased across intervals of interest to the study (See **Appendices A.1 – A.4**). Sediment for isotopic analysis was oven-dried at 30°C and weighed. Then, the sediment was disaggregated using deionized water and wet sieved at 63μm to remove fine clays. Samples were re-dried at 30°C, and the process repeated three times and the dry weight of the coarse fraction, >63μm, recorded. The planktonic species *Globigerina bulloides*,

Globorotalia inflata, and the benthic species *Planulina wuellerstorfi* were picked from the 150-250µm and 250-350µm size fraction for stable isotope and radiocarbon analysis. *G. bulloides*

Table 3.1

Core	Latitude	Longitude	Depth
RR0503 125 JPC	36°11.90' S	176°53.35'E	2,541 m
RR0503 87 JPC	37°15.81' S	176°39.86'E	663 m
RR0503 83 JPC & TC	36°44.25' S	176°38.39'E	1,627 m
RR0503 79 JPC	36°57.52' S	176°35.57' E	1,165 m
RR0503 64 JPC	37°25.34' S	177°00.41' E	651 m

Table 3.1| Bay of Plenty coring locations and depths.

and *G. inflata* species were run from the 250-350µm size fraction, and *P. wuellerstorfi* from the >250µm where available where scarce *P. wuellerstorfi* were pooled from the 150-250µm. Stable carbon and oxygen isotopes were run on a Micromass Optima mass spectrometer with a Multiprep device for automated analysis at Rutgers University Department of Geology stable isotope laboratory. The mass spectrometer has an analytical precision of 0.08‰ for $\delta^{18}O$ and .04‰ for $\delta^{13}C$ (+/-1 σ) based on the repeated analysis of an in-house marble standard. Raw data for each core can be found in **Appendix A.1-4**.

3.2.2 Ensemble Calculation

In order to quantitatively compare records from the five cores, a matching chronology for each core was created by interpolating to a centennial incremented age model for 0.0 to 30.0 thousand years (kyr BP). The isotopic values of cores 87 JPC, 64 JPC, 79 JPC, and 125 JPC were averaged using the *nanmean* function in Matlab to achieve a composite value or ensemble average for the Bay of Plenty (Appendix B.1). The splice of cores 83 JPC and 83 TC were not included in the ensemble calculations due to questions concerning the splice and age model.

3.2.3 Assemblage Counting

The raw isotope data suggested offsets in the timing of events between the two planktonic species. To asses the possible effect of changing abundances and differential bioturbation on the record, assemblage counts of these species were used to investigate bioturbation impacts on isotopic values (**Table 3.2**). Planktonic species of foraminifera from cores 87 JPC and 125 JPC were taken from ten 1cm sections of the core at depths surrounding the timing of deglacial isotopic depletions. All samples within the size fraction >150μm where successively split to yield a total of 300-500 planktonic foraminifera. For each sample population counts were conducted for *G. bulloides*, *G. inflata*, *N. pachyderma (left coiling), and N. pachyderma (right coiling)* according to the established taxonomy (Be, 1977; Thompson and Shackleton, 1980).To obtain overall numbers per gram assemblage counts were back multiplied for splits to yield the total number of each species, and any individuals previously removed for isotopic or trace metal analysis were added to the total count per species in the sample. The samples were then divided by the original dry weight (g) yielding an estimate of species population per gram of sediment.

Table 3.2

Core	Depth (average cm)	*G. bulloides (individuals/gram)*	*G. inflata (individuals /gram)*	*Pachyderma left (individuals /gram)*	*Pachyderma right (individuals/gram)*
125 JPC	152.5	293.3	369.3	273.5	0
125 JPC	156.5	223.3	331.4	216.1	13.2
125 JPC	164.5	312.8	416.2	259.5	0
125 JPC	172.5	97.5	187.2	109.8	0
125 JPC	184.5	121.4	329.6	149.4	4.4
125 JPC	220.5	122.2	204.9	158.3	8.6
125 JPC	228.5	177.4	395.4	289.3	5.4
87 JPC	70.5	864.6	889.8	327.6	0
87 JPC	78.5	1081.3	1250.7	820.1	71.3
87 JPC	82.5	3095.7	3941.8	3424.7	85.6
87 JPC	86.5	6880.9	6976.2	3812.8	653.6
87 JPC	94.5	5093.0	4572.1	3770.5	595.3

Table 3.2| Population counts of planktonic foraminifera within cores 125 JPC and 87 JPC. These assemblage counts were used to assess differential bioturbation between the several species. This can impact offsets in foraminiferal isotope data.

3.3 Results

3.3.1 Stratigraphy Chronology

RR0503 64 JPC

The age model for core RR0503-JPC-64was developed using tephra chronology and planktonic $\delta^{18}O$ stratigraphy. Tephra tie points for this core include the Whakatane tephra (5.5$\pm$.06 cal kyr BP), the Rotomoa tephra (9.5$\pm$.03 cal kyr BP), and the Waiohau tephra (13.6$\pm$.03 cal kyr BP). The age model for this core is described in greater detail in the supplementary on line information of *Rose et al.* (2010).

The development of the age model for the remaining RR0503-cores consisted of the also used stratigraphic tephra tie points (**Table 3.3;** Elmore, in prep). The presence of the Rotoma tephra (9.5 cal kyr BP), the Waiohau tephra (13.7 cal kyr BP), and the Okareka tephra (22.6 cal kyr BP) all suggest a continuous sedimentation rate between 4.8 and 13.3 cm/kyr throughout the Holocene. In core 79 JPC, the presence of the Te Rere tephra (25.5 cal kyr BP) at 289 cm indicates a higher sedimentation rate of 31 cm/kyr from the LGM to the end of MIS 2. A linear sedimentation rate was assumed between all chronological tie points allowing for the development of a continuous age model for the entire core (**Figure 3.2a**). The development

Table 3.3

Tephra Age (kyr BP)	64 JPC	79 JPC	83 JPC	83 TC	87 JPC	125 JPC
Kaharoa 0.6	89 cm	46 cm				
Waiohau 13.7		81 cm		125 cm		
Mayor Isle 6 14.0				156 cm		
Rerewhakaaitu 17.8	153 cm	187 cm	68 cm		74 cm	164 cm
Okareka 22.6	307 cm	199 cm	107 cm			282 cm
Te Rere 25.5	372 cm	289 cm				
Kawkawa 27.1		330 cm	164 cm		157 cm	346 cm

Table 3.3| Stratigraphic tie points used in the development of age models of cores *RR0503-125-JPC*, *RR0503-87-JPC*, *RR0503-83-TC*, *RR0503-79-JPC*, and *RR0503-64-JPC*.

Figure 3.2

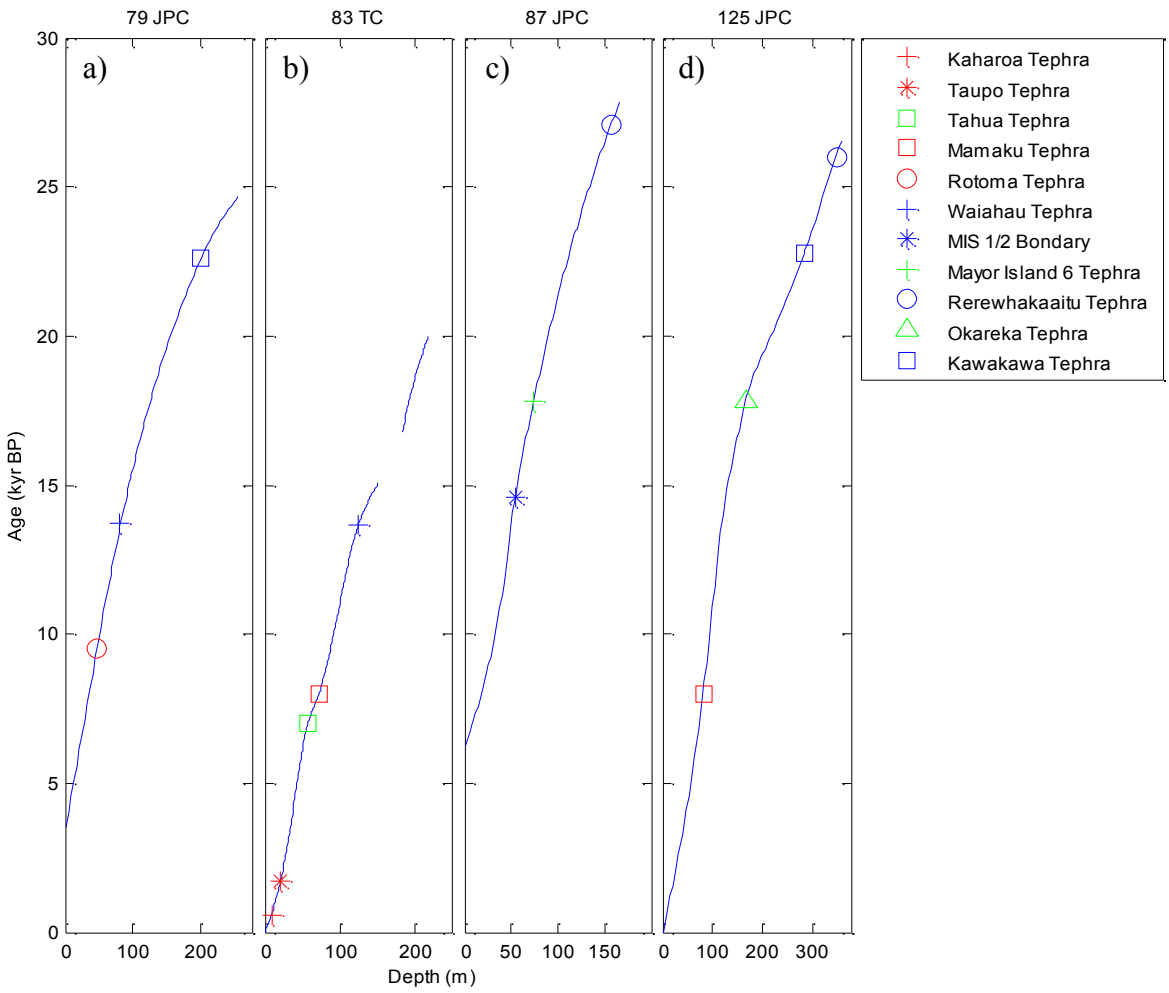

Figure 3.2| Age depth plots for the cores used in this study. Symbols illustrate stratigraphic tie points for cores 79 JPC, 83 TC, 87 JPC, and 125 JPC. Positively identified tephra (Shane et al, 2006) were combined with marine oxygen isotope events picked in the benthic record to create a high resolution chronological model for each core as indicated.

of the age model was the same for cores 83 TC, 87 JPC, and 125 JPC however the tephra tie points used varied (**Table 3.2*).*** The depth vs. age model for each core is presented in **Figure 3.2**.

3.3.2 Oxygen Isotopes

The *G. bulloides* $\delta^{18}O$ records variability throughout the Bay of Plenty depth transect of cores (**Figure 3.3**). In three cores: 87 JPC (600m), 79JPC (1200m), 125JPC (2500m), there was an increase in $\delta^{18}O_{bul}$ of 0.6‰ during the LGM to maximum values of 2.6‰, 2.2‰, and 2.6‰, respectively, prior to the termination of the LGM. After the LGM maximum the $\delta^{18}O_{bul}$ became steadily depleted by ~1.2‰ until the onset of the ACR. This continued into the Early Holocene to minimum values of ~0.0-0.15‰. A Holocene trend is not evident due to lower resolution data, however, in core 125JPC, whose age model extends to the modern era, and values level off between 0.3 and 0.5‰. The oxygen isotopes of the subsurface species *G. inflata* ($\delta^{18}O_{inf}$) in these cores showed a similar glacial to interglacial change but had much amplitude variability through the record (**Figure 3.3**). During the LGM core 79JPC $\delta^{18}O_{inf}$ ranged between 1.8‰ and 2.4‰. Results in cores 87JPC and 125 JPC were noisier during this interval but ultimately exhibit a similar enrichment. The maximum enrichment in all three cores occurs at 17.8 kyr BP approximately 2kyr after that seen in the *G. bulloides* record. After 17.8 kyr BP, there is a steady deglacial $\delta^{18}O_{inf\ depletion}$ into the Early Holocene to a minimum value of 0.7‰.

Core 64JPC (661m water depth; *Rose et al.* 2010) analyses do not extend into the LGM preventing an assessment of glacial isotopic values. However, after the LGM the deglacial trend in $\delta^{18}O_{bul}$ was steady depletion until a hiatus in the core at 14-9 kyr BP (**Figure 3.3**).

Figure 3.3

Figure 3.3| Oxygen isotope ($\delta^{18}O$) of the planktonic foraminifera *G. bulloides* for the Bay of Plenty cores used in this study. The cores 79 JPC (blue), 125 JPC (green), 64 JPC (red), 87 JPC (thin black line), were averaged to produce an ensemble record (thick black line) for the location.

When the record resumes after the ACR a notable $\delta^{18}O_{bul}$ minimum of 0.2‰ occurred in the early Holocene at ~8.7 kyr BP. The $\delta^{18}O_{inf}$ had a maximum of 2.1‰ at ~18kyr BP (**Figure 3.4**). After this maximum there was a steady decrease in $\delta^{18}O_{inf}$ to an Early Holocene minimum of .6‰ at 9 kyr BP; the steady depletion is exclusive of the aforementioned slump.

Benthic data in core 83 TC had anomalously enriched $\delta^{18}O$ values, from depths 154 to 184 cm not duplicated in other nearby cores. This is potentially due to a coring issue and limits from the use of the older sediments in this core and so it is reported for completeness but not utilized in the ensemble calculation (**Figure 3.5 and 3.6**). The two cores 83JPC and 83TC were spliced together using only the upper portion of TC87 to get a high resolution record. During the LGM there were several high amplitude swings extending from as low as 1.6 to as high as 2.4‰ (**Figure 3.5**). Unlike the other cores, *G. bulloides* in JPC83 do not begin the
The deglacial depletion until 19 kyr BP, and the noisy shift lasted until 5.8kyr BP when $\delta^{18}O_{bul}$ reached a minimum value of -0.1‰. This was much later than the Early Holocene minimum seen in the other cores. During the LGM, the $\delta^{18}O_{inf}$ values held steady at 2.2‰. The deglacial depletion began at 20 kyr BP (**Figure 3.6**); much earlier than the other cores and depleted until they reached a minimum value of .5‰ at 6.8 kyr BP.

Thermocline Proxy

The difference in $\delta^{18}O$ values between planktonic foraminiferal species has been used to estimate thermocline depths. In this study, the difference between *G. bulloides* and *G. inflata* ($\Delta\delta^{18}O$; e.g., Thornalley et al., 2009) were used to estimate near surface stratification. $\Delta\delta^{18}O$ values close to 0.0‰ signify as a deeper thermocline and whereas more negative values are interpreted as a shoaled thermocline. In the Bay of Plenty a deeper thermocline was present

Figure 3.4

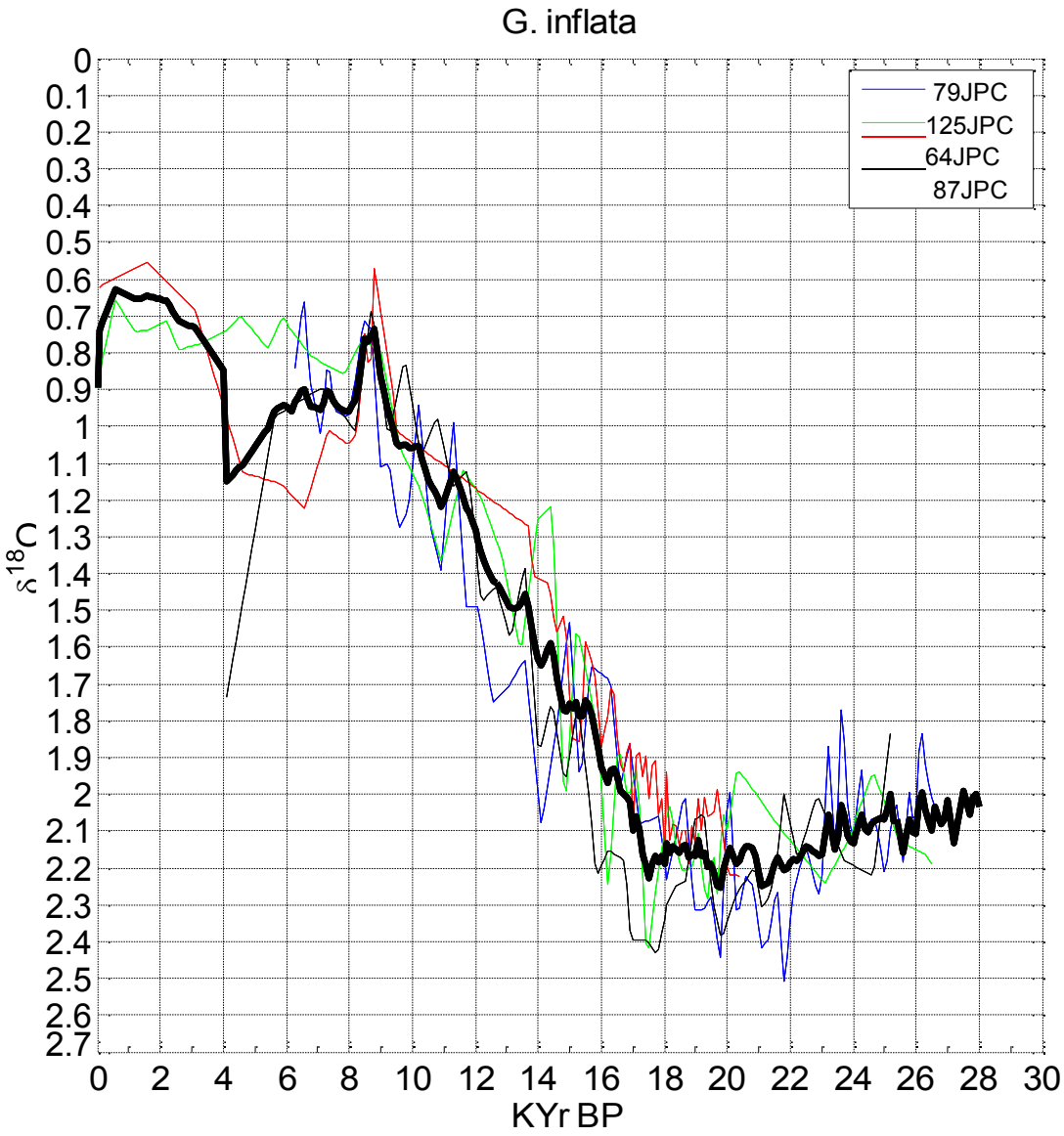

Figure 3.4| Bay of Plenty $\delta^{18}O$ inflata results for cores: 79 JPC (blue), 125 JPC (green), 64 JPC (red), 87 JPC (black). The average of the 4 cores was constructed by first linearly interpolating each core to a centennial time using step using the interp1 function in Matlab and then the namean function in MatLab was used to construct the ensemble average (thick black line).

Figure 3.5

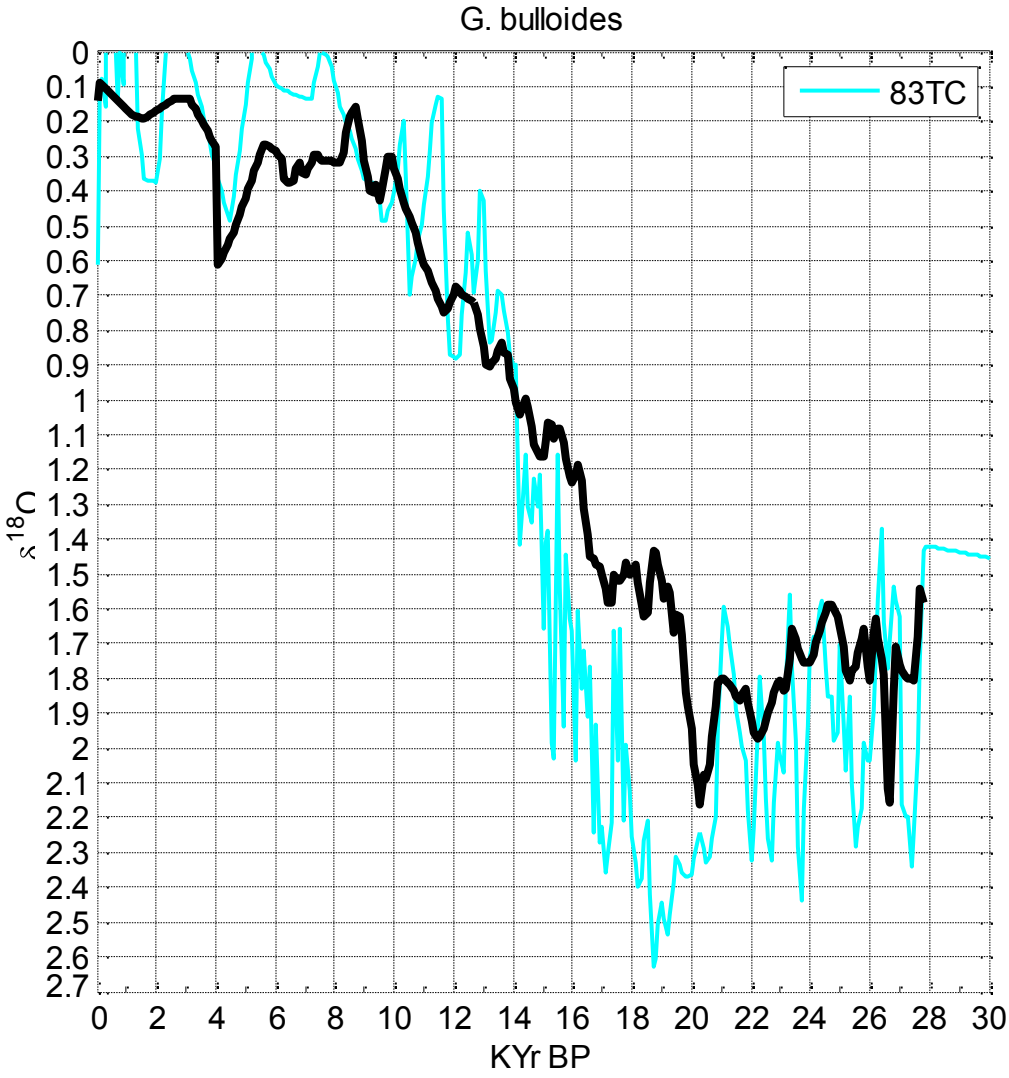

Figure 3.5| Bay of Plenty $\delta^{18}O$ bulloides data for core 83 TC/JPC splice (turquoise). The data from this combined core is compared with the ensemble average (thick black line). Note the offset in the onset of the deglacial shift, suggesting suspect stratigraphy.

Figure 3.6

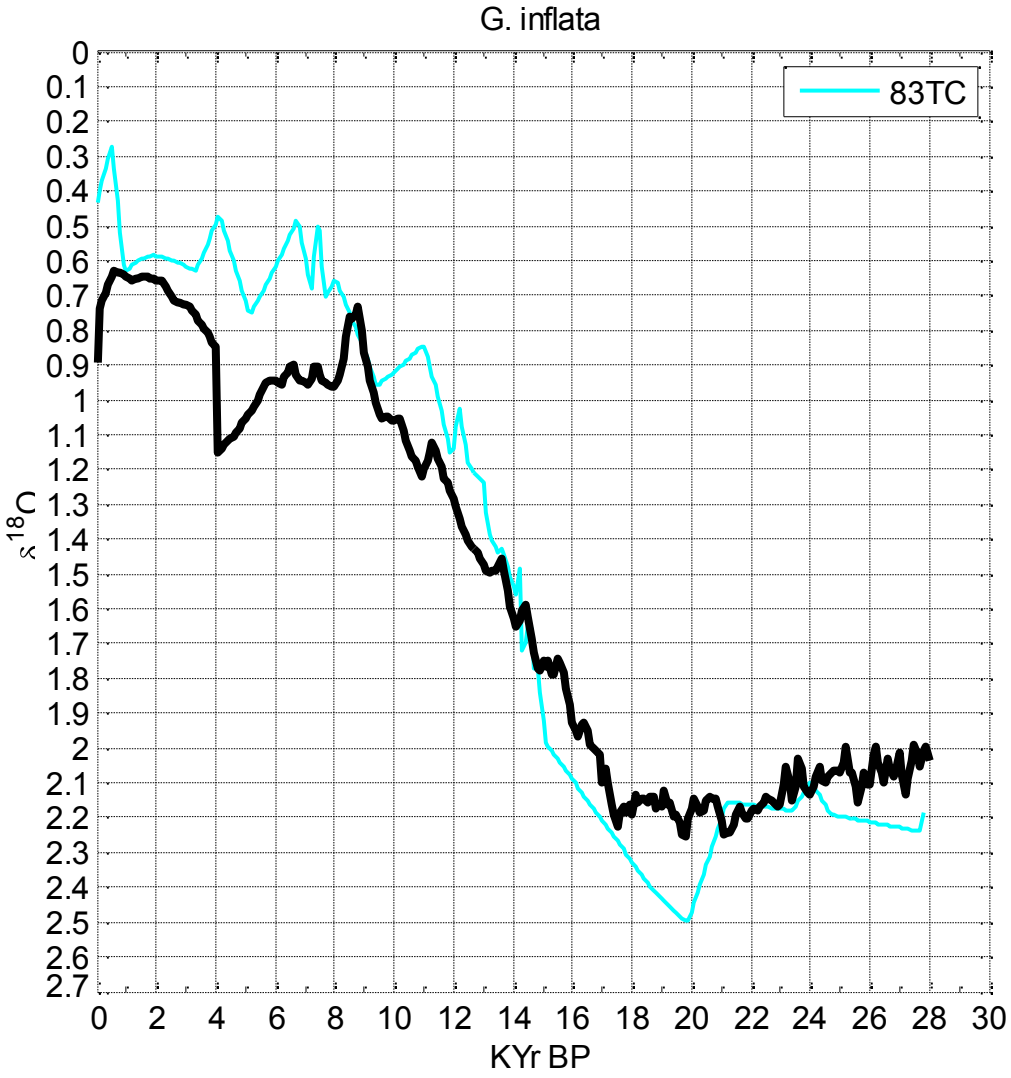

Figure 3.6 Bay of Plenty $\delta^{18}O$ *G. inflata* data for core 83 JPC/TC compared (turquoise). Results from this core are with the ensemble average of *G. inflata* (thick black line) for the other cores from this location.

in the LGM (**Figure 3.7**). At the deglacial onset, a step change in $\Delta\delta^{18}O$ enriched towards the zero line indicates the thermocline shoaled after which it continued to shoal into the Holocene. Two thermocline modes are clearly evident in this data set, a deeper glacial mode dominant prior to 20.1 kyr BP and a shallower post-glacial mode from 19.5 kyr BP through to the Holocene.

3.3.3 Carbon Isotopes

During the LGM the $\delta^{13}C$ of *G. bulloides* ($\delta^{13}C_{bul}$) in cores 79 JPC, 87 JPC, and 125 JPC had a mean of ~-0.4‰. At 20.1 kyr BP, there was a maximum $\delta^{13}C_{bul}$ value (-0.1-0.3‰) in all three cores (**Figure 3.8**). From 20.1-19.1, that is the 1kyr following the enrichment peak, there was a >1.0‰ depletion seen in the three cores. At the same time 64 JPC had a similar $\delta^{13}C_{bul}$ minimum of -1.7‰ but the onset is not resolvable due to the lack of LGM data. Throughout the deglaciation high amplitude noise in the $\delta^{13}C_{bul}$ in all cores dominates the record. After the deglacial shift, cores 79 JPC and 87 JPC averaged ~-0.9‰ through to the Holocene while core 125 JPC averaged -1.0‰, and 64JPC averaged -1.4‰. Despite variability between the four cores, the ensemble average allows for the interpretation of a clear regional trend.

The *G. inflata* carbon isotopes ($\delta^{13}C_{inf}$) are both less noisy and much more consistent between cores. Unlike $\delta^{13}C_{bul}$, the $\delta^{13}C_{inf}$ did not exhibit a high magnitude change at 20 kyr BP (**Figure 3.9**). In the interval from 25 to 18 kyr BP there were no significant trends in any core. 87JPC, 125 JPC, and 64 JPC, where data exists, all had a mean $\delta^{13}C_{inf}$ of 0.7‰, 79JPC had a slightly higher value of 0.8‰ during the interval. During the early deglaciation all cores

Figure 3.7

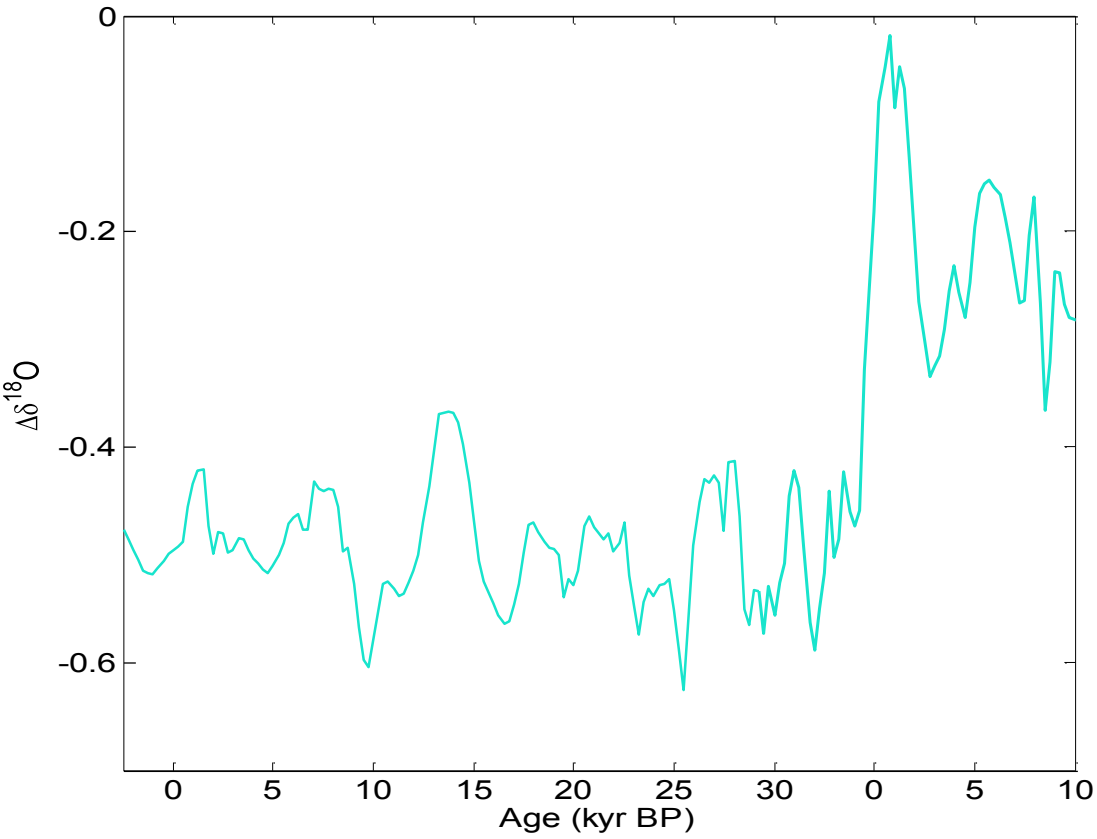

Figure 3.7| The difference between *G. inflata* $\delta^{18}O$ and *G. bulloides* $\delta^{18}O$ ($\Delta\delta^{18}O$) used to represent the depth of the surface mixed layer. When the $\Delta\delta^{18}O$ of the two species is more similar, that is, is closer to zero the thermocline is shoaled. When $\Delta\delta^{18}O$ is more negative there is a deeper thermocline.

Figure 3.8

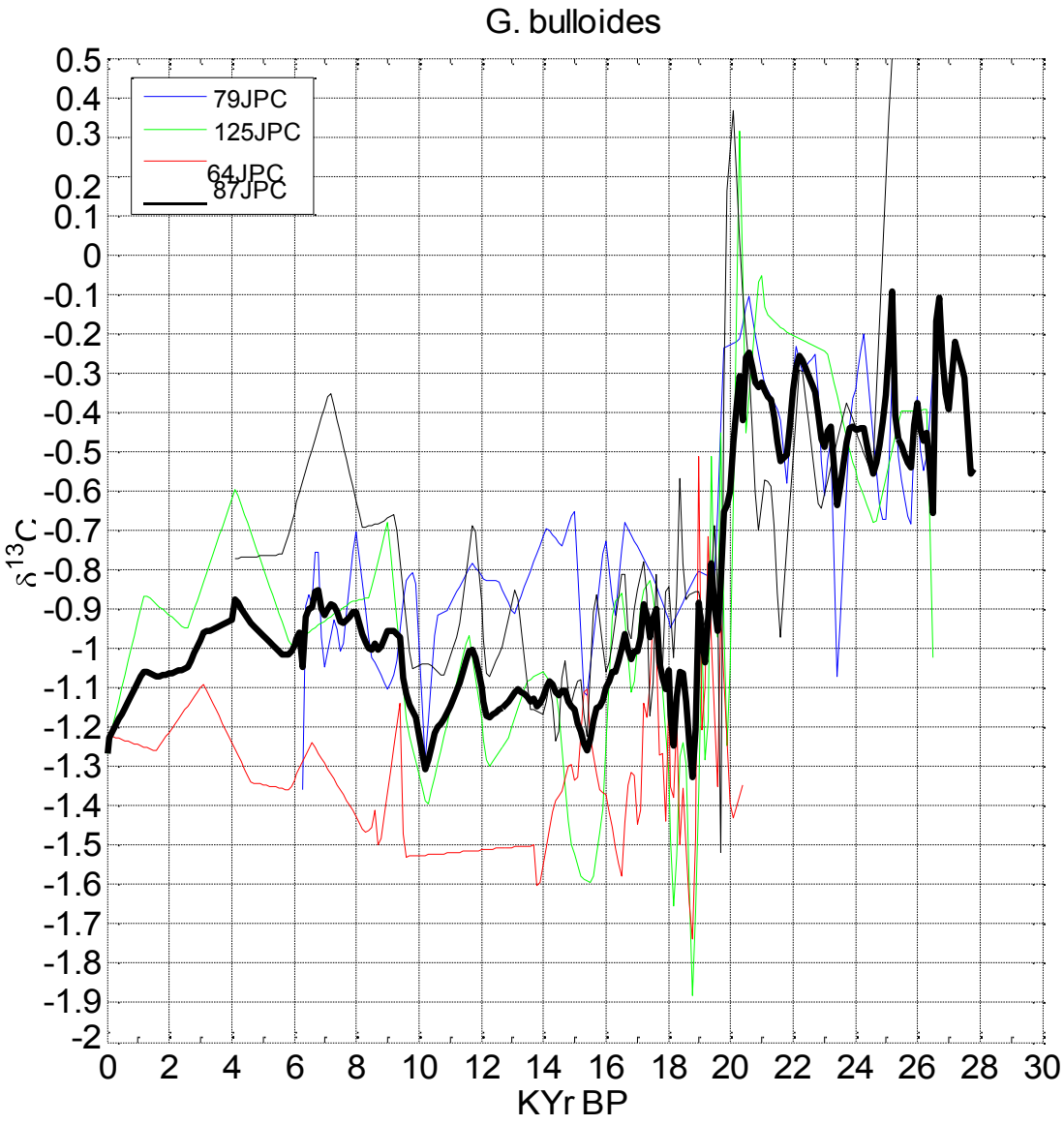

Figure 3.8| Bay of Plenty $\delta^{13}C$ for the planktonic foraminifera *G. bulloides* cores: 79 JPC (blue), 125 JPC (green), 64 JPC (red), 87 JPC (black), and the ensemble average for the cores (thick black line).

Figure 3.9

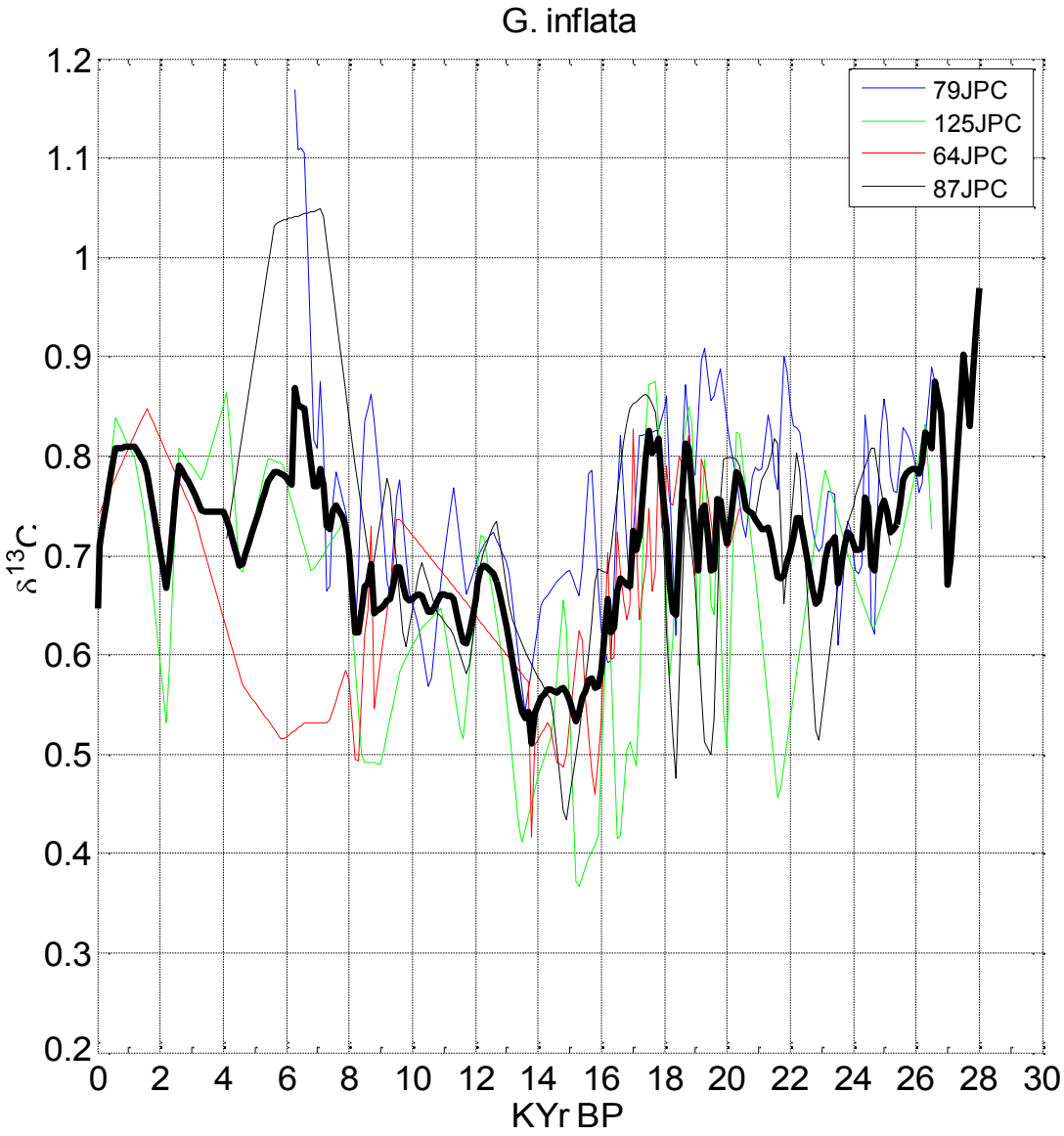

Figure 3.9| Bay of Plenty $\delta^{18}O$ for the planktonic species *G. inflata*. Cores: 79 JPC (blue), 125 JPC (green), 64 JPC (red), 87 JPC (black). The average of the several cores ensemble (thick black line).

exhibited a gradual depletion trend, 79 JPC shifting from 0.9‰ to 0.6‰, 125 JPC shifting from .9‰ to 0.4‰, 64 JPC and 87 JPC both shifted from 0.8‰ to 0.4‰, with minimum values in all cores between 15-14 kyr BP. During the ACR all cores had a 0.2‰ enrichment. Into the Holocene all cores possess had mean values of 0.7-0.8‰.

Combined cores 83 JPC/TC possessed an average $\delta^{13}C_{bul}$ of -.4‰ during the LGM (**Figure 3.10**). Between 21 and 19 kyr BP there was a major excursion from the rest of the ensemble with $\delta^{13}C_{bul}$ enriched by 1.0‰ from -.4‰ to .4‰. The subsequent deglacial depletion was similar in magnitude to the other cores (0.4 to -1.4‰) however the depletion spans a greater interval (20 to 15 kyr BP). After an extended deglacial step change $\delta^{13}C_{bul}$ values became highly irregular and differ from the ensemble average (**Figure 3.10**). This can be attributed to the stratigraphy issues with this core. The $\delta^{13}C_{inf}$ track well with the other cores during some intervals (**Figure 3.11**). During the LGM $\delta^{13}C_{inf}$ had a mean value of 0.8‰ with a maximum of 1.0‰ occurring at 20 kyr BP. A subsequent decrease to a value of 0.4‰ lasted until 13.8 kyr BP and after 13.8 kyr BP the $\delta^{13}C_{bul}$ averaged 0.7‰ with a maximum value of 1.1‰. Core 83 TC is highly variable and irregular when compared the rest of the ensemble.

3.3.4 Bioturbation

There is a 2,000 offset in the isotopic onset of the deglaciation between the results of the *G. bulloides* and *G. inflata* $\delta^{18}O$ records. In order to confidently interpret this lag as an oceanographic phenomenon it is important to ascertain that this lag is not the result of differential bioturbation impacting the foraminiferal isotopic signature. In this study two methods, population assemblage counting and bioturbation modeling, were employed to explore whether bioturbation was responsible for the offset between species.

Figure 3.10

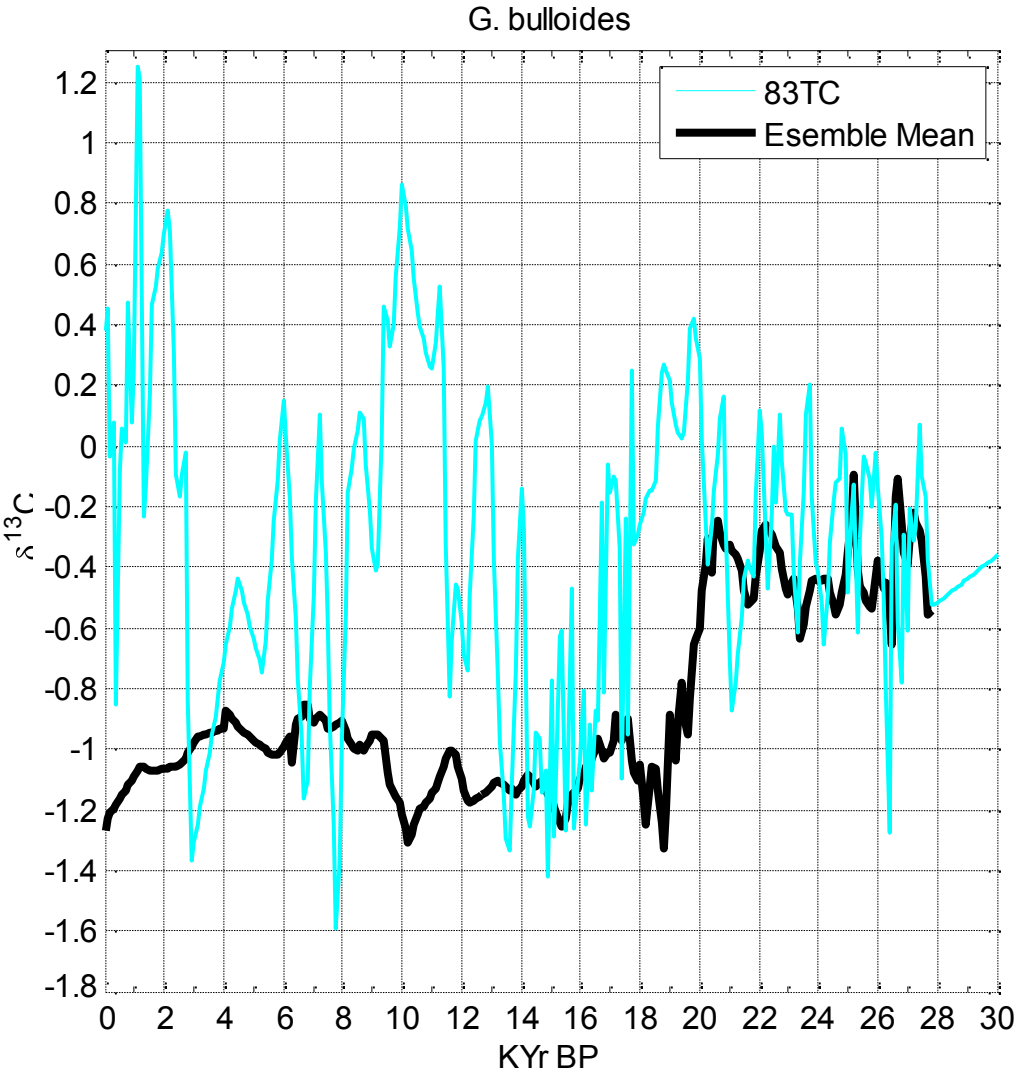

Figure 3.10| Bay of Plenty $\delta^{13}C$ from the planktonic species *G. bulloides*. Core 83 JPC/TC (turquois) is compared to the ensemble average (thick black line). Note the difference in timing of the deglacial shift in ^{13}C between 18 and 20 kyr BP.

Figure 3.11

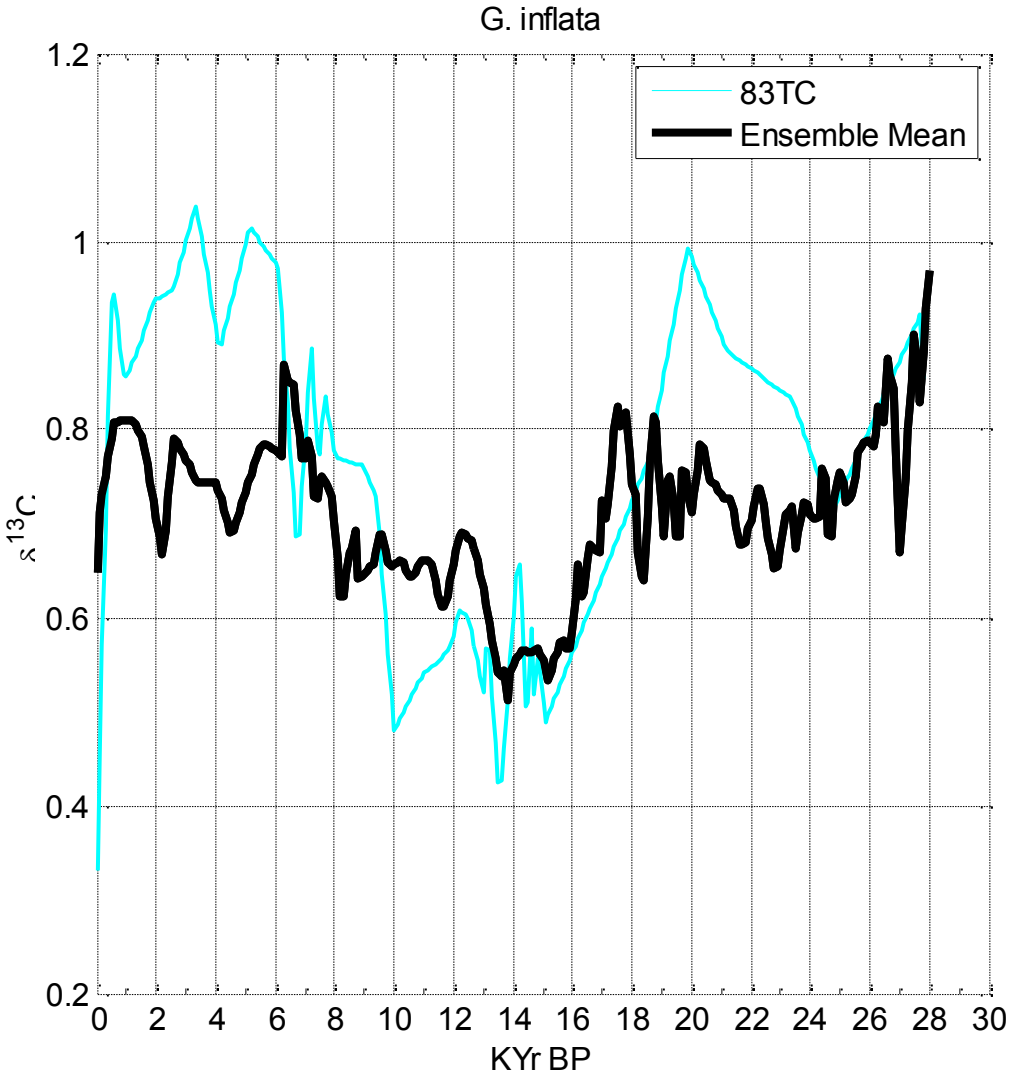

Figure 3.11| Bay of Plenty $\delta^{13}C$ of the planktonic species *G. inflata* in core 83 JPC/TC (turquoise) is compared to the ensemble average (thick black line). Note the difference in timing of the deglacial shift in ^{13}C between 18 and 20 kyr BP.

Assemblage Counts

Bioturbation is the mixing of sediment by benthic organisms which may differentially sort populations of foraminifera when they have differing abundances (e.g. Guinasso and Schink, 1975; Peng and Broecker, 1984). The magnitude of the effect can be assessed by examining population peaks of the different foraminifera and where in the core they occur (Peng and Broecker, 1984). It has been shown that if changing populations of different foraminifera do not track well with each other it may be a result of differential mixing of a younger population of foraminifera with an older population which can bias the isotopic signal among them (Broecker et al., 1999; Hutson, 1980). The relative species abundance for *G. bulloides* and *G. inflata* in both core 87 JPC and 125 JPC are similar (**Table 3.2**). In core 87 JPC there are distinct minima in both species of planktonic foraminifera at 70.5 cm and a distinct maximum at 84.5 cm. The similarity in both core 87JPC and 125 JPC suggests that bioturbation is not affecting the isotopic signal and bioturbation cannot account for the offset in the deglacial isotopic onset in the two species.

Bioturbation Model

A bioturbation model was used to verify empirically whether bioturbation affected the relative timing of the deglacial onset in the *G. bulloides* and *G. inflata*. An ideal model of isotopic values was developed in which the deglacial shift in isotopic values of *G. bulloides* and *G. inflata* were kept the same but the population counts were matched to test if a bioturbation impulse function is enough to create an offset in the resulting timing mimicking the observed deglacial onset. The bioturbation model takes the form of *Hutson* (1980):

$$I(d) = \frac{\sum_{i=1}^{m} ()\cdot P()\cdot ()}{\sum^{m}} ,$$
$$i=1\ ()\cdot P()$$

where $I(d)$ represents the mixed isotope value at depth d resulting from the impulse function; $H(i)$ represents the ith value of the impulse response function; $P(j)$ is the population total of the species at depth j; m is the vertical length of the impulse response function; j is the depth over which the impulse response function operates. The population assemblage data were linearly interpolated to represent every 1 cm of core from 155 to 230 cm (**Figure 3.12a**). The idealized isotopic values were constructed to have the onset of the glacial termination occur at 183cm for both species of foraminifera (**Figure 3.12b)**. For simplicity purposes the bioturbation impulse function was created as a Gaussian curve with an m of 31cm (**Figure 3.12c**). The bioturbation model illustrates that an isotopic offset cannot result from bioturbation if the population counts track with each other (**Figure 3.12d)**. This simulation confirmed that a bioturbation impulse function could not have caused the observed offset in the deglacial isotopic change. Therefore the offsets in the response of deglacial onset in *G. bulloides* and *G. inflata* must be real.

3.3.5 $\delta^{18}O$ Sea Water Estimation

The oxygen isotopic composition of foraminiferal calcite provides information about the oxygen isotope composition of the water mass. The, largest influences on $\delta^{18}O$ of ocean water ($\delta^{18}O_{SW}$) are the temperature at which the calcite precipitates and the ice volume effect on the global ocean. The effect of these two parameters must be removed to use $\delta^{18}O_{SW}$ to estimate changes in salinity and latitude of the source location of subsurface waters. The equation of *Shackleton* (1974) describes the thermal of effect on $\delta^{18}O$ during calcification

$$T°C = 16.9\text{-}4.0(\delta^{18}O_{calcite}\text{-}\delta^{18}O_{w})$$

Figure 3.12

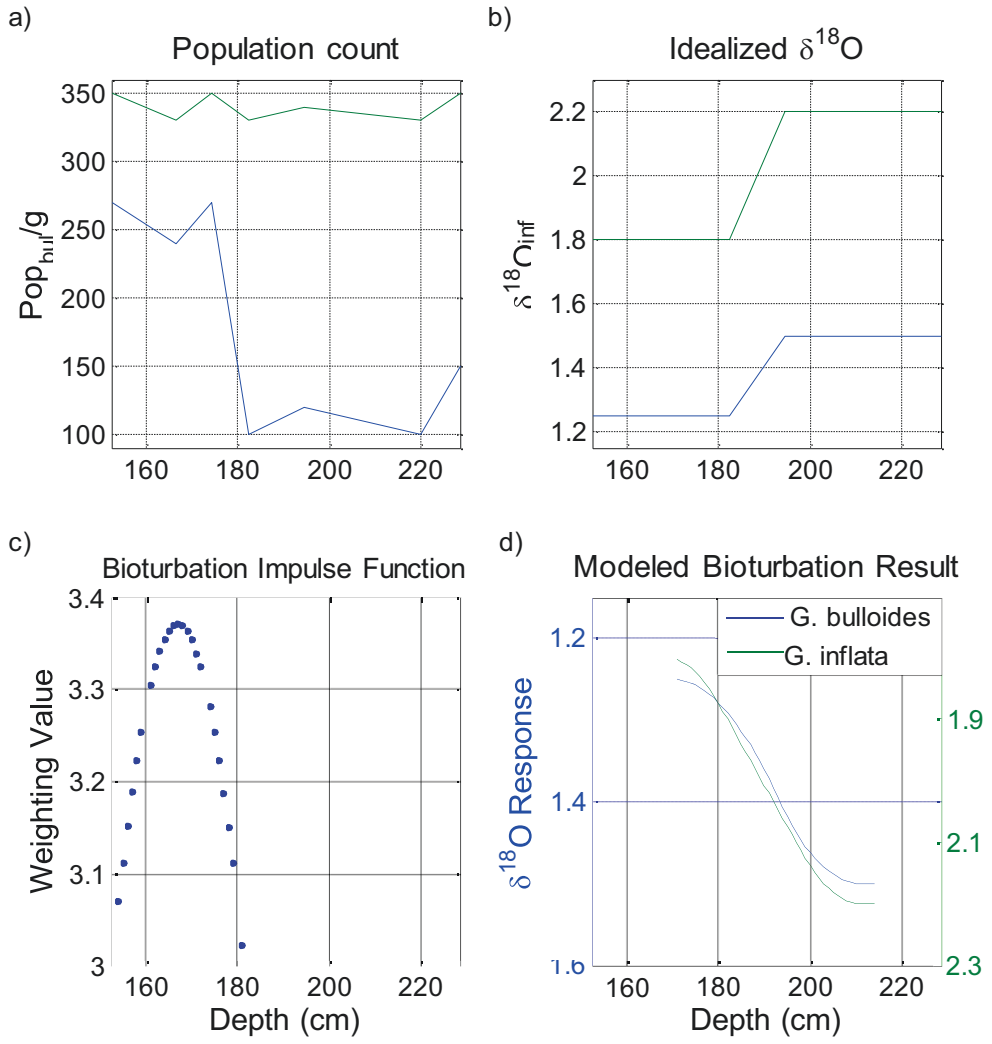

Figure 3.12| An evaluation of the influence of bioturbation on the offset in the timing of the deglacial onset in species *G. bulloides* and *G. inflata*. a) Assemblage counts of the population of *G. bulloides* (blue) and *G. inflata* (green) per gram of sediment. b) An idealized model of $\delta^{18}O$ for *G. bulloides* (blue) and *G. inflata* (green) with the isotopic signature of the deglacial onset occurring at the same depth in the core. c) A model of the bioturbation impulse function as is may affect the top 30 cm of sediment idealized to be a Gaussian filter which passes through the data set. d) The impulse response function as bioturbation affects the $\delta^{18}O$ for *G. bulloides* (blue) and *G. inflata* (green). Because the effect of our bioturbation impulse on oxygen isotopes does not impact the timing of the isotopic deglacial onset we can conclude the offset in our actual record is not a result of bioturbation.

To remove the ice volume effect on the $\delta^{18}O_{calcite}$ the, $\delta^{18}O_{bul}$ as measured (‰VBD), must be converted to units of units of standard mean ocean water used in the measurement of global mean ice volume:

$$\delta^{18}O_{bul}(‰ \text{ VBD}) = \delta^{18}O_{bul} (‰ \text{ SW}) - 0.27$$

The ice volume effect on $\delta^{18}O_{bul}$ (SW) can be back calculated by using the 30 kyr sea level reconstruction of *Peltier and Fairbanks* (2006) and converting their sea level height values to an estimate of $\delta^{18}O_{SW}$ caused by the storage of ice at high latitudes:

$$\delta^{18}O_{ice}(SW)=SLH*(-0.011)$$

This provides the effect of the ice volume, as interpreted by sea level change. The storage of ice at high latitudes results in the enrichment of ocean isotopic values, and the negative signal must be added back to the $\delta^{18}O_{bul}$ (SW) to acquire a $\delta^{18}O$ that no longer reflects a change in ice volume ($\delta^{18}O_{equ}$):

$$\delta^{18}O_{bul} + \delta^{18}O_{ice} = \delta^{18}O_{equ}$$

The SST as inferred from the Mg/Ca calibration (previous chapter), was used to estimate the thermal effect on $\delta^{18}O_{calcite}$. Substituting this SST into the *Shackleton* (1974) equation allows the calculation of $\delta^{18}O_{SW}$:

$$\delta^{18}O_{SW} (SW) = (T°C-16.9)/4.0 - \delta^{18}O_{calcite} (SW)$$

The resulting $\delta^{18}O_{SW}$ value now reflects only salinity and Rayleigh distillation and can be used to interpret the latitude and or salinity of the water masses (Broecker, 2002). Combining the 1σ standard error of the SST calibration, 0.8°C, with the 1σ standard error of the $\delta^{18}O_{bul}$ calculation, .08‰, yields a 1σ standard error of $\pm$.21‰ in the $\delta^{18}O_{sw}$ calculation (**Figure 3.13**).

Figure 3.13

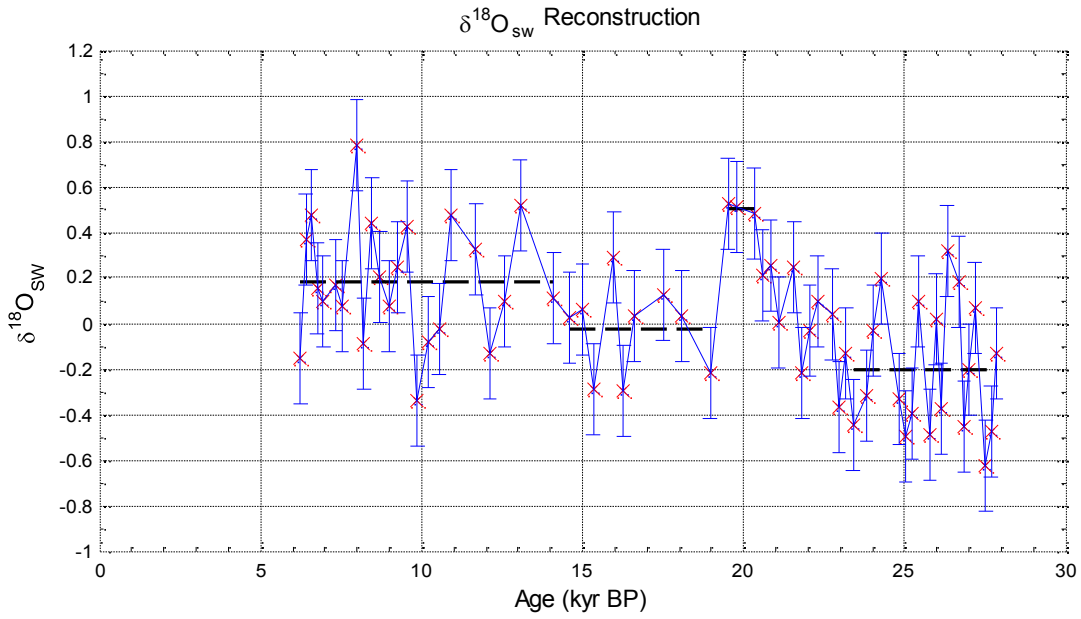

Figure 3.13| Reconstructed $\delta^{18}O$ of sea water ($\delta^{18}O_{SW}$) for core 87 JPC from the Bay of Plenty. In order to analyze $\delta^{18}O_{SW}$ the ice volume and temperature effect on $\delta^{18}O$ was first removed. The sea level reconstruction by Peltier and Fairbanks (2006) and the temperature equations of Shackleton et al. (1974) were used to remove these effects resulting in a reconstruction of $\delta^{18}O_{SW}$. The error bars reported are due to uncertainties in the variables input into these equations: $\delta^{18}O$ sea level estimation, the $\delta^{18}O$ of G. bulloides, and the Mg/Ca calibration. Because of the uncertainties here we highlight four large scale features in our reconstruction (black dashed line). The one sigma error bar of $\pm$0.2‰ associated with errors in the estimations translated through the $\delta^{18}O_{sw}$ calculation are reported. These four intervals of change are indicative of a four step change in surface water $\delta 18OS_W$ bringing our surface water mass from the last glacial maximum through to the Holocene.

The resulting $\delta^{18}O_{SW}$ reconstruction shows significant differences between the LGM and the Holocene (**Figure 3.13**). During the glaciation, $\delta^{18}O_{SW}$ values averaged -0.2‰. Beginning at 23 kyr BP a 0.2‰/kyr increase occurred with a three point maximum in $\delta^{18}O_{SW}$ of 0.5‰ at 20 kyr BP. After this peak there were two distinct shifts in surface water $\delta^{18}O_{SW}$. After the deglacial onset until the ACR, the $\delta^{18}O_{SW}$ average was 0.2‰ more enriched than the glacial average. After the ACR, $\delta^{18}O_{SW}$ values were highly variable but remained more enriched, on average by 0.2‰ into the Holocene. The depleted $\delta^{18}O_{SW}$ values during the LGM suggests that surface waters were either sourced at higher latitudes and/or were fresher at that time relative to modern waters in this region. The enrichment spike at the onset of the LGM suggests that a pulse of low latitude/saline water was advected into the Bay of Plenty followed by another rapid shift. After the shift back there was a gradual shift toward more enriched values, which persists into the Holocene indicating water masses gradually became either more saline or were sourced from lower latitudes. This series of three step changes between the glaciation and the Holocene.

3.4 Discussion

3.4.1 Evaluation of Bay of Plenty Stable Isotope Ensembles

Cores 64 JPC, 79 JPC, 87 JPC, and 125 JPC all have broadly similar deglacial isotopic records from the LGM to the Holocene with minor inter-core variability. At the $\delta^{18}O$ and $\delta^{13}C$ values for each species were interpolated to the same stratigraphy (0-30 kyr; n=301) and averaged; to create a collective ensemble representative of the Bay of Plenty (**Figure 3.6, 3.7, 3.8, 3.9**).

Within the Bay of Plenty ensemble the deglacial the $\delta^{18}O$ and $\delta^{13}C$ response of the shallower species, *G. bulloides,* differs from that of deeper subsurface species, *G. inflata*. There exists a two thousand year lag in the timing of the $\delta^{18}O$ deglacial onset between *G. inflata* to *G. bulloides* (**Figure 3.14**). The bioturbation modeling analysis conducted in two of the cores (described above; *Hutson*, 1980) verifies that this temporal offset is not a result of bioturbation. This suggests that the offset must result from the most shallow interior water mass, around 50 meters water depth, having experienced a $\delta^{18}O$ shift two thousand years earlier than the deeper subsurface water mass ~50 to 100 meters below the surface. At the same time ~20.1 kyr BP, there was a step change in the $\delta^{13}C$ of *G. bulloides* indicating the shallower interior water mass that did not occur in the deeper waters of the subsurface water column inhabited by *G. inflata* (**Figure 3.14**).

King and Howard (2004, 2005) showed that the calcite of *G. bulloides* and *G. inflata* possess different isotopic offsets compared the actual $\delta^{18}O$ and $\delta^{13}C_{DIC}$ in the water column. Acknowledging these offsets interpretations on the timing and amplitude of the isotopic changes as they relate to the water chemistry at these two different depths in the water column are possible and useful. The differences in the deglacial isotopic response between these two species indicate that there were fundamental changes in the two subsurface depths in the Southwest Pacific Ocean.

Shallow interior (<50m) Water Mass Shits

The *G. bulloides* record of shallowest interior water mass had depletions in $\delta^{18}O$ occurring at 20.1 kyr BP (**Figure 3.14a**). Three factors are known to affect the $\delta^{18}O$ isotopic composition of foraminifera on glacial to interglacial timescales: 1) the storage of isotopically

Figure 3.14

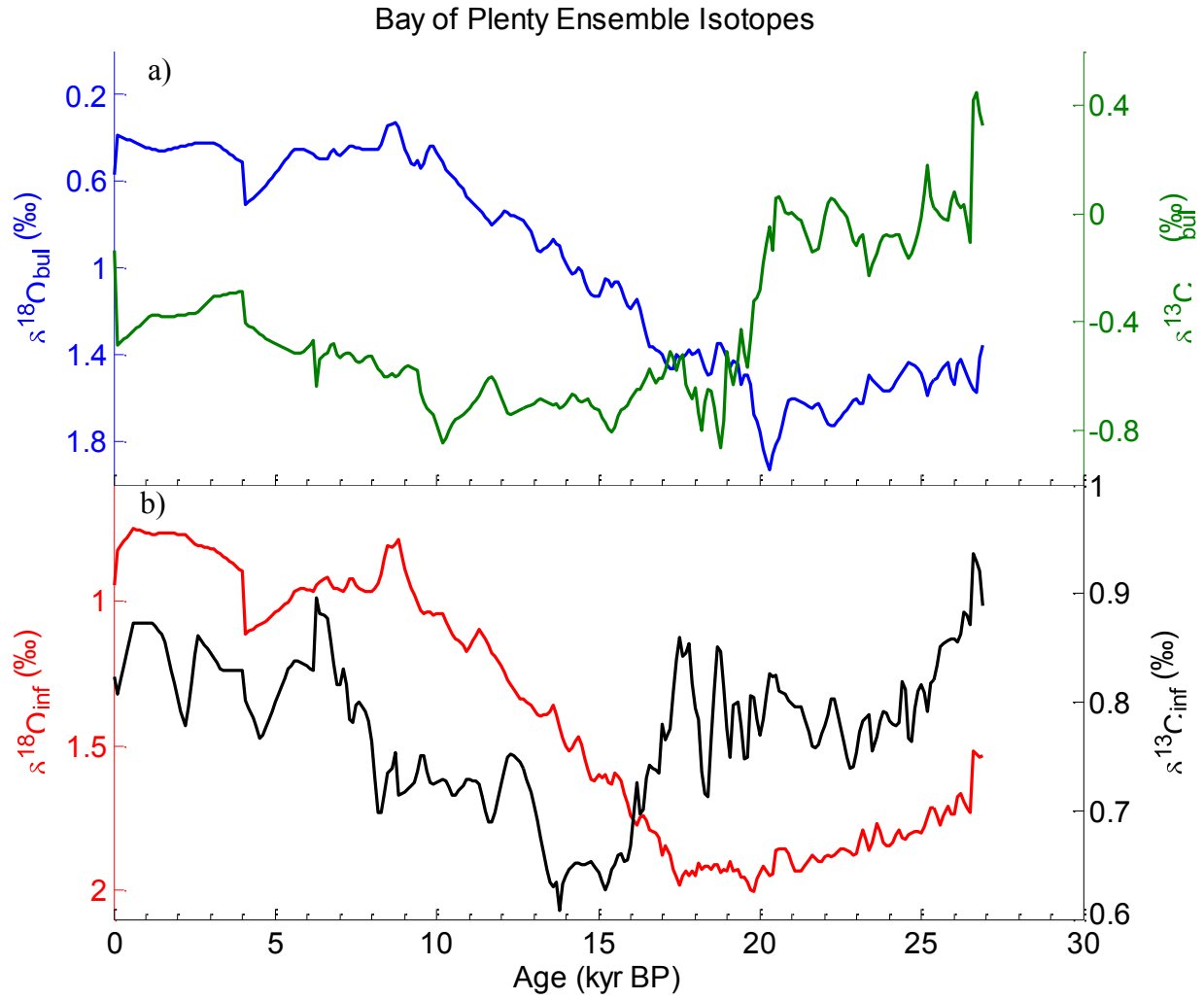

Figure 3.14| Bay of Plenty ensemble averages for *G. bulloides* $\delta^{18}O$ (blue) and $\delta^{13}C$ (green), along with *G. inflata* $\delta^{18}O$ (red) and $\delta^{13}C$ (black). Note the $\delta^{13}C$ step change in the shallow surface begins at ~20 kyr BP while the thermocline depletion does not occur until ~17.5 kyr BP. The timing of the deglacial $\delta^{18}O$ shift also occurs at 20 kyr BP in the shallow surface while the thermocline proxy does not begin until ~17.5 kyr BP. Recall these temporal differences cannot be a result of bioturbation.

depleted water in the form of large ice sheets 2) temperature impacting the thermal incorporation of water $\delta^{18}O$ into the shell 3) salinity and fractionation associated with the source latitude of the interior water mass. This shallow interior shift observed in the Bay of Plenty occurred before the major change in sea level at18.5 Kyr BP (*Peltier and Fairbanks,* 2006) and therefore must reflect a change in temperature and/or salinity. Isotopically depleted values are associated with fresher water masses and higher latitudes, such as the Southern Ocean, and enrichment with more saline water masses from lower subtropical latitudes (**Figure 1.1**). The reconstructed $\delta^{18}O_{SW}$ (**Figure 3.13**) spiked at the same time. Together these suggest there was a shift in source of these water from higher latitudes to lower, more tropical latitudes (**Figure 3.14**).

Concurrently, the *G. bulloides* $\delta^{13}C$ signal began a two thousand year 0.8‰ depletion from 21kyr BP to 19 kyr BP (**Figure 3.14a**). $\delta^{13}C$ changes can result from two processes: 1) changes in productivity with enhanced surface productivity taking in the lighter isotopes of carbon leaving the remaining dissolved inorganic carbon (DIC) pool available to shallow subsurface foraminifera isotopically heavy or 2) changes in the provenance and time of sequestration of the water masses with water masses that flow in from greater distances having accumulated a more depleted respired CO_2 signal along its flow path. This second mechanism implies $\delta^{13}C$ isotopic changes in this region resulted from a respired CO_2 signal with depleted $\delta^{13}C$ values having a distal and enriched $\delta^{13}C$ a more proximal source location. The $\delta^{13}C$ depletion at 20.1 kyr BP suggests there was a step change from a proximal source in the glaciation to more distally sourced thermocline waters at the start of the deglaciation. The concurrent $\delta^{13}C$ depletion and $\delta^{18}O_{SW}$ enrichment strengthens the interpretation that there was a shift in the source of shallow interior waters from the more proximal sourced Southern Ocean

in the LGM (**Figure 3.14a**) to more distal subtropical water that persisted throughout the deglaciation (**Figure 3.14b**).

Some portion of the $\delta^{13}C$ step change at the onset of deglacial warming may be attributable to $\delta^{13}C$ equilibrium theory as there is a high dependence of $\delta^{13}C$ fractionation on temperature (Mook, 1974). Air-sea exchange impacts $\delta^{13}C$ with colder waters able to hold more CO_2. In addition, during the dissolution of CO_2 into surface waters a fractionation occurs that is also temperature dependent. The greater capacity of colder waters to dissolve CO_2 and the greater fractionation at lower temperatures causes enriched $\delta^{13}C$ (Emerson and Hedges, 2008). However, in the New Zealand region, equilibrium is not usually reached because of the low residence time of surface waters. Therefore, air-sea exchange and the dependence of $\delta^{13}C$ fractionation on temperature is not a significant concern in the deglacial record around New Zealand.

After the deglacial step, the $\delta^{18}O$ and $\delta^{13}C$ data exhibited a slow continuous shift toward Holocene conditions. Most of the variability in the raw $\delta^{18}O$ signal is due to ice volume (Peltiers and Fairbanks, 2006) and the effect of SST changes (**Figure 2.3**) on the thermal incorporation of the $\delta^{18}O$. The $\delta^{18}O_{SW}$ reconstruction allows a clearer examination of the composition of shallow surface waters masses, and indicates there was a gradual shift to lower latitude, and or more saline source through the deglaciation (**Figure 3.15**). The supporting information from the $\delta^{13}C$ implicating a more distal source supports more input of tropically sourced waters similar to the STMW dominating in the modern era (Bostock et al, 2010). A more distal source location combined with the lower latitude source signal suggests that after the step change a greater volume of this water mass was sourced through the Equatorial Pacific.

Figure 3.15

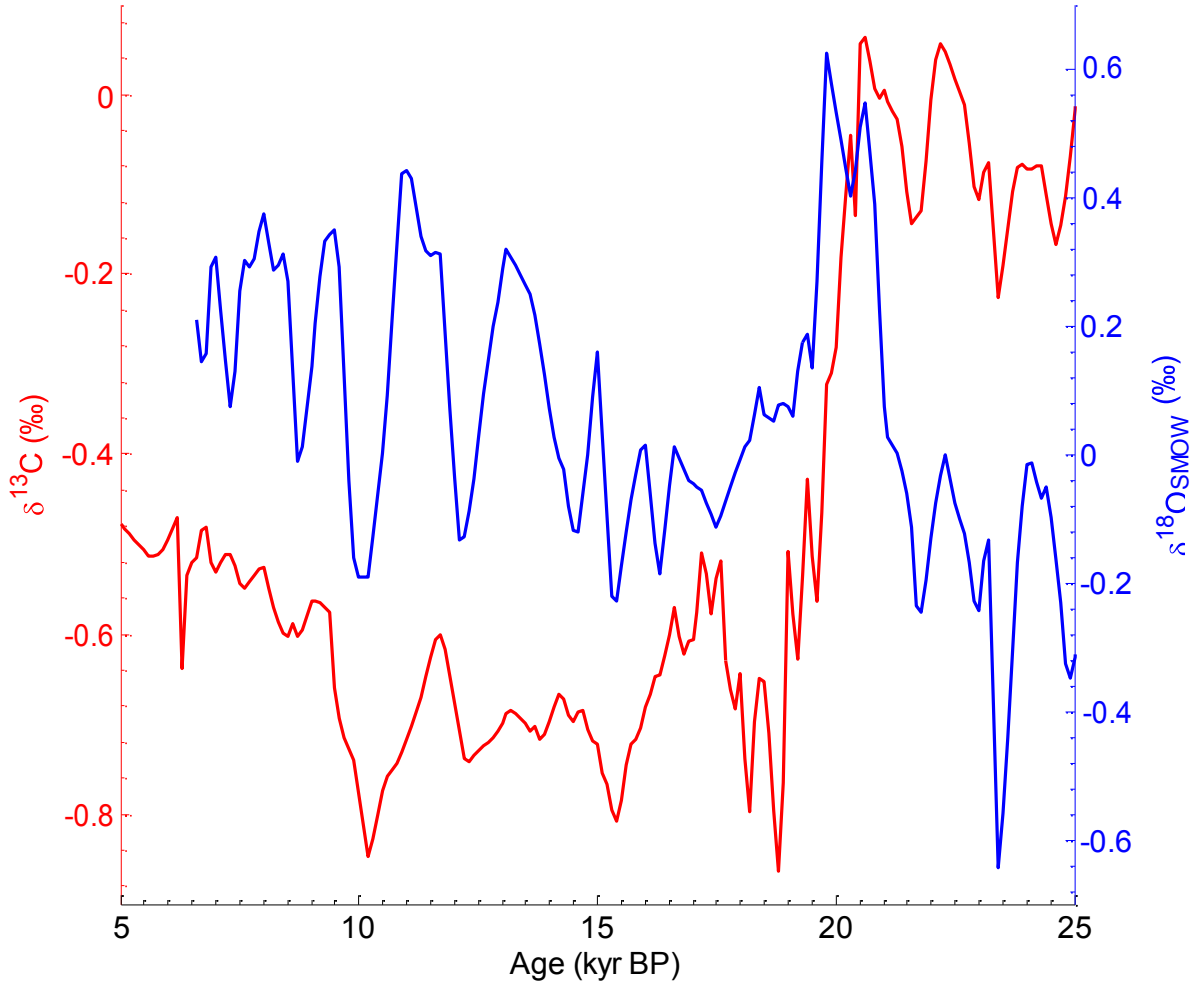

Figure 3.15| Comparison of deglacial changes in surface foraminifera $\delta^{13}C$ (red) with changes in the reconstruction of $\delta^{18}O_{SW}$ (blue) as depicted by Bay of Plenty sediment core 87JPC. Note that in the LGM, there is both a depleted $\delta^{18}O_{SW}$, which is indicative of a higher latitude fresher signal, and as enriched $\delta^{13}C$, which can be indicative of proximal source water locations. The combination strengthens the case for a Southern Ocean dominated source. In the Holocene enriched $\delta^{18}O_{SW}$, indicative of a lower latitude more saline signal, is accompanied by depleted $\delta^{13}C$, which can be indicative of longer flow path from source water locations. The combination suggests a dominance of waters from more distant tropical locations.

Deeper Subsurface (~100 m) Water Mass Shifts

The *G. inflata* record of deeper subsurface waters in the Bay of Plenty differs markedly from that of *G. bulloides*. The $\delta^{13}C$ was very steady with only a minor depletion of less than 0.3‰, beginning 17.5 kyr BP. Little to no change in subsurface water mass source occurred between the LGM and the Holocene. There was a low amplitude isotopic minimum at 14 kyr BP coincident with the global minimum $\delta^{13}C$ event described by *Spero and Lea* (2002) and discussed in greater detail in the subsequent section. The $\delta^{18}O_{inf}$ depletion was coincident with sea level increase (Peltier and Fairbanks, 2006) suggesting that global ice volume was the principle component of the deglacial $\delta^{18}O$ depletion. This is in stark contrast to the major source water shifts in shallower subsurface waters in the Bay of Plenty recorded by *G. bulloides*. This strongly suggests that water masses with different histories are present in the subsurface water column at the Bay of Plenty with a northern end member influencing the deeper subtropical shallow water column in the New Zealand region.

3.4.2 Regional near-surface circulation changes LGM to Present

Last Glacial Maximum (22-20 kyr BP) and Deglacial Onset (20-19 kyr BP)

During the LGM the shallow-surface water column in the in the New Zealand region of the Southwest Pacific Ocean had a different vertical structure than the Holocene (**Figure 3.16a,c,d**) with the isotopic properties and different source location of the sub-thermocline water masses. The position of the subtropical front (STF), the convergence region of subtropical water masses to the north and subantarctic water masses to the south, remained in the same position during the Holocene and the LGM (Sikes et al. (2002) supporting previous arguments that the front remained bathymetrically fixed on glacial interglacial time scales

Figure 3.16

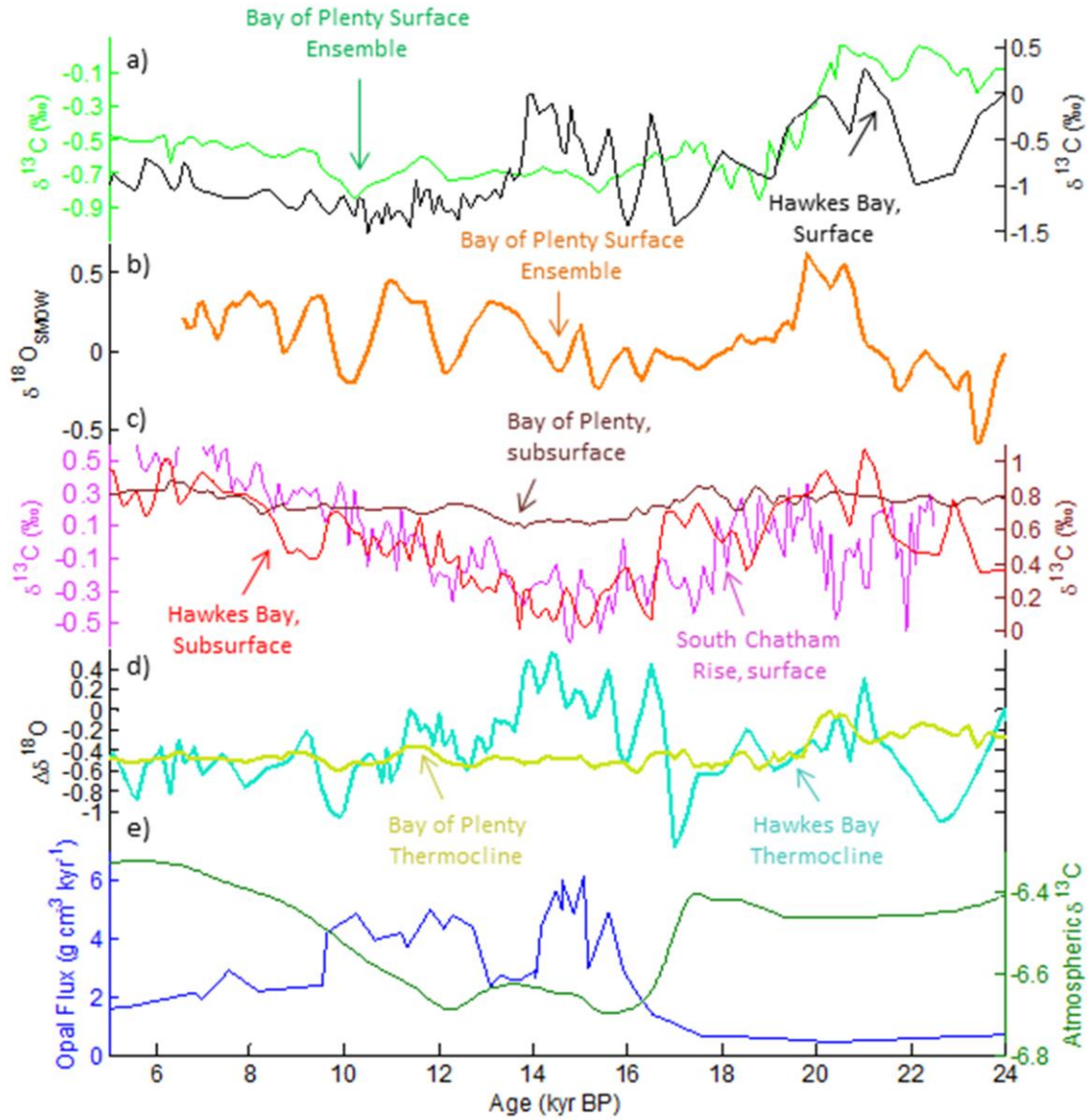

Figure 3.16 Compilation figure of the New Zealand region subsurface isotopes, Southern Ocean upwelling, and Antarctic atmospheric isotopes from the LGM to the Holocene. a, Bay of Plenty G. bulloides surface δ13C (green; this study) and G. bulloides surface δ13C (black; Carter et al., 2008) b, δ18OSW reconstruction derived from raw Bay of Plenty δ18Obul c, Bay of plenty G. inflata subsurface δ13C (maroon, right axis; this study), Hawks Bay G. inflata subsurface δ13C (red, right axis; Carter et al., 2008) and Chatham Rise G. bulloides surface δ13C (purple, left axis; Pahnke and Zahn, 2005) d, $\Delta\delta^{18}O$ for sub-thermocline foraminifera in the Bay of Plenty (vomit green) and Hawkes Bay (light teal) e, Opal fluxes (left), a proxy for Southern Ocean upwelling, from sediment core TN057-13-4PC (53°S, 5.1°E; blue), atmospheric δ13C (right) show as Monte Carlo mean reported by Schmitt et al., (2012) .

(Heath, 1972; Jillet, 1969; Shaw and Vennel, 2001). Today, core MD97-2120, on the western end of the south Chatham Rise, lies south of the STF underlying SAMW today (Pahnke and Zahn, 2005). Because the STF didn't move in the LGM, shallow dwelling foraminifera at this site can be assumed to have recorded the SAMW during the LGM. In this core the G. *bulloides* carbon isotope values during the LGM are enriched (**Figure 3.16a**) indicating the ventilation and proximal source of SAMW in the LGM was similar to today. In Hawkes Bay, isotopic values of *G. inflata* at MD97-2121, (Carter et al., 2007), track well with surface foraminifera at the south Chatham Rise suggesting the presence of SAMW in the subsurface (**Figure 3.16c**). This suggests that even well north of the STF a large component of the shallow ocean was under the influence of colder SAMW (Weaver et al., 1998; Carter et al., 2002; Pahnke and Sachs, 2006; Carter et al., 2007) during the LGM. Carbon isotopes of *G. bulloides*, surface foraminifera at Hawkes Bay were more enriched than modern values during the glaciation (Carter et al., 2008; **Figure 3.16a**). This suggests that there was a difference in water mass provenance at the LGM. The combined $\delta^{13}C$ and $\delta^{18}O_{SW}$ from the Bay of Plenty indicated shallow subsurface waters there came from a nearby high latitude source similar to Hawkes Bay and the South Chatham Rise. Unlike today, a component of shallow interior SAMW may have advected along a more direct path north from the STF thru Hawkes Bay to the Bay of Plenty carrying with it a proximal Southern Ocean signal.

The thermocline proxy can assist in placing the source water changes in the context of volume. The thermocline depth for the Hawkes Bay was calculated from previously published *G. bulloides* and *G. inflata* $\delta^{18}O$ for comparison to the Bay of Plenty discussed in section 3.3.2 (**Figure 3.17**). During the LGM in Hawkes Bay more negative $\Delta\delta^{18}O$ values suggest that the thermocline was shallow and there had been shoaling of the thermocline placing a thicker layer

Figure 3.17

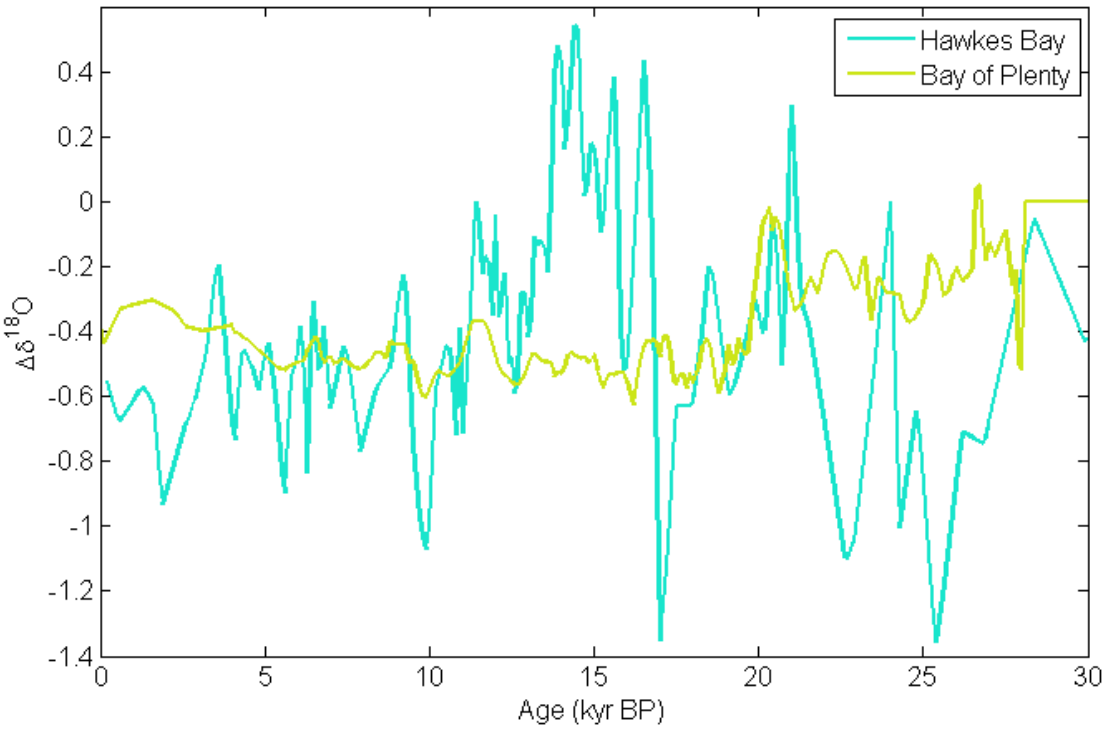

Figure 3.17| A comparison of Hawkes Bay (light blue) and Bay of Plenty (gold) $\Delta\delta^{18}O$. Note the during the deglaciation (20-18kyr BP) Hawkes Bay and the Bay of Plenty both have a shoaling of the thermocline evidenced by $\Delta\delta^{18}O$. The Bay of Plenty thermocline remains shoaled into the Holocene whereas the Hawkes Bay thermocline depth is highly variable until the ACR after which the thermocline remains permanently shoaled with similar $\Delta\delta^{18}O$ values to the Bay of Plenty.

of SAMW in the subsurface ocean to the east of the North Island (**Figure 3.16d**). In the Bay of Plenty LGM, the thermocline proxy was close to zero (**Figure 3.16d**) indicating a deeper thermocline or a less stratified surface ocean. In the glacial Bay of Plenty, a thicker mixed layer contained a greater component of proximally sourced fresher SAMW (**Figure 3.16a,c,d**). *Anderson et al.* (2009) show reduced upwelling in the Southern Ocean during the LGM. This reduction may have resulted from southern hemispheric conditions where the southern hemisphere trade winds were weakened and shifted north (Russell et. al., 2006; Toggweiler et al., 2006; Toggweiler 1999) impacting the mixed layer in the Bay of Plenty. Nonetheless, SAMW was present at shallower depths near Hawkes Bay, resulting in a shoaled thermocline and allowing these water masses to become a more integral component of the surface water mass in the Bay of Plenty.

During the period of maximum ice sheet extension (20-19 kyr BP) changes began in the shallowest subsurface of the subtropical New Zealand region. In the Bay of Plenty, these changes were marked by a pulse of subtropical saline waters that occurred in tandem with a clear shift from proximal to distally-sourced shallow interior waters. In Hawkes Bay, a similar $\delta^{13}C$ depletion in *G. bulloides* indicated a shift to distally sourced subtropical waters, as in the Bay of Plenty. The lack of change of the south Chatham Rise $\delta^{13}C$ indicate no SAMW south of the STF. The *G. inflata* $\delta^{13}C$ show no depletion, indicating deeper depths in both the Bay of Plenty and Hawkes Bay, had proximally sourced, likely Southern Ocean, water mass (**Figure 3.18**). The common proximal signature at the latter three locations indicate the dominate water mass at deeper depths in the Bay of Plenty and at Hawkes Bay must be the SAMW seen in the shallow interior of the south Chatham Rise (**Figure 3.16a and 3.18a**).

Figure 3.18

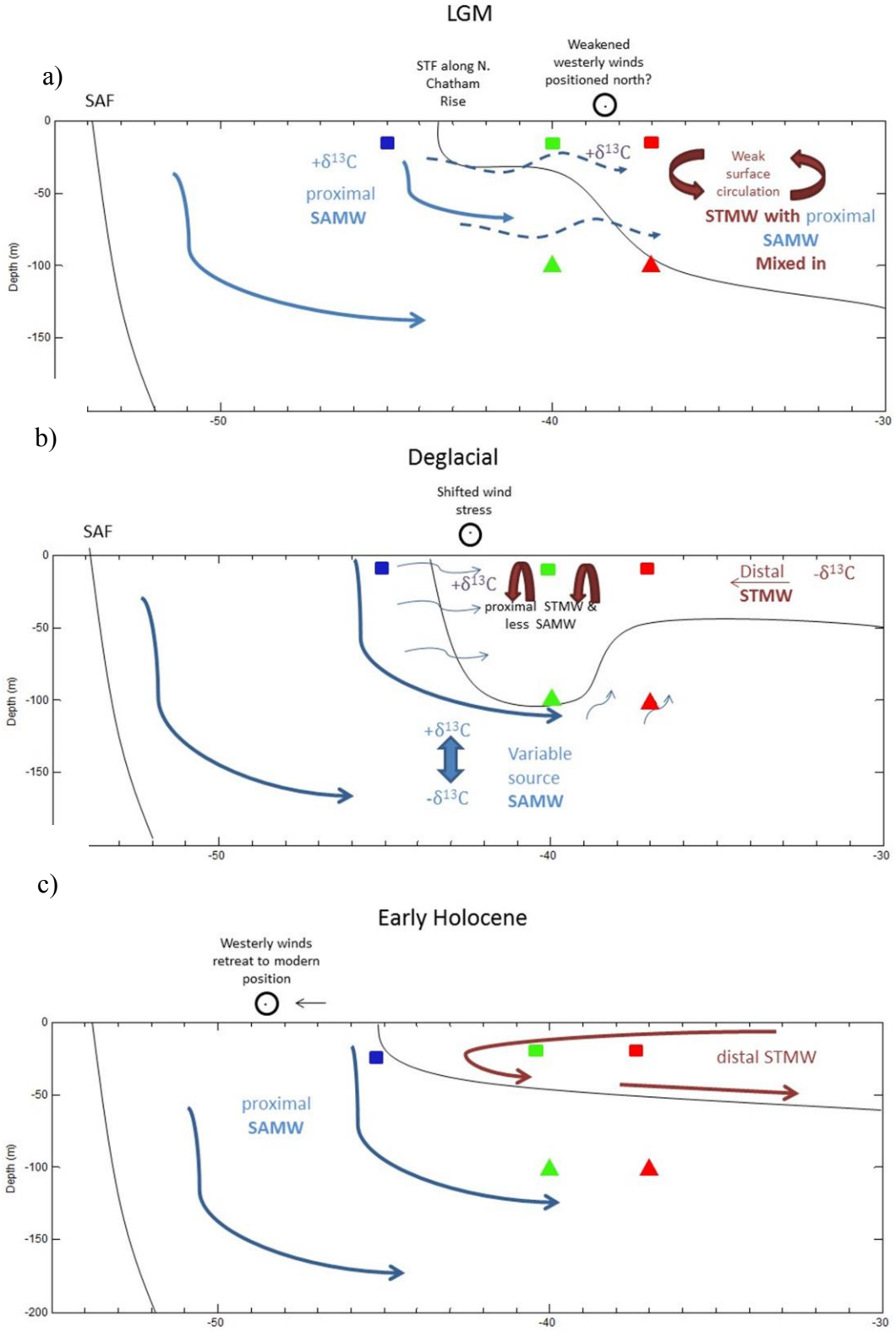
LGM
a)
SAF
STF along N. Chatham Rise
Weakened westerly winds positioned north?
+δ13C
proximal SAMW
+δ13C
Weak surface circulation
STMW with proximal SAMW Mixed in
Depth (m)
0
-50
-100
-150
-50
-40
-30
b)
Deglacial
Shifted wind stress
SAF
+δ13C
proximal STMW & less SAMW
Distal STMW
-δ13C
+δ13C
-δ13C
Variable source SAMW
Depth (m)
0
-50
-100
-150
-50
-40
-30
c)
Early Holocene
Westerly winds retreat to modern position
proximal SAMW
distal STMW
Depth (m)
0
-50
-100
-150
-200
-50
-40
-30

Figure 3.18| Two dimensional latitudinal transect of the shallow surface structure in the Southwest Pacific Ocean inferred from $\delta^{13}C$ and $\delta^{18}O$ of surface dwelling *G. bulloides* (square), and subsurface dwelling *G. inflata* (triangle). Data and interpretations from cores MD-97 2120 (blue; Pahnke and Zahn, 2005), MD-97 2121 (green; Carter et al. 2008), and the Bay of Plenty Ensemble (red; this study) are used to develop this model. Section **a**, is representative of likely glacial circulation and water column structure centered are 22-20 kyr BP **b,** represents circulatory patterns and water column structure defined by the early deglacial interval (16.7-14.5 kyr BP), and **c**, represents the early Holocene structure and circulation of the southwest Pacific Ocean.

Early Deglaciation (17-14.5 kyr BP) and ACR (14.1-12.4)

During the early deglaciation the waters which dominated at the Bay of Plenty and the south Chatham Rise became similar to modern. In the Bay of Plenty the thermocline shoaled due to an influx of distal subtropical water masses (**Figure 3.18b and Figure 19a**). Further south at the Chatham rise SAMW continued to dominate (**Figure 3.18b**). In contrast, Hawkes Bay appears to have been be a battle ground between competing proximal subantarctic and distal subtropical influences as evidenced by the large swings in the $\Delta\delta^{18}O$ the LGM to the ACR (**Figure 3.17**). In Hawkes Bay, after the initial deglacial shift, ~20 kyr BP from proximal to distally sourced waters there were swings between them a distal and a proximal source up until 12.1 kyr BP (**Figure 16, 17, 18b, 19a)**. Moreover, these shifts to more proximal waters were coincident with shifts to deeper thermocline depths while the shifts to distal coincided with shoaled thermocline depths. The same pattern was evident in the Bay of Plenty however, only the salinity reconstruction suggested a high to low latitude source shift (**Figure 3.16b**). At Hawkes Bay a salinity reconstruction was not available. But, if we assume the Bay of Plenty pattern held true for Hawkes Bay, the thermocline and source shifts suggest there was a continuing tradeoff between equatorial Pacific and Southern Ocean sources. At Hawkes Bay, this battle played out for the duration of the early deglacial interval establishing this mid-latitude location as key area for the tracing Southern Hemisphere source water shifts.

Early in the deglacial transition there was a $\delta^{13}C$ isotopic minimum event (Spero and Lea, 2002) that has been hypothesized to be related to a marked increase in Southern Ocean upwelling (**Figure 3.16e**) caused by the strengthening and southward shift of the southern hemisphere westerlies (Anderson et al., 2009; Toggweiler et al., 2006; Toggweiler, 1999). The carbon isotope minimum has been recorded in many locations of the world's oceans and is

Figure 3.19

a) b)

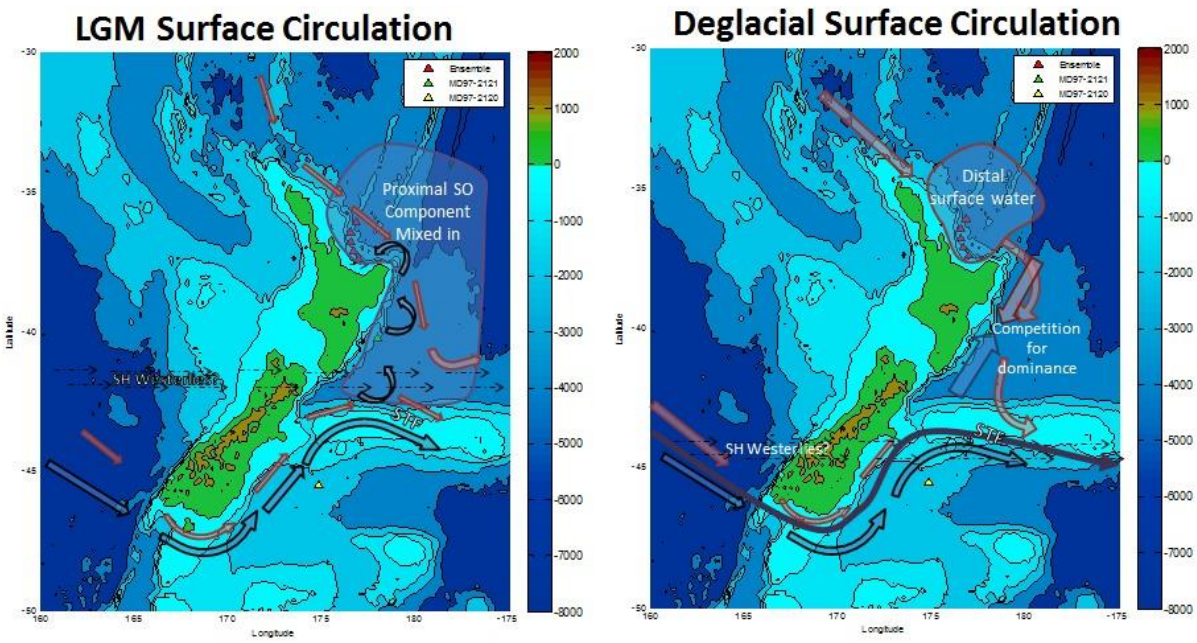

Figure 3.19 .Schematic maps of the suggested changes in circulation a) glacial b) deglacial surface circulation. Note that during the LGM subantarctic waters were a component of surface waters in the Bay of Plenty but after the onset of the deglaciation the Bay of Plenty is dominated by distally sourced Subtropical Mode Water (STMW; red) while the south Chatham Rise is dominated by proximally source Southern Ocean Subantarctic Mode Water (SAMW; blue). SAMW is getting passed the Subtropical Front (STF; purple) resulting in a deglacial battle for competing influence of SAMW and STMW at Hawkes Bay.

believed to have resulted from the transfer of highly depleted preformed $\delta^{13}C$, sourced from the deep water, that was advected north via AAIW and SAMW (Ninneman and Charles, 1997; Spero and Lea, 2002). Closely following this isotopic depletion in surface ocean waters, was depletion in atmospheric $\delta^{13}C$ of the indicating that stored carbon was vented into the atmosphere (Schmitt et al., 2012). The oceanic $\delta^{13}C$ minimum was recorded on the south Chatham Rise, in the shallow sub-surface at Hawke's Bay where SAMW was the dominant subsurface water mass, and in the deeper subsurface Bay of Plenty though at a much lower amplitude (F**igure 3.16c**). In shallower layers of the Bay of Plenty the isotopic minimum manifested as a secondary depletion event embedded within the step change that was in phase with Southern Ocean upwelling increase (**Figure 3.16e**). This secondary isotopic minimum may have resulted from either a subdued SAMW component in the Bay of Plenty (Marino et al., 1992; Spero and Lea, 2002) or from the transfer of this signal through STMW from the upwelling in the Equatorial Pacific. The increased stratification of the Bay of Plenty water column at the same time contradicts the interpretation that this signal was mixing up from greater depths. Therefore, it is more likely that an Equatorial Pacific component was responsible for the advection of this signal into the Bay of Plenty. Regardless of the mechanism, the carbon isotope minimum described by *Spero and Lea* (2002) was muted to the north, but evident in the shallow surface ocean in the region surrounding New Zealand attributable to increased venting of Southern Ocean deep water.

The Antarctic Cold Reversal (ACR; 14.5-12.1 kyr BP) appears to have been a tipping point in this region of the subtropical Pacific, after which oceanic conditions trend towards modern. During the ACR, at Hawkes Bay, the shallow surface waters shifted to distally sourced water masses and the thermocline shoaled, mirroring the initial early deglacial step

change in the Bay of Plenty (**Figure 3.18a and Figure 3.19**). After the ACR step, the shallow interior water masses permanently shifted towards modern values as STMW took over. The ACR was a tipping point at Hawkes Bay but apparently elsewhere in the subtropical Pacific. During the ACR was an invigoration of the EAC to volumes similar to modern (Bostock et al., 2004). Modeling studies indicate equatorial Pacific trade winds strengthened and shifted towards a more modern position (Bush and Philander, 2002). It is broadly evident that in the mid-latitude Pacific Ocean the ACR marks a step change towards surface circulation and water column structure more similar to that seen in the modern.

Early Holocene (12.1 kyr BP-)

After the ACR, water column structure in the New Zealand sector of the southwest Pacific Ocean resembled the modern ocean. At Hawkes Bay and in the Bay of Plenty the thermocline shoaled to a modern position with a newly established dominance of STMW across the region north of the STF. At the south Chatham Rise, and in the deeper subsurface depths at the two northern sites, SAMW was isotopically similar to modern, with a less respired CO_2 signal. The regional water column and the vertical structure of the water column began to resemble today (**Figure 3.16c**).

3.5 Conclusion

In summary, during the LGM the shallow subsurface water masses had a much greater component of locally sourced Southern Ocean (high latitude) water. In the mid-latitudes, the deglacial onset had a dramatic step change from nearby to more distant low latitude sources of subsurface water masses. In the Bay of Plenty, the deglaciation played out with a gradual deepening of the thermocline as dominant water masses began to advect from lower latitude, distal locations. At Hawkes Bay, the deglaciation played out as a battle for dominance between

proximal Southern Ocean source water and distal subtropical sources. The ACR appears to have been a tipping point in the transition from LGM to Holocene, after which subantarctic water masses were tamed and hold their present day configurations. Our results identify the mid-latitudes, such as the area offshore of the North Island, as a key region in deciphering Southern hemisphere source water shifts.

Chapter 4

4. Multi-proxy Synthesis

4.1 Summary

Multi-proxies were applied to cores in the Bay of Plenty to examine the deglacial Southwest Pacific Ocean SST and shallow subsurface properties. The Mg/Ca analysis of *G. bulloides* and the U^{37}_{3} index of alkenones from cores 87JPC/TC provided SST records of the deglacial spring and summer SST changes in the Bay of Plenty. The combination of these new SSTs records with previously published SSTs from Hawkes Bay (core MD97-2121) and the South Chatham Rise (core MD97-2120) allowed for a regional comparison of subtropical and subantarctic seasonal SSTs. The $\delta^{13}C$ and $\delta^{18}O$ of *G. bulloides* and *G. inflata* were used to track shallow and deep changes in the water changes in the sub-thermocline waters of the south Pacific Ocean. $\delta^{13}C$ tracks changes in respired CO_2 while the $\Delta\delta^{18}O$ tracks changes in shallow surface stratification. To estimate the $\delta^{18}O_{SW}$ the Mg/Ca SSTs were used to remove the temperature effect on $\delta^{18}O$ and the ice volume effect was removed using the reconstruction of *Peltier and Fairbanks* (2006). The combination of these proxy records leads to a more comprehensive picture of seasonal temperature and thermocline source water changes throughout the deglaciation.

The Bay of Plenty Mg/Ca and alkenone SST records in this study region are rectifiers for spring and summer temperatures. This study assumes modern seasonal growth preferences hold true in previous climates. During the LGM, 26-22 kyr BP, summer SSTs averaged 16.4°C after which they warmed until the ACR when SSTs plateaued at 19.5°C. Spring SSTs tracked well with summer SSTs through the ACR and remained 3.2-2.6°C cooler than summer SST.

Summer SSTs continued to rise after the ACR peaking as did local November insolation at 10kyr BP when SSTs reach 21.5°C. Spring SSTs also warmed but did not peak until 8 kyr BP at the time September insolation reaches a maximum. Comparing the Bay of Plenty spring and summer SST data to insolation models based on Milankovitch forcing indicates that the annual minimum insolation value tracked well with both seasons from the LGM through to the ACR, 14.1 kyr BP. After the ACR there was a tight correlation of the spring and summer proxies to September and November insolation, respectively, highlighting the ACR as a tipping point after which SSTs track well with the monthly insolation expected to drive temperatures during the peak flux. The results of this study suggest that local SSTs were driven primarily by local insolation with shifts from being driven by minimum insolation to the insolation of the specific proxy's season with the shift occurring at the ACR.

The multi-proxy SST comparison in three New Zealand cores demonstrates that the LGM-Holocene difference in the subantarctic waters is less than the difference evidenced in subtropical waters. In the Bay of Plenty, the greater difference of 4°C is a degree more than the south Chatham Rise site, 3°C. This greater SST change at the Bay of Plenty may have been caused by cooling from the influence of the northward shifted subantarctic winds during the LGM or warming resulting from enhanced influence of subtropical water masses sourcing in from the equatorial Pacific during the early Holocene.

Planktonic foraminiferal stable isotopes in the Bay of Plenty during the LGM had depleted $\delta^{18}O_{SW}$ values of ~-0.2‰, coincident with enriched $\delta^{13}C$ values. The combination of these two lines of evidence indicates proximally sourced Southern Ocean waters were advecting as far north as the Bay of Plenty. At the same time thermocline depth estimates from $\Delta\delta^{18}O$ values (-0.2‰) indicate that when the Southern Ocean influence was apparent in the Bay

of Plenty the shallow interior Ocean was less stratified. At the onset of the deglaciation there was a brief pulse of low latitude saline waters as $\delta^{18}O_{SW}$ values reached a 1 kyr peak of 0.5‰. This pulse was marked by a shoaling of the thermocline as $\Delta\delta^{18}O$ dropped to ~-0.4‰ and a shift to more distally sourced water evidenced by a rapid -0.4‰ shift in $\delta^{13}C$. After the pulse of low latitude/saline water masses $\delta^{18}O_{SW}$ dropped to ~0.0‰ and gradually rose to a Holocene average of ~0.3‰ suggesting a steady shift to more saline subtropical water masses. During this interval, 18 kyr BP to present the thermocline remained shoaled and waters remained distally sourced. This combination of $\delta^{18}O_{SW}$ and $\delta^{13}C$ data suggests that during the LGM the shallow Bay of Plenty was more greatly influenced by proximal Southern Ocean water and after the deglacial the sources shifted to a primarily distal, equatorially sourced, subtropical component.

At the Hawkes Bay site, the initial deglacial step change tracked well with the Bay of Plenty step change as evidenced by the 1.0‰ $\delta^{13}C$ depletion and a $\Delta\delta^{18}O$ shift similar to the Bay of Plenty. However at Hawkes Bay, the $\delta^{13}C$ deglacial step change is followed by a series of flip-flops with $\delta^{13}C$ varying between 0.3‰ and -1.4‰ until the onset of the ACR. Significantly, shifts to negative $\delta^{13}C$ accompany more negative $\Delta\delta^{18}O$ excursions. These swings suggest a battle between distal subtropical water shoaling the thermocline and proximal subantarctic influences deepening the thermocline. The ACR marked a shift at Hawkes Bay after which the thermocline deepened and waters were more distally sourced, marking the ACR as a major tipping point after which circulation is very similar to modern.

4.2 Deglacial History of the New Zealand shallow surface Ocean

During the LGM the Bay of Plenty and the Hawkes Bay shallow surface Ocean had a large component of cooler fresher subantarctic mode waters marked by a deepening

thermocline. In the Bay of Plenty, deglacial warming began 21 kyr BP coincident with the pulse of low latitude saline source waters. At 20.5 kyr BP $\delta^{18}O_{SW}$ peaked and $\delta^{13}C$ began a rapid deletion indicating a maximum influence of distally saline subtropical water masses sourced through the equatorial Pacific was present in the region. Concurrently, the Bay of Plenty thermocline began to shoal. At Hawkes Bay the summer SST rise also occurred at 21 kyr BP. The shoaling of the thermocline and depletion of $\delta^{13}C$ were concurrent with events in the Bay of Plenty. However, the Bay of Plenty $\delta^{13}C$ depletion leveled off at ~19 kyr BP after which point the thermocline remained shoaled while the Hawkes Bay depletion continued until 18 kyr BP after which the thermocline deepened and $\delta^{13}C$ enriched. Further south in the subantarctic waters at the south Chatham Rise spring and summer SSTs did not begin to increase until ~19 kyr BP at which point the surface $\delta^{13}C$ at this site also began a more gradual depletion.

SSTs continued to rise at all three through the early deglacial interval, 19 kyr BP to 14.1 kyr BP. At the Bay of Plenty, the thermocline remained shallow and the respired CO_2 signal persisted steadily while the deeper $\delta^{13}C$ began a moderate enrichment. In the shallow surface at Hawkes Bay the thermocline depth shoaled in phase with $\delta^{13}C$ enrichments flip-flopping throughout the entire interval. The deeper $\delta^{13}C$ at Hawkes Bay began a depletion which tracked well with that at seen in the south Chatham Rise surface Ocean. These depletions occur in phase with the increase Southern Ocean upwelling, all three peaking between 16-15 kyr BP during which time the Southern Ocean upwelling is at a maximum value. These depletions are attributed to the degassing of the Southern Ocean.

At the onset of the ACR, 14.1 kyr BP the deglacial warming slows at all three sites, declining during the Bay of Plenty summer. At this point the Hawkes Bay thermocline shoals

and distally sourced waters, similar to the Bay of Plenty, begin to dominate this region. Also at the onset of the ACR, Southern Ocean upwelling ceased and the deeper water masses in the subtropical Pacific began a $\delta^{13}C$ enrichment. After the ACR, 12.1 kyr BP, SSTs increased again and the shallow surface structure of in the New Zealand region began to resemble modern. At the south Chatham Rise the rate of increase in summer SSTs was much faster than the subtropical alkenone records; this increase caused SSTs at the south Chatham Rise to overshoot later-Holocene values by 4°C at ~12.6 kyr BP. Mid-Holocene peaks are evident in the Bay of Plenty at 10 kyr BP, and at Hawkes Bay around 9 kyr BP. However, south Chatham Rise SSTs decreased over 2°C to modern values abruptly between 9-10 kyr BP while the subtropical sites have a more gradual temperature decrease in phase with local insolation. By 8kyr BP the isotopic signatures in the vertical water column at all coring sites resembled modern values while the SSTs in the Bay of Plenty and Hawkes Bay continued to decrease steadily with local insolation.

4.3 Synthesis

The difference between LGM and Holocene SSTs is greater at the subtropical core sites than at the subantarctic core sites. The combination $\delta^{18}O_{SW}$, $\delta^{13}C$, and $\Delta\delta18O$ analyses indicate that during the LGM subantarctic sources had a proximal Southern Ocean component marked by a deeper thermocline while the Holocene was dominated by more distally sourced subtropical mode water and a shoaled thermocline. The comprehensive multi-proxy analysis shows that the increased subtropical influence which persisted into the Holocene contributed to a greater deglacial warming at subtropical sites than seen at the subantarctic site. The warmer SSTs which persisted in the Holocene also likely contributed to the more stratified shallow surface ocean marked by the shoaling of the thermocline. At 15 kyr BP the deeper

foraminiferal record had a $\delta^{13}C$ minimum in linked to subantarctic water masses which was muted in surface foraminifera record. Warmer SSTs caused by the increased influence of subtropical water masses may have more strongly stratified the surface ocean, shoaling the thermocline, and limiting the amount of respired CO_2 able to mix into the subtropical water masses muting the signal in surface foraminifera. Therefore, the combination of stable isotopes and SST proxies lead to a more detailed interpretation of the deglacial changes through the investigation of SSTs and thermocline source water changes at the Bay of Plenty.

The comparison of SST evidence to modeled insolation illustrates that the ACR was a tipping point in the deglacial progression. After the ACR, SSTs no longer track well with the annual minimum insolation but instead shift and appear to be driven by the insolation predicted to drive the season of maximum export flux. Maximum foraminifera flux occurs in October, SSTs lag insolation by two months causing August insolation to drive their SST signal. Alkenone flux maximum is November which fits well with September insolation driving the SST. These two independent data streams establish the ACR as both a tipping point after which the modern SST response to insolation is established and also a tipping point after which the mid-latitude sub-thermocline water mass structure appears to shift towards a more modern structure but also a time after which the relationship between seasonal SST responses to seasonal insolation become similar to the modern. The use of multiple proxies links the establishment of a more modern water column structure to the seasonal SST-seasonal insolation relationship.

This multi proxy approach leads to a more comprehensive understanding of deglacial changes in the southwest Pacific Ocean because changes in SST can be interpreted alongside the isotopic interpretation of source water changes.

Citations

Alley, R. B. & Clark, P. U., 1999.The deglaciation of the northern hemisphere: a global perspective. Annu. Rev. Earth Planet. Sci. 27, 149–182

Anderson, R. F., S. Ali, L. I. Bradtmiller, S. H. H. Nielson, M. Q. Fleisher, B. E. Anderson, and L. H. Burckle, 2009. Wind-driven upwelling in the Southern Ocean and the deglacial rise in atmospheric CO_2, *Science*, **323**, 1441-1448

Bard, E. (2001). Comparison of alkenone estimates with other paleotemperature proxies. Geochemistry Geophysics, Geosystems, 2(1). Doi: 10.1029/2000GC000050

Bard E., R.E.M. Rickaby, (2009) Migration of the subtropical front as modulator of glacial climate. Nature, 460, pp.380-384 doi: 10.1038/nature08189

Barrows, T. T., S. Juggins, P. Dedeckker, J. Theide, and J. I. Martinez, Sea surface temperatures of the southwest Pacific Ocean during the Last Glacial Maximum, Paleoceanography, 15, 95– 109, 2000.

Barrows, T., Juggins, S., De Deckker, P., Calvo, E. & Pelejero, C., 2007. Long-term sea surface temperature and climate change in the Australian–New Zealand region. *Paleoceanography* **22**, 1–17.

Be, A.W.H., 1960. Ecology of Recent Planktonic Foraminifera: Part 2: Bathymetric and Seasonal Distributions in the Sargasso Sea off Bermuda. *Micropaleontology, 6,4,* pp.373-392

Be, A.W.H., 1977. In: Ramsey, A.T.S. (Ed), An ecological, zoogeographic and taxonomic review of recent planktonic foraminifera. Oceanic Micropaleontology, col. 1. Academic Press, London, pp. 1-100

Be, A.W.H (1982). Biology of Planktonic Foraminifera. Studies in Geology, 6, pp.51-92

Be, A.W.H, D.S. Tolderlund, 1971. Distribution and ecology of planktonic foraminifera. In: Funnell, B.M., Reidel, W.R. (Eds), The Micropaleontology of Oceans. Cambridge University Press, London, pp. 105-150

Be, A.W.H., and Hamlin, W.H., 1967.Ecology of recent planktonic foraminifera, Part 3. Distribution in the North Atlantic during the summer of 1962. Micropaleontology, 13(1), pp.87-196

Belkin, I. M., and A. L. Gordon (1996), Southern Ocean fronts from the Greenwich meridian to Tasmania, J. Geophys. Res., 101, 3675– 3696, doi:10.1029/95JC02750.

Blunier, T., Brook, E.J., (2001) Timing of Millennial-Scale Climate Change in Antarctica and Greenland During the Last Glacial Period. Science, 291, pp.109-112

Blunier,T., J., Chappallaz, J., Schwander, A., Dallenbach, B., Staufer, T.F., Stocker, D. Ranaud, J., Jouzel, H.B. Clausen, C.U. Hammer, S.J. Johnsen 1998. Asynchrony of Antarctic and Greenland climate change during the last glacial period. *Nature, 394(6695),* pp. 739-743

Blunier, T., Schwander, J., Stauffer, B., Stocker, T., Dällenbach, A.,Indermühle, A., Tschumi, J., 1997. Timing of the Antarctic Cold Reversal and the atmospheric increase with respect to the Younger Dryas event. *Geophysical Research. Letters, 24,* pp. 2683–2686.

Bostock, H. C., B. N. Opdyke, M. K. Gagan, A. E. Kiss, and L. K. Fifield (2006), Glacial/interglacial changes in the East Australian current, Climate Dynamics , 26, doi:10.1007/s00382-005-0103-7.

Bostock, H.C., B.N. Opdyke, M.K. Gagan, L.K Field, 2004. Carbon isotope evidence for changes in Antarctic Intermediate Water circulation and ocean ventilation in the southwest Pacific during the last deglaciation Paleoceanography, 19, PA4013, doi:10.1029/2004PA001047

Bostock, H.C., Opdyke, B.N, Williams, M.J.M, 2010. Characterizing the intermediate depth waters of the Pacific Ocean using $\delta^{13}C$ and other geochemical tracers. Deep-Sea Research 1, 57 pp.847-859

Broecker, W.S., 1982. Glacial to interglacial changes in oceanography. Progressive Oceanography, 11, pp. 151-197

Broecker, W.s, 1994. Massive iceberg discharges as triggers for global climate change. Nature, 372, 421-424.

Broecker, W.S., (2002). The Glacial World According to Wally. Palisades, NY: Eldigio Press, Lamont-Doherty Earth Observatory

Bush, A.B.G, S.G.H. Philander, 1999. The climate of the Last Glacial Maximum: Results from a coupled atmosphere-ocean genereal circulation model. Journal of Geophysical Research, 104, pp.24,509-24,525

Callahan, J.E., 1972. The structure and circulation of deep water in the Antarcticic, *Deep-Sea Research Letters, 19,* 563-575.

Carter, L., Garlick, R. D., Sutton, P., et al., (1998). Ocean Circulation New Zealand. NIWA Chart Miscellaneous Series 76.

Carter, L., H. L. Neil, and I. N. M. Cave (2000) Glacial to interglacial changes in non-carbonate and carbonate accumulation in the SW Pacific Ocean, New Zealand, Palaeogeography Palaeoclimatology Palaeoecology, 162, 333–356.

Carter, L., B. Manighetti, G. Ganssen, L. Northcote, 2008. Southwest Pacific modulation of abrupt climate change during the Antarctic Cold Reversal-Younger Dryas. Paalaeogeography, Palaeoclimatology, Palaeoecology, 260, pp. 284-298

Carter, R.M., P.R. Gammon, L. Millwood, 2004. Glacial-interglacial (MIS 1-10) migrations of the Subtropical Front across ODP Site 1119, Canterbury Bight, Southwest Pacific Ocean. Marine Geology, 205, pp.29-58

Chapman, M.R., Shackleton, N.J., Zhao, M., Eglinton, G. (1996) Faunal and alkenone reconstructions of subtropical North Atlantic surface hydrography and paleotemperature over the last 28 kyr. *Paleoceanography,11(3),* pp343-357

Chapman, M.R., 2010. Seasonal production patterns of planktonic foraminifera in the NE Atlantic Ocean: Implications for paleotemperature and hydrographic reconstructions, *Paleoceanography, 25,* PA1101, doi:10.1029/2008PA001708

Chiswell, S.M., 1996. Variability in the Southland current, New Zealand. *New Zealand Journal Marine Freshwater Research,* 30, 1-17.

Clark, P. U. et al., 2009. The Last Glacial Maximum. *Science, 325,* 710–714

Cleroux, C., E. Cortijo, J.C. Duplessy, and R. Zahn, 2007. Deep-dwelling foraminifera as thermocline temperature recorders. *Geochemistry, Geophysics, Geosystems, 8,* Q04N11, doi:10.1029/2006GC001474.

Curry, W.B., Oppo, D.W., 2005. Glacial water mass geometry and the distribution of $\delta^{13}C$ of ΣCO_2 in the western Atlantic Ocean, *Paleoceanography, 20,* doi:10.1029/2004PA001021

Dansgaard,W., 1965. Stable isotopes in precipitation. *Tellus, 16,* pp. 436-468

Darling, K.F., Wade, C.M., (2008) The genetic diversity of planktic foraminifera and the global distribution of ribosomal RNA genotypes. *Marine Micropaleontology, 67,* 216-238

Deacon, G.E.R., 1937. The Hydrology of the Southern Ocean. Discovery Reports 15.

Emerson, S.R. and Hedges, J.I., 2008. Chemical Oceanography and the Marine Carbon Cycle, Cambridge University Press

Fairbanks , R.G., 1989. A 17,000 year glacio-eustatic sea level record: influence of glacial melting rates on the Younger Dryas event and deep ocean circulation. *Nature*, 342, 637-642.

Fenner, J., L. Carter, R. Stewart, 1992. Late Quaternary paleoclimatic and paleoceanographic change over Chatham Rise, New Zealand, *Marine Geology, 108*, 383–404

Field, D.B., 2004. Variability in vertical distributions of planktonic foraminifera in the California Current: Relationships to vertical ocean structure. *Paleoceanography, 19,*PA2014, doi:10.1029/2003PA000970.

Guinasso, N.L. Jr, Schink, D.R. (1975) Quantitative Estimates of Biological Mixing Rates in Abyssal Sediments. *Journal of Geophysical Research, 80(21)*

Hamon, B.V., 1965. The East Australian Current 1960-1964. *Deep Sea Research. 12(6)* pp. 899-921

Hays, J.D., Imbrie, J, Shackleton, N.J., 1976. Variations in the Earth's Orbit: Pacemaker of the Ice Ages, *Science*, 194*,* pp. 1121-1132

Hayward, B. W., et al. 2008, The effect of submerged plateaux on Pleistocene gyral circulation and sea-surface temperatures in the southwest Pacific, *Global Planetary Change*, *63*, 309 – 316, doi:10.1016/j.gloplacha.

Hayward, B.W., Sabaa, A.T., Kolodziej, A., Crundwell, M.P., Steph, S., Scott, G.H., Neil, H.L., Bostock, H.C., Carter, L., Grenfell, H.R., 2012. Planktic foraminiferabased sea-surface temperature record in the Tasman Sea and history of the Subtropical Front around New Zealand over the last one million years. *Marine Micropaleontology 82-83*, 13-27.

Heath, R.A., 1968. Geostrophic currents derived from oceanic density measurements north and south of the Subtropical Convergence east of New Zealand. *N.Z. Journal of Marine Freshwater Research, 2(4)* pp. 659-677

Heath, R.A., 1972. The Southland Current. *N.Z. Journal of Marine Freshwater Research* , *6,* 497–533.

Heath, R. A. 1981, Oceanic fronts around southern New Zealand, *Deep Sea Research, Part A, 28,* 547 – 560, doi:10.1016/0198-0149(81) 90116-3.

Heath, R. A. 1985, A review of the physical oceanography of the seas around New Zealand, 1982, *New Zealand Journal of Marine Freshwater Research, 19, 79*–124.

Hemleben, C., M. Spindler, I. Breitinger, and W. G. Deuser 1985, Field and laboratory studies on the ontogeny and ecology of some Globorotaliid species from the Sargasso Sea off Bermuda, *Journal Foraminiferal Research, 15,* 254–272.

Hopkins, J., A.G.P. Shaw, P. Challenor, 2010. The Southland Front, New Zealand: Variability and ENSO correlations, *Continental Self Research, 30,* 1535-1548

Hutson, W.H. (1980) Bioturbation of deep-sea sediments: Oxygen isotopes and stratigraphic uncertainty. CLIMAP. *Geology, 8,* pp.127-130

Huybers, P., and G. Denton, 2008. Antarctic temperature at orbital timescales controlled by local summer duration. *Nature Geoscience* doi:10.1038/ngeo311

Huybers, P., and C. Wunsch, 2003. Rectification and precession signals in the climate system, *Geophys. Res. Lett.*, *30*(19), 2011, doi:10.1029/2003GL017875

Huybers, P., C. Wunsch, 2005. Obliquity pacing of the late Pleistocene glacial terminations. *Nature, 434,* pp. 491-493

Imbrie, J., Boyle, E.A., Clemens, S.C., Duffy, A., Howard, W.R., Kukla, G., Kutzbach, J., Martinson, D.G., McIntyre, A., Mix, A.C., Molfino, B., Morley, J.J., Peterson, L.C., Pisias, N.G., Prell, W.L., Raymo, M.E., Shackleton, N.J., Toggweiller, J.R., 1992. On the structure and origin of major glaciation cycles. 1. Linear responses to Milankovitch forcing. *Paleoceanography, 7,* pp. 701-738

Jillett, J., 1969. Seasonal hydrology of waters off the Otago Peninsula south-eastern New Zealand. *N. Z. Journal of Marine Freshwater Research, 3(3),* 349–375.

Jouzel J, Lorius C, Merlivat L, Petit JR (1987a) Abrupt climatic changes: the Antarctic ice record during the late Pleistocene. In: Berger WH, Labeyrie LD (eds) Abrupt climatic change:evidence and implications. D. Reidel, Dordrecht, pp 235-245

Jouzel, J., V. Masson, O. Cattani, S. Falourd, M. Stievenard, B. Stenni, A. Longinelli, S.J.Johnsen, J.P. Steffensen, J.R. Petit, J. Schwander, R. Souchez, and N.I. Barkov. 2001. A new 27 ky high resolution East Antarctic climate record. *Geophysical. Research Letters, 28(16)* pp. 3199-3202

Kennett, J.P., 1982. Marine Geology. Prentice-Hall, Englewood Cliffs, New Jersey.

King, A. L., and W. R. Howard, 2001. Seasonality of foraminiferal flux in sediment traps at Chatham Rise, SW Pacific: Implications for paleotemperature estimates, *Deep Sea Research, Part I, 48,* 1687 – 1708, doi:10.1016/S0967-0637(00)00106-0.

King, A.L., W.R. Howard, 2005. $\delta^{18}O$ seasonality of planktonic foraminifera from Southern Ocean sediment traps: Latidudinal gradients and implications for paleoclimate reconstructions. Marine Micropaleontology, 56,pp.1-24

King, A.L., Howard, W.R., 2003. Planktonic foraminiferal flux seasonality in Subantarcitc sediment traps: a test for paleoclimate reconstructions. *Paleoceanography, 18,* pp.1000-1019

Laepple, T., and G. Lohmann , 2009. Seasonal cycle as template for climate variability on astronomical timescales, Paleoceanography, 24, PA4201, doi:10.1029/2008PA001674.

Loubere, P., Bennett, S., 2008. Southern Ocean biogeochemical impact on the tropical ocean: Stable isotope records from the Pacific for the past 25,000 years. *Global and Planetary Change, 63,* 333-340

Lowe, A.L., Anderson, J.B., 2002. Reconstruction of the West Antarctic Ice Sheet in Pine Island Bay during the Last Glacial Maximum and its subsequent retreat history. *Quaternary Science Review, 21,* 1879-1897.

Lowe DJ, Shane PAR, Alloway BV, Newnham RM (2008a) Fingerprints and age models for widespread New Zealand tephra marker beds erupted since 30,000 years ago: A framework for NZ-INTIMATE. *Quaternary Science Reviews* **27**, 95-126.

B. D. Marino, M. B. McElroy, R. J. Salawitch, W. G. Spaulding, (1992) Glacial to interglacial variations in 13C for atmospheric CO2. *Nature* **357**, 461

Mashiotta, T.A., Lea, D.W., Spero, H.J., 1999. Glacial-interglacial changes in the Subantarctic sea surface temperature and delta O-18-water using foraminiferal Mg. *Earth Planetary Science Letters, 170,* 417-432.

McCartney, M. S., Subantarctic Mode Water, in A Voyage of Discovery: George Deacon 70th Anniversary Volume, edited by M. Angel, Pergamon, New York, pp. 103-119, 1977.

McManus, J.F., Francois, R., Gherardi, J.-M., Keigwin, L.D., Brown-Leger, S., 2004. Collapse and rapid resumption of Atlantic meridional circulation linked to deglacial climate changes. *Nature 428,* 834-837.

Milankovitch, M. (1930), *Mathemtatische Klimalehre und Astronomische Theorie der Klimaschwankungen,* 176 pp., Gebruder Borntraeger, Stuttgart, Germany.

Mix, A. C., E. Bard, G. Eglinton, L. D. Keigwin, A. C. Ravelo, and Y. Rosenthal, 2000, Alkenones and multiproxy strategies in paleoceanographic studies, *Geochemistry Geophysics Geosystems, 1(11),* 1033, doi:10.1029/2000GC000056.

Mix, A.C., Bard, E., Schneider, R., 2001. Environmental processes of the ice age: land, oceans, glaciers (EPILOG). Quaternary Science Review, 20, 627-657.

Monnin E., A. Indermuhle, A. Dallenbach, J. Fucklicker, B. Stauffer., T., Stocker, D., Raynaud, J.M. Barnola, 2001. Atmospheric CO_2 Concentrations over the Last Glacial Termination. *Science, 291, 5501*, pp. 112-114

Müller, P. J., G. Kirst, G. Ruhland, I. von Storch, and A. Rosell-Mele´ (1998), Calibration of the alkenone paleotemperature index U37 K0 based on core-tops from the eastern South Atlantic and the global ocean (60_N–60_S), *Geochimica Cosmochima Acta, 62,* 1757– 1772, doi:10.1016/S0016-7037(98)00097-0.

Nees, S., Armand, L., De Deckker, P., Labracherie, M., Passlow, V., 1999. A diatom and benthic foraminiferal record from the South Tasman Rise (southeastern Indian Ocean): implications for palaeoceanographic changes for the last 200,000 years. *Marine Micropaleontology, 38,* 69-89. http://dx.doi.org/10.1016/S0377-8398(99)00039-0.

Nelson,C.S., Cooke, P.J., Hendy, C.H., Cuthbertson, A.M.,1993. Oceanographic and climate changes over the past 150,000 years at Deep Sea Drilling Project Site 594 of southeastern New Zealand, southwest Pacific Ocean. *Paleoceanography, 8,* pp. 435-458
Ninnemann, U.S., Charles, C.D., 1997. Regional differences in Quaternary Subantarctic nutrient cycling: link to intermediate and deep-water ventilation. Paleoceanography, 12, 560-567.

Orsi, A.H., Whitworth III, T., Nowlin Jr., W.D., 1995. On the meridional extent and fronts of the Antarctic Circumpolar Current. *Deep Sea Research I, 42,* 641-673. http://dx.doi.org/10.1016/0967-0637(95)00021-W.

Orsi A. H., C. L.Wiederwohl, (2009) A recount of Ross Sea waters, Deep-Sea Research II *56* 778–795,

Pahnke, K., R. Zahn, H. Elderfield, M. Shulz, 2003. 340,000 year centennial-scale marine record of Southern Hemisphere climatic oscillation. *Science, 301,* pp. 948-952

Pahnke, K., Zahn, R., 2005. Southern Hemisphere water mass conversion linked to North Atlantic climate variability. *Science, 307*, 1741-1746.

Pahnke, K., Sachs, J.P., 2006. Sea surface temperatures of southern mid-latitudes 0-160 kyr B.P. *Paleoceanography 21,* PA2003. http://dx.doi.org/10.1029/2005PA001191.

Park, S., Longdill, P., 2006. Synopsis of SST and Chl-a in Bay of Plenty. *Environment Bay of Plenty*, Environment Bay of Plenty Regional Council, Whakatane, NZ, ISSN 1175-9372

Peltier, W.R. and R.G. Fairbanks, 2006. Global glacial ice volume and Last Glacial Maximum duration from an extended Barbados sea level record. *Quaternary Science Reviews*, 25, 3322-3337.

Peng, T.H., Broecker, W.S. (1984) The impacts of Bioturbation on the age difference between benthic and planktonic foraminifera in deep sea sediments, *Nuclear Instruments and Methods in Physics Research B5* pp. 346-352

Petit, J.R., Jouzel, J., Raynaud, D., Barkov, N.I., Barnola, J.-M., Basile, I., Bender, M., Chappellaz, J., Davis, M., Delaygue, G., Delmotte, M., Kotlyakov, V.M., Lipenkov, V., Lorius, C., Pepin, L., Ritz, C., Saltzman, E., Stievenard, M., 1999. Climate and atmospheric history of the last 420,000 years from the Vostok ice core, Antarctica. Nature 399, 429–436.

Prahl, F. G., L. A. Muehlhausen, and D. L. Zahnle, 1988. Further evaluation of long-chain alkenones as indicators of paleoceanographic conditions, *Geochimica Cosmochimica Acta, 52,* 2303 – 2310, doi:10.1016/0016-7037(88) 90132-9.

Prahl, F. G., M. A. Sparrow, and G. V. Wolfe, 2003. Physiological impacts on alkenone paleothermometry, *Paleoceanography, 18(2),* 1025, doi:10.1029/2002PA000803.

Prell, W. L., W. H. Hutson, D. F. Williams, A. W. H. Be´, K. Geitzenauer, and B. Molfino, 1980. Surface circulation of the Indian Ocean during the Last Glacial Maximum, approximately 18,000 yr B.P., *Quaternary Research, 14,* 309–336, doi:10.1016/0033-5894(80)90014-9.

Ridgway, K. R., and J. S. Godfrey, 1994. Mass and heat budgets in the East Australian Current: A direct approach, *Journal of Geophysical Research, 99,* 3231–3248, doi:10.1029/93JC02255.

Rose, K.A, E.L. Sikes, T.P. Guilderson, P. Shane, T.M. Hill, R. Zahn, H. J. Spero, 2010. Upper-ocean-to-atmosphere radiocarbon offsets imply fast deglacial carbon dioxide release. *Nature, 466,* pp. 1093-1097

Rosenthal, Y., and E. A. Boyle, 1993. Factors controlling the fluoride content of planktonic foraminifera: An evaluation of its paleoceanographic applicability. *Geochim. Cosmochim. Acta* 57: 335-346.

Rosenthal, Y., Boyle, E. A. and N. Slowey, 1997. Temperature control on the incorporation of Mg, Sr, F and Cd into benthic foraminiferal shells from Little Bahama Bank: prospects for thermocline paleoceanography. *Geochim. Cosmochim. Acta.* 61: 3633-3643.

Rosenthal, Y., Lohmann, G.P. Lohmann, K.C. and R.M. Sherrell. 2000. Incorporation and preservation of Mg in G. sacculifer: Implications for reconstructing sea surface temperatures and the oxygen isotopic composition of seawater. Paleoceanography, 15: 135-145

Russell, J. L., Dixon, K. W., Gnanadesikan, A., Stouffer, R. J. & Toggweiler, J. R., 2006. Southern Ocean westerlies in a warming world: propping open the door to the deep ocean. *Journal of Climate 19,* 6382–6390

Samson, C.R, E.L. Sikes, and W. R. Howard (2005) Deglacial paleoceanographic history of the Bay of Plenty, New Zealand. *Paleoceaongraphy*, 20, PA4017, doi:10.1029/2004PA001088.

Schaefer, G., Rodgers, J.S., Hayward, B.W., Kennett, J.P., Sabaa, A.T., Scott, G.H., 2005. Planktic foraminiferal and sea surface temperature record during the last 1 Myr across the Subtropical Front, Southwest Pacific. *Maine Micropaleontology, 54,*191-212.

Schmitt, J et al. (2012): Monte Carlo average of stable carbon isotope ratio of atmospheric CO_2 from three Antarctic ice cores. doi:10.1594/PANGAEA.772711

Schmitt, Jochen; Schneider, Robert; Elsig, Joachim; Leuenberger, Daiana;Lourantou, Anna; Chappellaz, Jérôme A; Köhler, Peter; Joos, Fortunat; Stocker, Thomas F; Leuenberger, Markus; Fischer, Hubertus (2012): Carbon isotope constraints on the deglacial CO_2 rise from ice cores. *Science*, 336**,** 711-714, doi:10.1126/science.1217161

Shackleton, N.J., 1974. Attainment of isotopic equilibrium between ocean water and benthonic foraminifera genus Uvigerina: isotopic changes in the ocean during the last glacial. *Les Méthodes Quantitatives D'étude Des Variations Du Climat Au Cours Du Pleistocene; Colloq. Int. CNRS, vol. 219,* pp. 203–209.

Shackleton, N.J., 1987. Oxygen isotopes, ice volume and sea level. *Quaternary Science Reviews, 6(3)*, pp. 183-190

Shackleton, N.J., 2000. The 100,000-year ice-age cycle identified and found to lag temperature, carbon dioxide, and orbital eccentricity, *Science, 289,* pp. 1897-1902

Shakun J., P. Clark, F. He, S. Marcott, A. Mix, Z. Liu, B. Otto-Bliesner, A. Schmittner, E. Bard 2012. Global Warming Preceded by Increasing Carbon Dioxide Concentrations during the Last Deglaciation,.*Nature* 484, No. 7392, 49–54. DOI 10.1038/nature10915.

Shane, P. A., Sikes, E. L. & Guilderson, T. P., 2006. Tephra beds in deep-sea cores off northern New Zealand: implications for the history of Taupo Volcanic Zone, Mayor Island, and White Island volcanoes. *Journal of Volcanic and Geothermal Research 154*, pp. 276-290

Sigman, D. M., M. P. Hain, and G. H. Haug (2010), The polar ocean and glacial cycles in atmospheric CO_2 concentration, *Nature*, *466*, 47-55

Shaw, A. G. P. 1998, The temporal and spatial variability the Southland Front, New Zealand using AVHRR SST imagery, Ph.D thesis, University of Otago Dundin, New Zealand 248pp.

Shaw, A.G.P. and R. Vennell, Measurements of an Oceanic Front using a Front-Following Algorithm for AVHRR SST Imagery. *Remote Sensing of the Environment 75(1):*47-62. (2001).

Sikes, E.L. and L.D. Keigwin (1994) Equatorial Atlantic sea surface temperatures for the last 30 kyr: A comparison of Uk'37, δ18O, and foraminiferal assemblage estimates., *Paleoceanography*, 9, 31-45.

Sikes, E.L., Samson, C., Guilderson, T., Howard, W.R., 2000. Old radiocarbon ages in the southwest Pacific Ocean during the last glacial period and deglaciation. *Nature 405,* 555-559.

Sikes, E.L., Howard, W.R., Neil, H.L., Volkman, J.K., 2002. Glacial-interglacial sea surface temperature changes across the subtropical front east of New Zealand based on alkenone unsaturation ratios and foraminiferal assemblages. *Paleoceanography 17* (1012). http://dx.doi.org/10.1029/2001PA000640.

Sikes, E.L., Nodder, S.D., O'Leary, T., Volkman, J.K., 2005. Alkenone temperature records and biomarker flux at the subtropical front on the Chatham Rise, SW Pacific Ocean. *Deep Sea Research I 52,* 721-748.

Sikes, E.L., Howard, W.R., Samson, C.R., Mahan, T.S., Robertson, L.G., Volkman, J.K., 2009. Southern ocean seasonal temperature and subtropical front movement on the South Tasman Rise in the late Quaternary. *Paleoceanography 24*, PA2201. http://dx.doi.org/10.1029/2008PA001659.

Sikes, E.L., and J.K. Volkman, Calibration of alkenone unsaturation ratios (U37K1) for paleotemperature estimation in cold polar waters, Geochim. Cosmochim. Acta, 57, 1883-1889, 1993.

Skinner, L.C., Fallon, S., Waelbroeck, C., Michel, E., Barker, S., (2010) Ventilation of the Deep Southern Ocean and Deglacial CO_2 Rise, *Science 328,* 1147 DOI: 10.1126/science.1183627

Sowers, T., and M. Bender (1995) Climate records covering the last deglaciation. *Science, 269*, 210-214.

Spero, H.J., K.M. Mielke, E.M. Kalve, D.W., Lea, D.K. Pak, 2003. Multispecies approach to reconstructing easter equatorial Pacific thermocline hydrograpgy during the past 360 kyr. *Paleoceanography, 18(1),*1022, doi:10.1029/2002PA000814

Spero, H.J., Lea, D.K., 2002. The cause of the Carbon Isotope Minimum on glacial terminations. *Science, 296(5567)* pp. 552-555

Stott, L.D., Timmerman, A, Thunell, R. (2007) Southern hemisphere and deep-sea warming led deglacial atmospheric CO2. *Science, 318 (5849),* pp. 435-438

Talley, L.D., 1996. Antarctic Intermediate Water in the South Atlantic. The South Atlantic: Present and Past Circulation, pp. 219–238

Thompson P.R., Shackleton N.J. 1980. North Pacific paleoceanography. Late Quaternary coiling variation of planktonic foraminifer *Neogloboquadrina pachyderma*. Nature, 287:829-833.

Thornalley, D.J.R., Elderfield, H., Mccave, N. (2009) Holocene oscillations in temperatures and salinity of the surface subpolar North Atlantic. *Nature, 457,* pp. 711-714 doi:10.1038/nature07717

Toggweiler, J. R., 1999. Variation of atmospheric CO_2 by ventilation of the ocean's deepest water. *Paleoceanography 14,* 571–588

Toggweiler, J.R, Key, R.M., 2001. Thermohaline circulation. In: Steele J, Thorpe S, Turekian K, editors. *Encyclopedia of ocean science.* London: Academic Press Ltd. 2941-2947

Toggweiler, J. R., Russell, J. L. & Carson, J. R.,2006. Mid-latitude westerlies, atmospheric CO2, and climate changes during the ice ages. *Paleoceanography 21,* PA2005.

Tsuchiya, M.,Talley,L.D.,1996.Water property distributions along an eastern Pacific hydrographic section at 1351W. *Journal of Marine Research 54,*541–564.

Weaver, A. J., Eby, M., Fanning, A. F. & Wiebe, E. C., 1998. Simulated influence of carbon dioxide, orbital forcing and ice sheets on the climate of the Last Glacial Maximum. *Nature 394,* 847–853

Wells, P.E., Connell, R., 1997. Movement of hydrological fronts and widespread erosional events in the southwestern Tasman Sea during the late Quaternary. *Australian Journal Earth Science 44,* 105-112. http://dx.doi.org/10.1080/08120099708728297.

Wijffels, S.E., J.M Tool, R. Davis, 2001. Revisiting the South Pacific subtropical circulation: A synthesis of World Ocean Circulation Experiments observations along 32ºS. *Journal of Geophysical Research, 106, C9* pp.19481-19513

Wong, A.P.S., G.C Johnsons, 2003. South Pacific Eastern Subtropical Mode Water. *Journal of Physical Oceanography, 33* pp. 1493-1509

Appendix A.1: RR0503 79 JPC Stable Isotopes

Depth (cm)	Ages (kyr BP)	G. inflata (Delta 13C PDB)	G. inflata (Delta 18O PDB)	G. inflata RUID#	G. bulloides (Delta 13C PDB)	G. bulloides (Delta 18O PDB)	G. bulloides RUID#
4.5	4.0591	0.71	1.76	20100527	-0.77	1.29	20100433
16.5	5.6136	1.03	0.97	20100528	-0.76	0.14	20100434
28.5	7.1682	1.05	0.90	20100529	-0.34	0.28	20100435
36.5	8.2045	0.79	1.01	20100530	-0.69	0.34	20100436
40.5	8.7227	0.68	0.67	20101379	-0.68	-0.04	20101387
44.5	9.2409	0.79	1.04	20100531	-0.66	0.37	20100437
48.5	9.7591	0.60	0.81	20101380	-1.05	-0.06	20101388
52.5	10.271	0.70	1.08	20100532	-1.04	0.49	20100438
56.5	10.773	0.64	0.97	20101381	-1.07	0.26	20101389
60.5	11.266	0.62	1.17	20100533	-0.96	0.45	20100439
64.5	11.749	0.58	1.12	20101382	-0.66	0.75	20101392
68.5	12.224	0.70	1.48	20100534	-1.08	0.67	20100441
72.5	12.688	0.74	1.44	20101383	-1.00	0.57	20101393
76.5	13.144	0.64	1.58	20100535	-0.84	1.00	20100442
80.5	13.59	0.60	1.37	20101384	-1.15	0.53	20101394
84.5	14.025	0.58	1.90	20100536	-1.17	1.09	20100445
88.5	14.448	0.55	1.75	20101385	-1.28	1.01	20101395
92.5	14.859	0.43	1.97	20100539	-1.15	1.34	20100446
96.5	15.259	0.51	1.75	20101386	-1.08	1.19	20101396
100.5	15.647	0.61	2.03	20100540	-0.83	1.33	20100447
112.5	16.748	0.83	2.18	20101127			
124.5	17.762	0.84	2.44	20100541	-1.12	1.61	20100448
128.5	18.082	0.63	2.30	20101128	-0.88	1.69	20101120
132.5	18.395	0.47	2.25	20101129	-0.56	2.02	20101121
136.5	18.698	0.76	2.24	20101132	-0.86	1.43	20101122
140.5	18.994	0.68	2.07	20101133	-0.85	1.42	20100829
144.5	19.283	0.51	2.05	20101134	-0.98	1.39	20101123
148.5	19.564	0.50	2.29	20101135	-0.60	1.82	20100824
152.5	19.838	0.80	2.40	20100542	0.10	2.49	20100449
156.5	20.105	0.80	2.32	20101136	0.37	2.63	20100825
160.5	20.366	0.80	2.26	20101137	-0.07	2.20	20101124
164.5	20.62	0.75	2.23	20101138	-0.30	1.91	20100826
168.5	20.868	0.73	2.20	20101139	-0.72	1.43	20101125
172.5	21.11	0.78	2.31	20101140	-0.57	1.61	20100827
176.5	21.347	0.79	2.28	20101141	-0.59	1.59	20100828
180.5	21.577	0.83	2.18	20100543	-1.00	1.65	20100450
184.5	21.802	0.65	2.00	20101142			
192.5	22.236	0.82	2.18	20101143	-0.25	1.92	20101126

204.5	22.846	0.50	2.00	20100544	-0.66	1.63	20100451
224.5	23.695	0.72	2.18	20100545	-0.37	1.76	20100452
251.5	24.582				-0.56	1.54	20100453

Appendix A.2: RR0503 83 TC Stable Isotopes

Depth (cm)	Ages (kyr BP)	G. inflata (Delta 13C PDB)	G. inflata (Delta O18 PDB)	G. inflata RU#	G. bulloides (Delta C13 PDB)	G. bulloides (Delta O18 PDB)	G. bulloides RU#
0.5	0	0.33	0.43	20101520	0.38	0.61	
1.5	0.05882				0.82	0.15	
2.5	0.11904				0.29	0.12	
3.5	0.18073				-0.19	-0.02	
4.5	0.24541				0.34	0.30	
5.5	0.3117				0.02	0.12	
6.5	0.37981				-1.19	-0.35	
7.5	0.45128				0.01	-0.11	
8.5	0.52461	0.97	0.27	20101220	-0.13	0.04	
9.5	0.60017				0.05	-0.06	
10	0.63958				-0.91	0.01	
10.5	0.67935				-0.20	0.20	
11.5	0.76037				0.63	-0.03	
13.5	0.93026	0.85	0.64	20101521	-0.04	0.13	
14.5	1.0186				0.32	-0.41	
15.5	1.1091				1.35	-0.37	
16.5	1.2026				1.21	-0.16	
17.5	1.2977				-0.23	-0.04	
18.5	1.3951	0.89	0.60	20101221	-0.15	0.22	
20.5	1.5966				0.46	0.37	
23.5	1.9224	0.94	0.59	20101522			
24.5	2.0415				0.72	0.37	
25.5	2.1666				0.84	0.23	
27.5	2.43				-0.22	-0.27	
28.5	2.5694	0.95	0.60	20101222			
29.5	2.7119				-0.01	-0.09	
30.5	2.8593				-1.39	-0.06	20101515
33.5	3.3217	1.04	0.63	20101523			
38.5	4.1419	0.88	0.47	20101223			
40.5	4.4792				-0.43	0.50	
44.5	5.1515	1.02	0.76	20101224			
45.5	5.316				-0.75	-0.06	20101516
50	6.0224				0.18	0.10	
50.5	6.0973	0.97	0.60	20101524			
55.5	6.7493	0.66	0.48	20101225	-1.26	0.13	20101517
60.5	7.1953	0.89	0.69	20101525	0.11	0.14	
64.5	7.4451	0.76	0.46	20101226			

65.5	7.5051				-0.59	0.00	20101518
68.5	7.6914	0.84	0.71	20101227			
70.5	7.8249				-1.67	0.02	20101519
73.5	8.0438	0.77	0.65	20101228			
75.5	8.2055				-0.13	0.16	
80.5	8.6622				0.15	0.27	
83.5	8.9684	0.76	0.85	20101229	-0.32	0.36	
85.5	9.1835				-0.47	0.37	
87.5	9.407	0.73	0.96	20101230	0.49	0.38	
89.5	9.6369				0.30	0.50	
92.5	9.9923	0.48	0.92	20101233	0.87	0.41	
95.5	10.357				0.61	0.16	
96.5	10.48				0.45	0.71	
100.5	10.975	0.54	0.84	20101234	0.23	0.46	
103.5	11.346				0.57	0.17	
104.5	11.468	0.55	0.98	20101235			
105.5	11.59				-0.84	0.11	
107.5	11.832				-0.40	0.86	
108.5	11.951	0.57	1.17	20101236			
110.5	12.184	0.61	1.02	20101397	-0.78	0.89	
113.5	12.522	0.60	1.19	20101237	0.08	0.50	
115.5	12.737				0.10	0.73	
117.5	12.942				0.22	0.31	
118.5	13.04	0.51	1.24	20101238			
119.5	13.135	0.60	1.37	20101398			
120.5	13.228				-0.86	0.89	
123.5	13.483	0.43	1.44	20101239	-1.29	0.68	
125.5	13.634	0.43	1.42	20101528	-1.35	0.70	
127.5	13.774	0.50	1.47	20101240			
130.5	13.971				-0.11	0.91	
132.5	14.095	0.64	1.56	20101241	-0.23	0.87	
134.5	14.214	0.66	1.47	20101529	-1.35	1.49	
136.5	14.327	0.60	1.79	20101399			
138.5	14.435	0.46	1.65	20101242	-1.10	1.10	
140.5	14.539				-0.85	1.43	
142.5	14.639	0.62	1.66	20101243			
144.5	14.735	0.46	1.84	20101530	-1.21	1.19	
146.5	14.826	0.60	1.75	20101400	-1.01	1.36	
148.5	14.915	0.53	1.86	20101244	-1.51	1.18	
150.5	15				-0.77	1.66	
152.5	15.085	0.49	1.98	20101245			

154.5		0.67	1.77	20101531	-0.90	1.36
156.5		0.76	1.56	20101532	-1.55	1.35
158.5					-1.23	0.79
160.5					0.08	0.65
162.5		0.63	0.80	20101401	-0.47	0.23
166.5		0.61	1.02	20101533		
170.5					-0.25	1.16
172.5		0.58	1.35	20101402		
176.5		0.68	1.53	20101534		
180.5					-0.57	1.89
182.5		0.79	2.17	20101403	0.23	2.37
184.5	16.753				0.52	2.69
186.5	16.999	0.86	2.12	20101535	-0.47	2.47
190.5	17.468				0.37	2.40
192.5	17.691	0.80	2.09	20101404	-0.17	2.16
196.5	18.113				-0.42	1.89
198.5	18.31	0.83	2.24	20101536	-0.34	2.25
200.5	18.499				-0.32	1.95
205.5	18.939	0.73	2.31	20101537	-0.29	2.14
210.5	19.337	0.53	2.24	20101538	-0.49	2.01
215.5	19.7	0.69	2.19	20101539	0.37	2.46
219.5	19.967	0.70	2.19	20101540	-1.20	1.76

Appendix A.3: RR0503 87 JPC Stable Isotopes

Depth (cm)	Ages (kyr BP)	G. inflata (Delta 13C PDB)	G. inflata (Delta O18 PDB)	G. inflata RU#	G. bulloides (Delta C13 PDB)	G. bulloides (Delta O18 PDB)	G. bulloides RU#
0.5	6.25	1.2	0.88	20090069	-1.59	0.49	20100432
2.5	6.4146	1.10	0.76	20100799	-0.82	0.53	20100701
4.5	6.5851	1.12	0.64	20100800	-0.91	0.47	20100702
6.5	6.7618	0.95	0.87	20100801	-0.67	0.23	20100703
8.5	6.9452	0.77	0.94	20100802	-1.07	0.47	20100704
10.5	7.1366	0.9	1.04	20090070			
12.5	7.3354	0.61	0.81	20100818	-0.92	0.27	20100455
14.5	7.542	0.79	0.96	20100805	-1.03	0.40	20100714
16.5	7.7574						
18.5	7.9827	0.73	0.98	20100806	-0.69	0.51	20100715
20.5	8.2175	0.61	0.87	20090076	-0.84	0.32	20100456
22.5	8.4623	0.83	0.71	20100807	-1.02	0.33	20100716
24.5	8.7189	0.86	0.74	20100808	-1.05	0.09	20100717
26.5	8.9879	0.77	1.11	20100809	-1.11	0.22	20100718
28.5	9.2694	0.64	1.10	20100810	-1.06	0.59	20100719
30.5	9.5641	0.79	1.28	20090077	-0.83	0.72	20100457
32.5	9.8748	0.67	1.23	20100811	-0.80	0.27	20100722
34.5	10.202	0.63	0.94	20100812	-1.29	0.31	20100723
36.5	10.545	0.56	1.26	20100813	-0.92	0.60	20100724
38.5	10.907	0.68	1.39	20100814	-0.90	1.00	20100725
40.5	11.291	0.77	0.98	20091028			
42.5	11.697	0.66	1.49	20100838	-0.78	1.02	20100458
44.5	12.126	0.70	1.49	20100839	-0.83	0.60	20100726
46.5	12.58	0.72	1.75	20100840	-0.83	0.95	20100727
48.5	13.072	0.69	1.71	20100255	-0.92	1.28	20100200
50.5	13.59	0.54	1.63	20091030			
52.5	14.112	0.65	2.09	20100256	-0.69	1.20	20100201
54.5	14.598	0.67	1.82	20100841	-0.74	1.04	20100729
56.5	14.991	0.69	1.52	20100257	-0.64	1.32	20100202
58.5	15.334	0.66	1.99	20100842	-1.17	0.92	20100730
60.5	15.658	0.81	1.65	20090080			
62.5	15.973	0.63	1.67	20100258	-0.71	1.21	20100203
64.5	16.282	0.58	1.69	20100843	-0.93	1.02	20100731
66.5	16.589	0.83	1.98	20100270	-0.68	1.34	20100204
68.5	16.893	0.66	1.86	20100844			
70.5	17.196	0.82	2.08	20091034			
72.5	17.498				-0.82	1.36	20100205
74.5	17.8	0.83	2.06	20100271			

76.5	18.099	0.86	2.23	20100272	-0.95	1.51	20100206
78.5	18.392	0.61	2.12	20100847			
80.5	18.681	0.88	1.99	20090082			
82.5	18.966	0.76	2.31	20100273	-0.80	1.75	20100207
84.5	19.246	0.92	2.32	20100849			
86.5	19.521	0.85	2.28	20100274	-0.82	1.61	20100208
88.5	19.792	0.89	2.46	20100850	-0.24	2.23	20100767
90.5	20.059	0.82	1.93	20090083			
92.5	20.322	0.77	2.35	20100275	-0.21	2.18	20100209
94.5	20.581	0.71	2.22	20100851	-0.10	2.22	20100768
96.5	20.836	0.79	2.25	20100276	-0.22	2.05	20100769
98.5	21.087	0.78	2.42	20100852	-0.33	1.78	20100770
100.5	21.334	0.85	2.39	20090084			
102.5	21.578	0.75	2.24	20100277	-0.40	1.90	20100213
104.5	21.818	0.91	2.53	20100853	-0.59	1.69	20100771
106.5	22.055	0.83	2.28	20100278	-0.22	1.96	20100774
108.5	22.288	0.83	2.20	20100854	-0.30	1.98	20100775
110.5	22.517	0.77	2.14	20090085			
112.5	22.744	0.72	2.24	20100279	-0.25	1.88	20100215
114.5	22.967	0.70	2.29	20100855	-0.65	1.74	20100776
116.5	23.187	0.76	1.85	20100546	-0.44	1.88	20100216
118.5	23.404	0.76	2.14	20100086	-1.08	1.38	20100777
119.5	23.511	0.59	2.01	20100547			
120.5	23.618	0.66	1.72	20090086			
122.5	23.829	0.75	2.07	20100087	-0.38	1.87	20100217
124.5	24.037	0.69	2.12	20100856	-0.33	1.94	20100778
126.75	24.293	0.68	1.92	20100088	-0.20	1.78	20100218
128.5	24.445	0.91	2.13	20100857			
130.5	24.645	0.55	2.05	20090087			
132.5	24.842	0.80	2.11	20100548	-0.67	1.54	20100780
134.5	25.036	0.87	2.23	20100089	-0.67	1.54	20100781
136.5	25.228	0.76	2.07	20100858	-0.25	1.78	20100783
138.5	25.417	0.76	2.02	20100859	-0.54	1.57	20100784
140.5	25.604	0.83	2.19	20090088			
142.5	25.789	0.82	1.99	20100090	-0.71	1.40	20100220
144.5	25.971	0.80	2.11	20100819	-0.32	1.86	20100792
146.5	26.151	0.75	1.79	20100091	-0.57	1.44	20100221
148.5	26.328	0.83	1.94	20100820	-0.50	1.72	20100793
150.5	26.503	0.89	2.01	20090089			
152.5	26.677				-0.08	2.23	20100794
154.5	26.847	0.84	2.09	20100549	-0.33	1.69	20100222

156.5	27.016	0.65	2.01	20100821	-0.40	1.77	20100795
158.5	27.184	0.74	2.14	20100092	-0.22	1.79	20100796
160.5	27.351						
162.5	27.519	0.91	1.98	20100822	-0.32	1.81	20100797
164.5	27.686	0.82	2.06	20100085	-0.56	1.54	20100084
166.5	27.854	0.91	1.98	20100822	-0.54	1.61	20100798

Appendix A.4: RR0503 125 JPC Stable Isotopes

Depth (cm)	Ages (kyr BP)	G. inflata (Delta 13C PDB)	G. inflata (Delta O18 PDB)	G. inflata RU#	G. bulloides (Delta C13 PDB)	G. bulloides (Delta O18 PDB)	G. bulloides RU#
0.5	0	0.65	0.89	20100124	-1.27	0.14	20100259
8.5	0.5913	0.84	0.66	20104451			
16.5	1.2157	0.80	0.74	20100099	-0.86	0.24	20100045
20.5	1.5413	0.74	0.74	20104452			
28.5	2.2209	0.53	0.71	20104453			
32.5	2.577	0.81	0.79	20100100	-0.95	0.15	20100046
40.5	3.3218	0.78	0.77	20104454			
48.5	4.1138	0.86	0.74	20100101	-0.59	0.22	20100047
52.5	4.5288	0.67	0.70	20104455			
60.5	5.402	0.80	0.79	20104456			
64.5	5.8614	0.79	0.70	20100102	-0.99	0.07	20100048
72.5	6.8285	0.68	0.81	20104457			
80.5	7.8656	0.74	0.86	20100103	-0.88	0.07	20100049
84.5	8.4181	0.49	0.77	20104458	-0.87	0.08	20111840
88.5	9.0063	0.49	0.80	20104459	-0.68	0.65	20111841
92.5	9.6231	0.59	1.06	20100104	-1.20	0.29	20100050
96.5	10.263	0.63	1.18	20100108	-1.41	0.27	20100260
100.5	10.918	0.65	1.37	20100106	-1.19	0.45	20100052
104.5	11.58	0.51	1.12	20104460	-0.96	0.59	20111842
108.5	12.237	0.73	1.20	20100107	-1.30	0.73	20100053
112.5	12.873	0.60	1.35	20100105	-1.23	0.51	20100051
116.5	13.466	0.41	1.62	20100111	-1.09	0.82	20100054
120.5	13.993	0.48	1.25	20104461	-1.06	0.74	20111843
124.5	14.446	0.52	1.21	20104462	-1.11	0.85	20111844
128.5	14.848	0.67	2.07	20100112	-1.48	0.79	20100261
132.5	15.217	0.36	1.54	20104463	-1.58	0.72	20111845
136.5	15.565	0.39	1.69	20104464	-1.60	0.67	20111846
140.5	15.897	0.42	1.84	20104465	-1.41	1.11	20111847
144.5	16.218	0.66	2.27	20100113	-0.89	1.21	20100057
148.5	16.53	0.39	1.85	20104466	-0.86	1.51	20111848
152.5	16.836	0.52	2.01	20104469	-1.15	1.58	20111849
156.5	17.137	0.48	1.92	20104470	-0.86	1.63	20111850
160.5	17.434	0.87	2.46	20100114	-0.82	1.63	20100058
164.5	17.727	0.87	2.25	20104471	-1.03	1.52	20111851
168.5	18	0.72	2.10	20104472	-1.32	1.38	20111854
172.5	18.229	0.56	2.02	20104473	-1.70	1.25	20111855
176.5	18.43	0.72	2.16	20100115	-1.20	1.40	20100059

180.5	18.613	0.81	2.21	20104474	-1.30	1.32	20111856
184.5	18.783	0.85	2.20	20104475	-1.92	1.18	20111857
188.5	18.946	0.83	2.20	20104476	-1.58	1.32	20111858
192.5	19.103	0.58	2.10	20100116	-0.96	1.65	20100060
196.5	19.257	0.82	2.24	20104477	-1.47	1.42	20111859
200.5	19.409	0.74	2.29	20104478	-0.45	1.98	20111860
204.5	19.56	0.60	2.13	20104479	-1.18	1.43	20111861
208.5	19.71	0.76	2.28	20100117	-0.40	1.93	20100061
212.5	19.861	0.55	2.04	20104480	-1.33	1.28	20111862
216.5	20.013	0.50	2.10	20104481	-1.02	1.57	20111863
224.5	20.319	0.85	1.93	20100118	0.40	2.67	20100062
228.5	20.475				-0.48	2.02	20111951
240.5	20.954	0.66	2.00	20100119	-0.02	2.00	20100063
244.5	21.118				-0.15	2.02	20111864
256.5	21.624	0.45	2.09	20100120	-0.19	2.05	20100064
288.5	23.086	0.79	2.24	20100121	-0.25	2.02	20100262
304.5	23.863	0.69	2.12	20100122	-0.52	1.67	20100065
320.5	24.66	0.62	1.94	20100526	-0.69	1.56	20100066
336.5	25.478	0.71	2.13	20100265	-0.40	2.01	20100067
352.5	26.315	0.83	2.16	20100268	-0.39	1.69	20100199
356.5	26.524	0.71	2.19	20100269	-1.10	1.60	20100264

Appendix B.1: RR0503 87 JPC G. bulloides SST

Depth (cm)	Age (Kyr BP)	SST (°C)	Mg/Ca
0.50	6.25	15.08	2.38
2.50	6.41	17.05	2.94
4.50	6.59	17.73	3.16
6.50	6.76	17.43	3.06
8.50	6.95	16.28	2.70
10.50	7.14	17.69	3.15
12.50	7.34	17.42	3.06
14.50	7.54	16.54	2.78
16.50	7.76	16.68	2.82
18.50	7.98	18.97	3.61
20.50	8.22	16.30	2.71
22.50	8.46	18.38	3.39
24.50	8.72	18.45	3.41
26.50	8.99	17.44	3.06
28.50	9.27	16.82	2.87
30.50	9.56	17.16	2.97
32.50	9.87	15.92	2.60
34.50	10.20	17.03	2.93
36.50	10.55	16.19	2.68
38.50	10.91	16.70	2.83
40.50	11.29	16.24	2.69
42.50	11.70	16.76	2.85
43.50	11.91	17.13	2.96
44.50	12.13	16.69	2.83
45.50	12.35	16.06	2.64
46.50	12.58	16.30	2.71
47.50	12.83	15.23	2.42
48.50	13.07	16.90	2.89
50.50	13.59	16.30	2.71
51.50	13.85	15.93	2.61
52.50	14.11	16.66	2.82
53.50	14.36	15.70	2.54
54.50	14.60	17.06	2.94
55.50	14.79	16.80	2.86
56.50	14.99	16.20	2.68
58.50	15.33	16.46	2.76
60.50	15.66	16.68	2.82
61.50	15.82	16.67	2.82
62.50	15.97	17.78	3.18
64.50	16.28	16.27	2.70
66.50	16.59	16.38	2.74
68.50	16.89	16.19	2.68
70.50	17.20	14.91	2.34
72.50	17.50	16.85	2.88
75.50	17.95	16.13	2.66
78.50	18.39	15.40	2.46
80.50	18.68	15.88	2.59
82.50	18.97	14.26	2.18
83.50	19.11	15.77	2.56
84.50	19.25	16.00	2.63
85.50	19.38	15.80	2.57
86.50	19.52	17.38	3.04
87.50	19.66	14.34	2.20
89.50	19.93	15.37	2.46
92.50	20.32	14.89	2.33
94.50	20.58	13.64	2.04
96.50	20.84	14.44	2.22
97.50	20.96	16.89	2.89
98.50	21.09	14.49	2.23
100.50	21.33	12.15	1.74
102.50	21.58	14.93	2.34
103.50	21.70	12.54	1.81
104.50	21.82	13.90	2.10
106.50	22.06	13.54	2.02
108.50	22.29	13.96	2.11
110.50	22.52	12.49	1.80
112.50	22.74	14.05	2.13
114.50	22.97	12.99	1.90
116.50	23.19	13.37	1.98
118.50	23.40	14.09	2.14
120.50	23.51	12.96	1.90
122.50	23.62	12.82	1.87
123.50	23.83	12.60	1.83
124.50	24.04	13.43	1.99
126.50	24.29	14.95	2.35
127.50	24.37	14.07	2.14

128.50	24.45	14.33	2.20
131.50	24.74	13.77	2.07
132.50	24.84	13.71	2.06
133.50	24.94	13.40	1.99
136.50	25.23	12.49	1.80
137.50	25.32	15.32	2.44
138.50	25.42	15.30	2.44
142.50	25.60	13.54	2.02
143.50	25.88	13.57	2.03
144.50	25.97	13.73	2.06
146.50	26.15	13.82	2.08
150.50	26.50	17.08	2.95
152.50	26.68	12.86	1.88
154.50	26.85	12.46	1.80
156.50	27.02	13.12	1.93
158.50	27.18	14.08	2.14
160.50	27.35	12.73	1.85
162.50	27.52	11.22	1.57
164.50	27.69	12.89	1.88
166.50	27.85	13.97	2.11

Appendix B.2: RR0503 87 JPC/TC Alkenone SST

Core	Depth (cm)	Age (kyr BP)	UK37	Temp. (ºC) Prahl et al. 1988	Temp. (ºC) Sikes & Volk 1993
RR0503-87TC	2	0.1318	0.669	18.5	19.9
RR0503-87TC	12	1.0097	0.689	19.1	20.4
RR0503-87TC	22	1.8848	0.698	19.4	20.6
RR0503-87TC	32	2.7568	0.738	20.6	21.6
RR0503-87TC	42	3.6259	0.718	20.0	21.1
RR0503-87TC	52	4.4922	0.732	20.4	21.4
RR0503-87TC	60.5	5.2259	0.752	21.0	21.9
RR0503-87TC	62	5.3554	0.695	19.31	20.6
RR0503-87TC	62.5	5.3985	0.713	19.8	21.0
RR0503-87TC	66.5	5.7425	0.723	20.1	21.2
RR0503-87TC	70.5	6.0866	0.764	21.3	22.2
RR0503-87TC	72	6.2156	0.725	20.2	21.3
RR0503-87TC	72.5	6.2586	0.733	20.4	21.5
RR0503-87TC	76.5	6.6014	0.761	21.2	22.2
RR0503-87TC	80.5	6.9443	0.730	20.3	21.4
RR0503-87TC	82	7.0728	0.683	19.0	20.3
RR0503-87TC	82.5	7.1157	0.750	20.9	21.9
RR0503-87TC	84.5	7.2865	0.755	21.1	22.0
RR0503-87TC	88.5	7.6282	0.724	20.1	21.3
RR0503-87TC	90.5	7.7991	0.741	20.6	21.7
RR0503-87TC	92	7.9272	0.745	20.8	21.8
RR0503-87TC	92.5	7.9699	0.721	20.1	21.2
RR0503-87TC	96.5	8.3104	0.733	20.4	21.5
RR0503-87TC	98.5	8.4806	0.745	20.8	21.8
RR0503-87TC	100.5	8.6509	0.744	20.7	21.7
RR0503-87TC	102	8.7785	0.724	20.1	21.3
RR0503-87TC	104.5	8.9908	0.734	20.5	21.5
RR0503-87TC	108.5	9.3301	0.745	20.8	21.8
RR0503-87TC	112	9.627	0.737	20.5	21.6
RR0503-87TC	114.5	9.8385	0.759	21.2	22.1
RR0503-87TC	116.5	10.008	0.776	21.7	22.5
RR0503-87TC	120.5	10.346	0.709	19.7	20.9
RR0503-87TC	122	10.473	0.693	19.2	20.5
RR0503-87TC	122.5	10.515	0.710	19.7	20.9
RR0503-87TC	126.5	10.852	0.706	19.6	20.8
RR0503-87TC	128.5	11.02	0.741	20.6	21.7
RR0503-87TC	130.5	11.189	0.710	19.7	20.9
RR0503-87TC	132	11.315	0.727	20.2	21.3

RR0503-87TC	132.5	11.357	0.721	20.0	21.2
RR0503-87TC	136.5	11.693	0.705	19.6	20.8
RR0503-87TC	140.5	12.028	0.699	19.4	20.7
RR0503-87TC	142	12.154	0.678	18.8	20.1
RR0503-87TC	142.5	12.196	0.699	19.4	20.6
RR0503-87TC	144.5	12.363	0.683	18.9	20.3
RR0503-87TC	146.5	12.531	0.679	18.8	20.2
RR0503-87TC	150.5	12.866	0.712	19.8	21.0
RR0503-87TC	152	12.991	0.689	19.1	20.4
RR0503-87TC	152.5	13.033	0.679	18.8	20.2
RR0503-87TC	160.5	13.7	0.686	19.0	20.3
RR0503-87TC	164.5	14.033	0.717	19.9	21.1
RR0503-87TC	168.5	14.366	0.597	16.4	18.2
RR0503-87TC	169	14.408	0.582	16.0	17.8
RR0503-87TC	170.5	14.533	0.625	17.2	18.9
RR0503-87TC	172.5	14.699	0.593	16.3	18.1

Appendix C.1: RR0503 87 JPC $\delta^{18}O_{SW}$ Calculation

Age (kyr BP)	$\delta^{18}O_{SW}$
6.6	0.209
6.7	0.145
6.8	0.157
6.9	0.292
7	0.307
7.1	0.223
7.2	0.146
7.3	0.074
7.4	0.129
7.5	0.255
7.6	0.301
7.7	0.291
7.8	0.303
7.9	0.345
8	0.373
8.1	0.330
8.2	0.286
8.3	0.293
8.4	0.310
8.5	0.269
8.6	0.129
8.7	-0.012
8.8	0.012
8.9	0.075
9	0.137
9.1	0.205
9.2	0.277
9.3	0.332
9.4	0.340
9.5	0.348
9.6	0.291
9.7	0.124
9.8	-0.041
9.9	-0.162
10	-0.191
10.1	-0.192
10.2	-0.192
10.3	-0.129
10.4	-0.064
10.5	0.001
Age (kyr BP)	$\delta^{18}O_{SW}$
10.6	0.092
10.7	0.208
10.8	0.323
10.9	0.437
11	0.442
11.1	0.429
11.2	0.383
11.3	0.338
11.4	0.317
11.5	0.309
11.6	0.313
11.7	0.310
11.8	0.190
11.9	0.070
12	-0.036
12.1	-0.135
12.2	-0.128
12.3	-0.090
12.4	-0.038
12.5	0.029
12.6	0.093
12.7	0.147
12.8	0.200
12.9	0.237
13	0.290
13.1	0.318
13.2	0.307
13.3	0.293
13.4	0.279
13.5	0.264
13.6	0.248
13.7	0.216
13.8	0.171
13.9	0.123
14	0.072
14.1	0.027
14.2	-0.006
14.3	-0.024
14.4	-0.081
14.5	-0.118
Age (kyr BP)	$\delta^{18}O_{SW}$
14.6	-0.122
14.7	-0.062
14.8	-0.001
14.9	0.088
15	0.158
15.1	0.031
15.2	-0.095
15.3	-0.222
15.4	-0.229
15.5	-0.175
15.6	-0.120
15.7	-0.072
15.8	-0.030
15.9	0.007
16	0.013
16.1	-0.062
16.2	-0.138
16.3	-0.187
16.4	-0.118
16.5	-0.048
16.6	0.011
16.7	-0.007
16.8	-0.025
16.9	-0.042
17	-0.047
17.1	-0.051
17.2	-0.057
17.3	-0.076
17.4	-0.095
17.5	-0.113
17.6	-0.096
17.7	-0.074
17.8	-0.051
17.9	-0.029
18	-0.008
18.1	0.010
18.2	0.021
18.3	0.061
18.4	0.104
18.5	0.061
Age (kyr BP)	$\delta^{18}O_{SW}$
18.6	0.056
18.7	0.052
18.8	0.077
18.9	0.079
19	0.073
19.1	0.060
19.2	0.129
19.3	0.173
19.4	0.187
19.5	0.135
19.6	0.269
19.7	0.454
19.8	0.624
19.9	0.577
20	0.532
20.1	0.488
20.2	0.444
20.3	0.400
20.4	0.442
20.5	0.508
20.6	0.547
20.7	0.468
20.8	0.388
20.9	0.224
21	0.073
21.1	0.026
21.2	0.014
21.3	0.002
21.4	-0.025
21.5	-0.060
21.6	-0.115
21.7	-0.237
21.8	-0.247
21.9	-0.196
22	-0.132
22.1	-0.077

		23.5	-0.560	24.8	-0.327	26.1	-0.151
22.2	-0.034	23.6	-0.441	24.9	-0.350	26.2	-0.207
22.3	-0.001	23.7	-0.307	25	-0.316	26.3	-0.063
22.4	-0.039	23.8	-0.169	25.1	-0.206	26.4	0.072
22.5	-0.077	23.9	-0.082	25.2	-0.049	26.5	0.204
22.6	-0.102	24	-0.017	25.3	-0.092	26.6	0.335
22.7	-0.124	24.1	-0.013	25.4	-0.198	26.7	0.365
22.8	-0.168	24.2	-0.043	25.5	-0.223	26.8	0.055
22.9	-0.228	24.3	-0.070	25.6	-0.231	26.9	-0.132
23	-0.244	24.4	-0.051	25.7	-0.298	27	-0.210
23.1	-0.167	24.5	-0.098	25.8	-0.334	27.1	-0.248
23.2	-0.134	24.6	-0.164	25.9	-0.081		
23.3	-0.390	24.7	-0.230	26	0.098		
23.4	-0.645						